

AD-A040 895

XEROX CORP/ELECTRO-OPTICAL SYSTEMS PASADENA CALIF
THERMAL ENERGY STORAGE DEMONSTRATION UNIT FOR VUILLEUMIER CRYOGEN--ETC(U)

F/G 10/2

FEB 77 R RICHTER

F33615-75-C-2045

UNCLASSIFIED

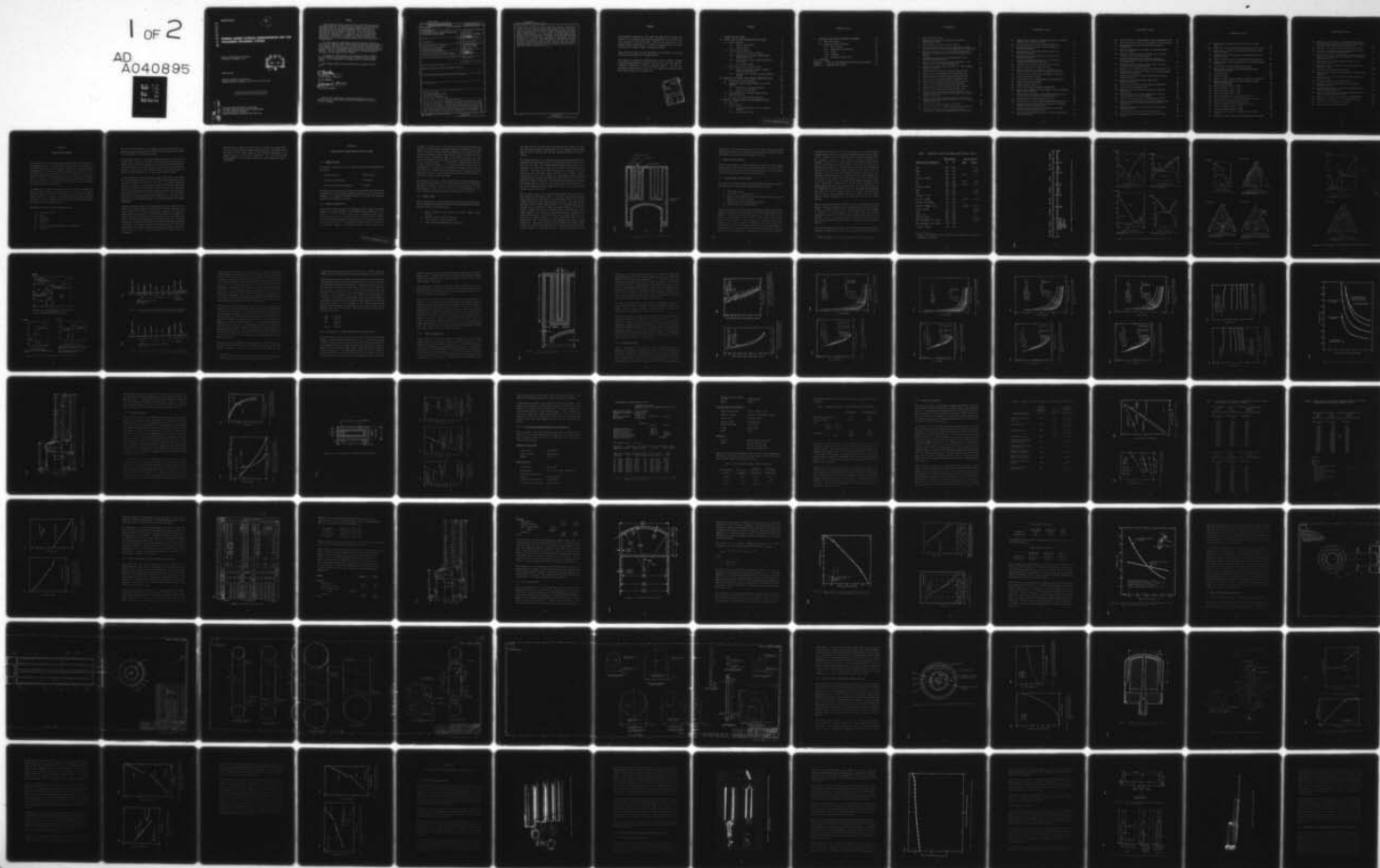
2340-I-1

AFAPL-TR-76-110

NL

1 of 2

AD
A040895



AD A 040895

AFAPL-TR-76-110

12
NW

THERMAL ENERGY STORAGE DEMONSTRATION UNIT FOR VUILLEUMIER CRYOGENIC COOLER

XEROX ELECTRO-OPTICAL SYSTEMS
PASADENA, CALIFORNIA 91107



FEBRUARY 1977

TECHNICAL REPORT AFAPL-TR-76-110
INTERIM REPORT FOR PERIOD 2 JUNE 1975 to 31 AUGUST 1976

Approved for public release; distribution unlimited

DDC FILE COPY

AIR FORCE AERO PROPULSION LABORATORY
AIR FORCE WRIGHT AERONAUTICAL LABORATORIES
AIR FORCE SYSTEMS COMMAND
WRIGHT-PATTERSON AIR FORCE BASE, OHIO 45433

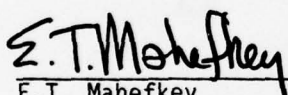
NOTICE

When Government drawings, specifications, or other data are used for any purpose other than in connection with a definitely related government procurement operation, the United States Government thereby incurs no responsibility nor any obligation whatsoever; and the fact that the government may have formulated, furnished, or in any way supplied the said drawings, specifications, or other data, is not to be regarded by implication or otherwise as in any manner licensing the holder or any other person or corporation, or conveying any rights or permission to manufacture, use, or sell any patented invention that may in any way be related thereto.

This final report was submitted by Xerox/Electro Optical Systems Inc. under Contract F3361575-C-2045. Robert Richter was the principal investigator. The effort was sponsored by the Air Force Space and Missile Systems Organization (SAMSO), under the technical direction of the Air Force Aero Propulsion Laboratory, with E.T. Mahefkey/AFAPL/POE-2/513-255-6237 the cognizant project engineer. The Air Force greatly acknowledges Dr. Richter's technical contribution in the conduct of this research.

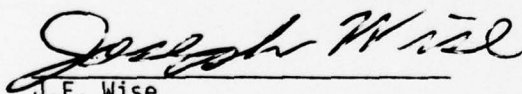
This report has been reviewed by the Information Office, (ASD/OIP) and is releasable to the National Technical Information Service (NTIS). At NTIS, it will be available to the general public, including foreign nations.

This technical report has been reviewed and is approved for publication.



E.T. Mahefkey
Project Engineer, AFAPL/POE-2

FOR THE COMMANDER



J.F. Wise
Technical Area Manager

Copies of this report should not be returned unless return is required by security considerations, contractual obligations, or notice on a specific document.

UNCLASSIFIED

SECURITY CLASSIFICATION OF THIS PAGE (When Data Entered)

REPORT DOCUMENTATION PAGE		READ INSTRUCTIONS BEFORE COMPLETING FORM
1. REPORT NUMBER AFAPL-TR-76-110	2. GOVT ACCESSION NO.	3. RECIPIENT'S CATALOG NUMBER
4. TITLE (and Subtitle) THERMAL ENERGY STORAGE DEMONSTRATION UNIT FOR VUILLEUMIER CRYOGENIC COOLER	5. TYPE OF REPORT & PERIOD COVERED Interim Report, 2 June 1975 to 31 August 1976	6. PERFORMING ORG. REPORT NUMBER 2340-Interim-1
7. AUTHOR(s) Robert Richter	8. CONTRACT OR GRANT NUMBER(s) F33615-75-C-2045	
9. PERFORMING ORGANIZATION NAME AND ADDRESS Xerox Electro-Optical Systems 300 North Halstead Street Pasadena, California 91107	10. PROGRAM ELEMENT, PROJECT, TASK AREA & WORK UNIT NUMBERS Project No. 2126 Task No. 03 Work Unit No. 10	
11. CONTROLLING OFFICE NAME AND ADDRESS Air Force Aero Propulsion Laboratory/POE Wright Patterson Air Force Base, Ohio 45433	12. REPORT DATE February 1977	13. NUMBER OF PAGES 154
14. MONITORING AGENCY NAME & ADDRESS (if different from Controlling Office)	15. SECURITY CLASS. (of this report) Unclassified	15a. DECLASSIFICATION DOWNGRADING SCHEDULE
16. DISTRIBUTION STATEMENT (of this Report) Approved for public release; distribution unlimited.		
17. DISTRIBUTION STATEMENT (of the abstract entered in Block 20, if different from Report)		
18. SUPPLEMENTARY NOTES		
19. KEY WORDS (Continue on reverse side if necessary and identify by block number) Thermal Space Power Heat Pipe and Energy Transport Space Power System Study Thermal Energy Storage Material		
20. ABSTRACT (Continue on reverse side if necessary and identify by block number) This report covers the work performed under the Thermal Energy Storage Demonstration Unit Program. The report presents the analysis, design, fabrication, and testing of a thermal energy storage demonstration unit which was to be mated to an existing Vuilleumier cooler (AFLIR) to demonstrate the concept of powering such a device directly with stored thermal energy. The Thermal Energy Storage Demonstration Unit was to be sized for delivering 1000 watts thermal power for one hour at a temperature of 1250° ± 25°F. The		

DD FORM 1 JAN 73 1473 EDITION OF 1 NOV 65 IS OBSOLETE

UNCLASSIFIED

SECURITY CLASSIFICATION OF THIS PAGE (When Data Entered)

UNCLASSIFIED

SECURITY CLASSIFICATION OF THIS PAGE(When Data Entered)

ternary eutectic 64 MgF_2 -30 LiF -6 KF , which has a eutectic temperature of 1310 $^\circ\text{K}$, was selected as the thermal energy storage material. The report presents the approach and the assumptions underlying the design of the unit, which incorporates a heat pipe for the transfer of energy from the thermal energy storage material to the hot cylinder of the Vuilleumier cooler. Details of the fabrication and the testing of the Thermal Energy Storage Demonstration Unit are presented. The analysis of the test data led to the conclusion that the basic design satisfied all requirements that were established for a TES unit. The thermal energy storage material, however, was found to apparently release its latent heat of fusion over a wider temperature range than had been anticipated. This fact can be attributed to nonisothermal phase transformation or a bulk thermal conductivity that is lower than had been assumed for the salt.

UNCLASSIFIED

SECURITY CLASSIFICATION OF THIS PAGE(When Data Entered)

FOREWORD

The information presented in this report was generated during the performance of the Thermal Energy Storage Demonstration Unit contract, Air Force Contract No. F33615-75-C-2045. The work was carried out in the Advanced Systems Department of the Radiation Systems Division of Xerox Electro-Optical Systems, (XEOS), Pasadena, California.

Robert Richter was the principal investigator of the program. Individual contributors were members of the XEOS Division.

The program was sponsored by SAMSO/SZ under Project 21260310, "Thermal Energy Storage Demonstration Program," with the Air Force Aero Propulsion Laboratory (AFAPL/POE-2) acting as technical monitor. The work was performed during the period 1 June 1975 to 31 August 1976 with the draft final report submitted in November 1976.

ACCESSION IN	
NTIS	White Section <input checked="" type="checkbox"/>
DIC	Buff Section <input type="checkbox"/>
UNANNOUNCED	
JUSTIFICATION	
BY	
DISTRIBUTION AVAILABILITY CODES	
Dist.	AVAIL. AND OF SPECIAL

CONTENTS

I. INTRODUCTION AND SUMMARY	1
II. THERMAL ENERGY STORAGE DEMONSTRATION UNIT DESIGN	5
2.1 General Approach	5
2.1.1 Heating Configuration	5
2.1.2 General Layout	6
2.2 Detailed Design Approach	9
2.2.1 Thermal Energy Storage Material	9
2.2.2 Optimization of Thermal Energy Storage Demonstration Unit	19
2.2.3 Final Thermal Energy Storage Demonstration Unit Design	45
2.2.4 Hot Cylinder Design	49
2.3 Special Heat Transfer Considerations	56
2.3.1 Effect of Volumetric Change of Thermal Energy Storage Material	56
2.3.2 Cooling of Hot Cylinder During Performance Testing	63
III. FABRICATION OF THERMAL ENERGY STORAGE DEMONSTRATION UNIT	73
3.1 Machining and Initial Assembly	73
3.2 Loading of Thermal Energy Storage Unit with TES Material	75
3.2.1 Evaluation of Loading Procedures	75
3.2.2 Casting of TES Material	79
3.3 Final Assembly of the Thermal Energy Storage Demonstration Unit	82
3.4 Filling of Heat Pipe With Working Fluid	84
IV. TESTING OF THERMAL ENERGY STORAGE DEMONSTRATION UNIT	91
4.1 Test Setup	91
4.2 Initial Testing	93
4.2.1 Steady State Thermal Losses and Thermal Capacity	93
4.2.2 Test Data Evaluation	98

CONTENTS (Contd)

V.	CONCEPTUAL FLIGHT DEVICE PARAMETER DEVELOPMENT	119
5.1	Basic Requirements	119
5.2	Conceptual Design Parameters	120
5.2.1	Basic Design	120
5.2.2	Temperature Distributions	123
5.2.3	Weight	123
5.2.4	Structure	128
5.2.5	Conceptual Flight Device	132
VI.	CONCLUSIONS	135
APPENDIX A	- EFFECT OF NONCONDENSABLE GAS ON HEAT PIPE OPERATION	137
APPENDIX B	- TRANSIENT WICK EFFECTS	141

ILLUSTRATIONS

1	General TES Unit Lay-out	8
2	Temperature Distribution Along the Solar Collector Thermal Power System	12
3	Phase Diagrams of Fluoride Eutectic Salts	13
4	Temperature Distribution in the Thermal Energy Storage Unit for a VM Cooler with 64 LiF-30 MgF ₂ -6 KF as TES Material	17
5	Temperature Distribution in the Thermal Energy Storage Unit for a Vuilleumier Cooler with 67 LiF-33 MgF ₂ as TES Material	17
6	Parameters Investigated in the Optimization of the Thermal Energy Storage Unit	21
7	Effect of Thermal Energy Storage Salt Thickness on the Length of the Thermal Energy Storage Unit	23
8	Correlation Between Primary Dimensions of 1 kW-Hr Thermal Energy Storage Unit	23
9	Thermal Losses from Thermal Energy Storage Heat Pipe	24
10	Power Losses from Thermal Energy Storage Heat Pipe	24
11	Thermal Losses from Thermal Energy Storage Heat Pipe	25
12	Power Losses from Thermal Energy Storage Heat Pipe	25
13	Thermal Losses from Thermal Energy Storage Heat Pipe	26
14	Power Loss from Thermal Energy Storage Heat Pipe	26
15	Thermal Losses from Thermal Energy Storage Heat Pipe	27
16	Power Loss from Thermal Energy Storage Heat Pipe	27
17	Effect of Vapor Flow Annular Width and Thermal Energy Storage Material Thickness on Thermal Loss of the Thermal Energy Storage Unit	28
18	Effect of Vapor Flow Annular Width and Thermal Energy Storage Material Thickness on Thermal Loss of the Thermal Energy Storage Unit	28
19	Power Losses from Hot Cylinder of VM Cooler	29
20	Optimum Design for a 1 kW-Hr Thermal Energy Storage Unit	30
21	Power Loss as Function of Insulation Thickness of Final Thermal Energy Storage Demonstration Unit Design	32

ILLUSTRATIONS (Contd)

22	Temperature Distribution in Thermal Insulation of Thermal Energy Storage Demonstration Unit	32
23	Insulation Design of Thermal Energy Storage Unit	33
24	Pressure Drops and Available Suction Pressure for Various Wire Screens	34
25	Pressure Drops and Available Suction Pressure for Various Wire Screens	34
26	Pressure Drops and Available Suction Pressure for Various Wire Screens	34
27	Heat Pipe Design Calculations for Final Design of a 1 kW-Hr Thermal Energy Storage Unit	36
28	Conductivity of Various Combinations of Fiberfrax	41
29	Thermal Conductivity of Super Insulation	41
30	Effect of Insulation Thickness on the Total Loss of Thermal Energy from the Thermal Energy Storage Unit	44
31	Thermal Losses as Affected by the Amount of Insulation	44
32	Available Inconel 600 Pipes	46
33	Final Design for a 1 kW-Hr Thermal Energy Storage Unit	48
34	Original Hot Cylinder Design	50
35	Rupture Stress of René 41	52
36	Life of Cold-Rolled, Annealed and Aged Sheet	53
37	Larson-Miller Parameter Plot of Rupture Life of Cold-Rolled Sheet, 0.025-0.250-Inch	53
38	Effect of Plate Thickness on the Maximum Stresses in the Hot Cylinder of the AFLIR Vuilleumier Cooler	55
39	Thermal Energy Storage Demonstration Unit	57
40	Configuration of Thermal Energy Storage Demonstration Unit	64
41	Volumetric Void as a Function of Half Angle for Thermal Energy Storage Demonstration Unit	65
42	Volumetric Void and Surface Void Relation for Thermal Energy Storage Demonstration Unit	65
43	Gas Flow for Performance Testing of Thermal Energy Storage Demonstration Unit	66

ILLUSTRATIONS (Contd)

44	Flow Test Insert - Thermal Energy Storage Demonstration Unit	67
45	Total Heat Transfer from the Hot Cylinder to the Cooling Air	68
46	Power Extraction from the Hot Cylinder as Function of Flow Rate	68
47	Final Air Temperature as Function of Flow Rate Through the Hot Cylinder	70
48	Pressure Drop Along the Heat Transfer Path of the Hot Cylinder of the Vuilleumier Cooler	70
49	Flow Rate Requirement for Cooling Hot Cylinder of Vuilleumier Cooler During Thermal Energy Storage Unit Performance Test	72
50	Pressure Drop Along the Heat Transfer Path of the Hot Cylinder of the Vuilleumier Cooler	72
51	Exploded View of Thermal Energy Storage Demonstration Unit	74
52	Thermal Energy Storage Unit Prior to Loading with Thermal Energy Storage Material	76
53	Temperature of Thermal Energy Storage Material Capsule During Melt-Down	78
54	Bottom Plate of Casting Fixture SK2340-004-1 Material: Graphite	80
55	Tubes and Center Rod of Casting Fixture SK2340-004-2	80
56	Casting Fixture (Exploded View)	81
57	Distribution of Wick Material Consisting of Mesh 70 Bolting Cloth	83
58	TES Demonstration Unit After Application of Wicking Structure and Prior to Final Welding	85
59	Completed Thermal Energy Storage Demonstration Unit	85
60	Insulation and Thermocouple Locations of Thermal Energy Storage Demonstration Unit for Vuilleumier Cooler Application	86
61	Predicted Thermal Losses from Thermal Energy Storage Demonstration Unit	87
62	Fully Thermally Insulated TES Demonstration Unit	88
63	Thermal Energy Storage Demonstration Unit Test Setup (View I)	92

ILLUSTRATIONS (Contd)

64	Thermal Energy Storage Demonstration Unit Test Setup (View II)	92
65	Energy Loss from Thermal Energy Storage Demonstration Unit	95
66	Temperature of Thermal Energy Storage Demonstration Unit During Cool-Down	100
67	Temperature of Thermal Energy Storage Demonstration Unit During Cool-Down	100
68	Apparent Thermal Capacity of Thermal Energy Storage Unit	101
69	Measured Temperature of Thermocouple No. 3 During Charging of TES Unit	101
70	Cooling Data of Thermal Energy Storage Unit	105
71	Temperature of Thermal Energy Storage Demonstration Unit During Cool-Down	106
72	Extracted Energy	107
73	Extracted Energy	107
74	Amount of Stored Thermal Energy as Function of Temperature	109
75	Apparent Thermal Capacity of Thermal Energy Storage Unit During Charging	109
76	Extracted Energy (June 7, 1976)	111
77	Extracted Energy (June 7, 1976)	111
78	Extracted Energy (June 4, 1976)	112
79	Extracted Energy (June 4, 1976)	112
80	Measured Temperatures During Energy Extraction	114
81	Measured Temperatures by Thermocouples Nos. 10 and 12	114
82	Temperatures During Charging of TES Unit	115
83	Measured Temperature During Energy Extraction	117
84	Extracted Energy (August 5, 1976)	118
85	Extracted Energy (August 5, 1976)	118
86	Thermal Energy Storage Unit Mounted on a Hi-Cap Hot Cylinder	121
87	Correlation Between Power Requirement and TES Unit Length	122

ILLUSTRATIONS (Contd)

88	Temperature Distribution in the Thermal Energy Storage Unit and the Hot Cylinder of the Long Life, High Capacity Vuilleumier Refrigerator for Space Application	124
89	Temperature Drop Across Thermal Energy Storage Material	125
90	Vuilleumier Refrigerator Operating Temperature During Discharge of Thermal Energy Storage Unit	125
91	Operating Temperature of Vuilleumier Refrigerator During a Full Cycle of Charging and Discharging of the Thermal Energy Storage Unit	126
92	Total Weight of a Thermal Energy Storage Unit for a Vuilleumier Cooler	127
93	Specific Energy of a Thermal Energy Storage Unit for a Vuilleumier Cooler	129
94	Thermal Energy Storage Material Weight	130
95	Total Container Weight Including Insulation and Heat Pipe Components	130
96	Dynamic Modulus of Elasticity E and Yield Strength of Inconel 600 Alloy	131
97	Collapsing Pressure of Thin-Walled Vessel	131
98	Conceptual Thermal Energy Storage Unit for Hi-Cap Vuilleumier Cooler	133
99	Long Life, High Capacity Vuilleumier Refrigerator with Thermal Energy Storage Units	134
100	Long Life, High Capacity Vuilleumier Refrigerator with Battery Energized Electric Heaters	134
A-1	Temperature Differentials and Pressure Differentials	138
A-2	Temperature Differential Due to Noncondensable Gas	139
A-3	Vapor Pressure of Sodium and Potassium	139
B-1	Test Fixture for Wick Investigation	143

SECTION I

INTRODUCTION AND SUMMARY

The objective of the Thermal Energy Storage Demonstration Unit program was the demonstration of a thermal energy storage (TES) unit capable of providing thermal energy to a Vuilleumier (VM) cooler by releasing thermal energy which had been stored in the form a latent heat of fusion of a salt. The requirements were to deliver 1 kW of thermal power for 1 hour at a temperature between 1200° and 1400°F to the hot cylinder of a Vuilleumier cooler. In addition, the TES capability had to be sufficient to account for all thermal losses occurring due to limitations on the size and weight of thermal insulation of the TES unit.

The program was to generate background data for the design of flight test devices which can operate in a power range of 1 to 3 kW, while having a lifetime of better than 5 years. The data were to include costing for the design, fabrication, testing, and delivery of such devices, projected efficiency in satellite application, their weight, volume, and the operating temperature as a function of load.

The program was organized into seven major tasks:

- I. Analytical Studies
- II. Design
- III. Fabrication
- IV. Test Setup
- V. Testing
- VI. Conceptual Flight Device Parameter Development
- VII. Reporting

The total technical effort of the program extended over a period of 12-months, and was concluded with the delivery of the tested TES unit mounted on a hot cylinder of a Vuilleumier cooler.

For successful mating of the thermal energy storage unit with the Vuilleumier cooler, the heat pipe concept was considered for transferring the stored energy from the storage material to the point of energy requirement. This appeared most valid in this application in which the amount of thermal energy is large and the heat transfer surface of the hot cylinder over which the thermal energy had to be applied was relatively small.

As the optimization studies indicated, weight considerations and thermal loss considerations dictated a unit with a relatively large diameter, which was about one-third the length of the unit. The largest acceptable diameter of the unit was determined by the restriction that the temperature at the hot cylinder of the Vuilleumier cooler should not vary by more than 50°F from the beginning of the energy extraction process until the completion of the freezing of the thermal energy storage salt. This stipulation determined the largest thermal energy storage material thickness in the unit and, thus, the greatest diameter for an annular design of the storage compartment.

During the heat pipe design, the elevation pressure drop, which is determined by the height to which the working fluid of the heat pipe has to be raised, proved to be the major pressure drop component. The final wick design of the heat pipe had to utilize almost 75 percent of its theoretical suction capacity to overcome the elevation pressure drop. The wick design proved to be adequate, although great uncertainty existed for a time when the heat pipe did not function properly for reasons which later were traced to a gas leak. The dynamic behavior of wick structures has not been fully investigated and therefore introduced uncertainties into the design of large diameter heat pipe structures which have to be operated in a 1-g environment.

The test results seemed to indicate that the eutectic salt, $\text{MgF}_2\text{-LiF-KF}$, used in the thermal energy storage demonstration unit, released only about 50 percent of the fusion energy of the individual components of the eutectic mixture at the eutectic temperature. The total stored energy could therefore not be extracted within the design temperature range of $1250^\circ \pm 25^\circ\text{F}$.

SECTION II

THERMAL ENERGY STORAGE DEMONSTRATION UNIT DESIGN

2.1. GENERAL APPROACH

The specific requirements for the thermal energy storage demonstration unit were:

Thermal capacity to	1 kW-hr thermal
Power to the hot cylinder	1 kW thermal
Hot cylinder operating tempeature	1250 $\pm 25^{\circ}\text{F}$

The energy to the unit was to be supplied from an electric source which was to energize the thermal energy storage unit without the use of electrical heaters, i.e., using the container material of the unit as resistance elements for the electrical current.

2.1.1 HEATING CONFIGURATION

Considerable thought was given to eliminating electric heaters and using solely the structural material of the thermal energy storage unit as the electrical pass for resistance heating. For a reasonable current level, the electric pass has to be long and, therefore, many structural elements of the thermal energy storage unit would have had to be placed electrically in series with each other. This would have required electrical insulation of structural components by insulating material, which appeared very

difficult to achieve when at the same time requiring high thermal conductivity for maintaining a reasonable temperature distribution in the TES unit. An even more serious problem was thought to be the galvanic effect to which the thermal energy storage material would be exposed and about which little or nothing was known for the ternary eutectic salt. Any galvanic separation of the individual elements could cause a serious attack on the container material. It was therefore suggested that the electrically resistive heating of the container material should first be investigated in a smaller device specifically developed for such a test. This test could furnish long time operating data in parallel with the operation of the full scale thermal energy storage unit which could be heated with standard resistance heaters.

The elimination of electric heaters appeared to be of great advantage, as many electric heater failures have been experienced with the VM cooler. When the hot cylinder is heated directly by electric heaters, the heat transfer area is only 7.241 in.^2 (46.7 cm^2). For a power input of 1 kW, this indicates the relatively high power density of 21.4 watt/cm^2 .

2.1.2 GENERAL LAYOUT

After electing separate electric heating for the power input into the unit, the most appropriate configuration for that heating scheme was considered. The most critical considerations were:

- a. Lowest temperature drop across the thermal energy storage material
- b. Smallest thermal losses from the unit
- c. Lowest weight of structural material
- d. Lowest operating temperature of the heaters

The design that evolved from these considerations was a tubular unit with two interconnected annular compartments for the thermal energy storage material and an annular well for the resistance heaters as shown in Figure 1.

The highest temperature drop across the thermal energy storage material is determined by the greatest thickness of the TES material and the heat flow rate per unit area. The annular design provides large surfaces for a relatively low heat flux as well as a relatively small TES material thickness. By placing the electric heaters into an annular well, the heaters can give off their power from their entire surface, thereby operating at a lower power density and corresponding lower operating temperature than a heater that transfers energy only from one side while having its other side insulated. Furthermore, by placing the heater inside the thermal energy storage unit, the outer surface of the TES unit is at the lowest temperature during heating of the unit. This minimizes the thermal losses from the unit.

For the initial layout of the thermal energy storage unit, the effective heat transfer area was about 1700 cm^2 . During the time when the heaters supply energy for the operation of the Vuilleumier cooler as well as for storage, the highest power density is only 1 watt/cm^2 . This compares very favorably with the heater power density of 21.4 watt/cm^2 when the hot cylinder of the Vuilleumier cooler is heated directly with electric heaters. Despite the fact that the heaters have to transfer power to the higher temperature of the thermal energy storage material, compared to the operating temperature of the hot cylinder which is about 90°F lower, the heaters will actually operate at a lower temperature because of the considerably lower power density when energizing the thermal energy storage unit. Thus, the reliability of the heaters in the thermal energy storage unit would be higher than that of the heaters that directly power the hot cylinder of a Vuilleumier cooler. This might suggest that the

56720

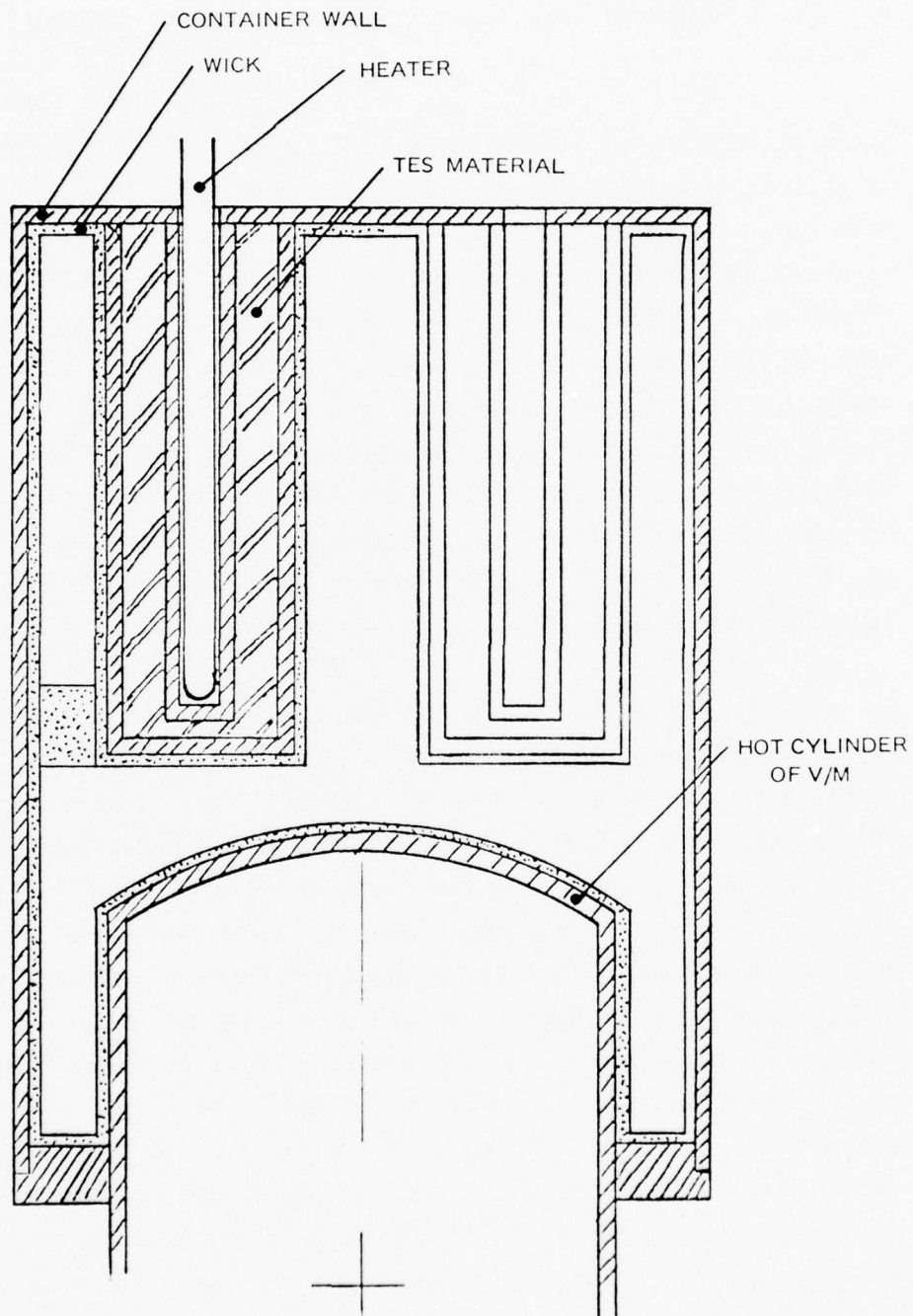


Figure 1. General TES Unit Layout (Center Cut Through Cylindrical Configuration)

urgency for eliminating the heaters and for turning to resistance heating the container material of the thermal energy storage unit might have been eliminated by the thermal energy storage unit design.

2.2 DETAILED DESIGN APPROACH

With the establishment of the general approach to the design of the thermal energy storage demonstration unit, the detailed design of the unit required the selection of the thermal energy storage material and the optimization of the unit with respect to size and thermal losses.

2.2.1 THERMAL ENERGY STORAGE MATERIAL

The design of the thermal energy storage demonstration unit had to consider the selection of a thermal energy storage material that had:

- a. High fusion energy
- b. Low volume, i.e., high density
- c. Melting point appropriate for maintaining the desired operating temperature of the hot cylinder
- d. Compatibility with the structural material
- e. Stability over many melting cycles

In the Solar Collector Thermal Power System program which preceded this program, lithium fluoride was selected as the the thermal energy storage material. Lithium fluoride has a melting point of 1558⁰F and a heat of fusion of 0.259 kWh/kg. For the solar collector thermal power train, lithium fluoride proved to be the appropriate thermal energy storage material as it had the melting temperature that could provide the Vuilleumier cooler with the thermal energy at the desired temperature as shown in Figure 2. Since in the present application the thermal energy did not have to be transferred across a thermal radiation joint, which required

a temperature differential of 220°F in the thermal train, a thermal energy storage material with a lower melting temperature appeared to be appropriate. A number of the most promising thermal energy storage materials are presented in Table 1, while Figure 3 presents pertinent phase diagrams.¹ From Table 1 the binary eutectic 67 LiF-33 MgF_2 and the ternary eutectic 64 LiF-30 MgF_2 -6 KF were selected for possible application in the thermal energy storage unit. In Figures 4 and 5 the calculated temperature distributions in the thermal energy storage unit are shown for the two materials. The ternary eutectic LiF- MgF_2 -KF appeared to provide the more appropriate melting temperature for achieving the desired operating conditions at the hot cylinder of the Vuilleumier cooler. The inner surface of the hot cylinder, which is cooled by the flowing helium gas in the cooler, would have a temperature of 1267.5°F at the beginning of the thermal energy extraction cycle, while at the end of the extraction cycle the temperature will have dropped to 1227.5°F . This temperature range was well within the desired operating range of $1250 \pm 25^{\circ}\text{F}$. The temperature level as well as the temperature range for a system using the binary eutectic LiF- MgF_2 appeared not to be better than that of the ternary eutectic.

Another ternary system which appeared to have a melting point near the desired operating temperature for the storage material was 62 LiF-19 NaF-19 MgF_2 . It fuses at 708°C (1306°F). However, this system was recognized as unstable as it can transition into a system which has a melting temperature of only 630°C (1166°F) when NaF and MgF_2 form the double salt $\text{MgF}_2 \cdot \text{NaF}$. This is in conformance with the double melting point of the binary system consisting of NaF and MgF_2 , as shown in the phase diagram of Figure 3.

The assumed thermal energy storage capacity of the ternary eutectic mixture composed of LiF- MgF_2 -KF was based on the published data of the heat of

1. "Phase Diagrams for Ceramists," American Ceramic Society (1964).

TABLE 1. PROPERTIES OF APPLICABLE THERMAL ENERGY STORAGE MATERIALS

<u>Eutectic Molar Composition</u>	<u>Melting Point</u>		<u>Heat of Fusion*</u>	
	<u>°C</u>	<u>°F</u>	<u>kWh/l</u>	<u>kWh/kg</u>
CaF ₂	1382	2520		0.105
MgF ₂	1263	2305		0.265
NaF	996	1825	0.603	0.216
56 CaF ₂ + 44 MgF ₂	985	1805		
KF	860	1580	0.310	0.125
LiF	848	1558	0.464	0.259
67 CaF ₂ + 33 NaF	813	1495		
NaCl	800	1472		0.132
KCl	776	1429		0.098
79 CaF ₂ + 21 LiF	765	1409		
67 LiF + 33 MgF ₂	742	1368	(0.537)	(0.238)
42.5 LiF + 57.5 MgF ₂	735	1355		
64 LiF + 30 MgF ₂ + 6 KF	713	1315	(0.465)	(0.219)
40 KF + 60 NaF	710	1310		(0.172)
LiH	686	1267		0.716
50 KF + LiF	650	1202		
48 LiF + 52 NaF	652	1206		(0.261)
NaF + NaF-MgF ₂ + LiF + MgF ₂	630	1166		(0.261)
NaF + NaF-MgF ₂ + LiF + MgF ₂	708	1306		
62 ZnF ₂ + 38 LiF	622	1152		

* Values in parentheses are of questionable accuracy and subject to modifying definitions.

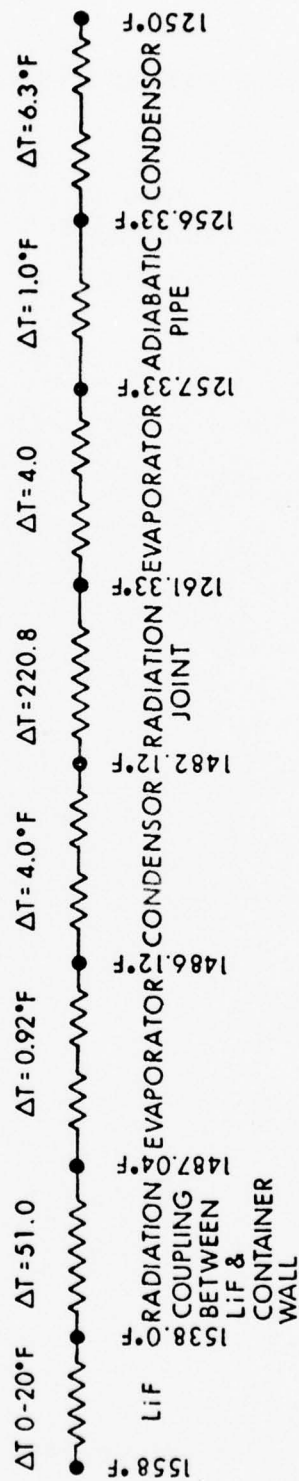


Figure 2. Temperature Distribution Along the Solar Collector Thermal Power System

LiF-NaF

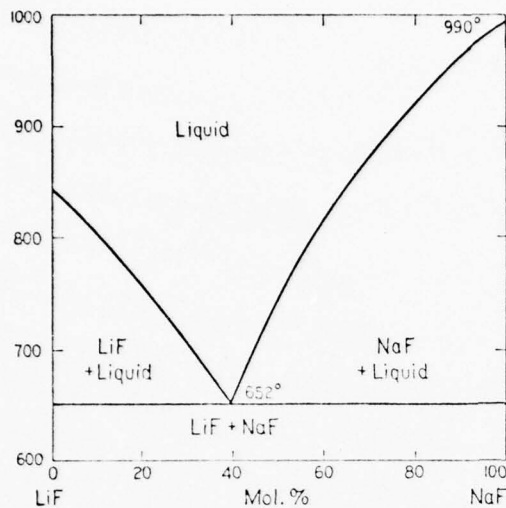


FIG. 1467.—System LiF-NaF.

A. G. Bergman and E. P. Dergunov, *Compt. rend. acad. sci., U.R.S.S.*, **31**, 755 (1941).

LiF-MgF₂

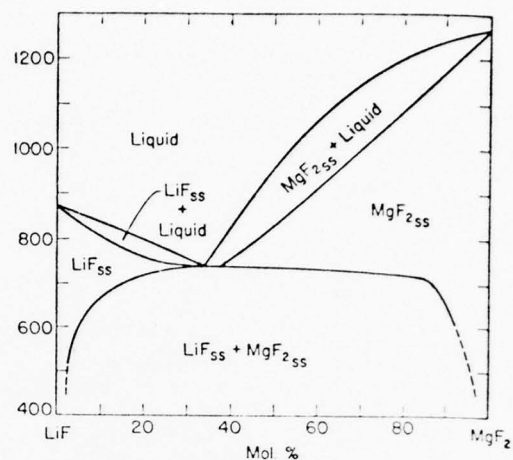


FIG. 1471.—System LiF-MgF₂.

W. E. Counts, Rustum Roy, and E. F. Osborn, *J. Am. Ceram. Soc.*, **36** [1] 15 (1953).

NaF-CaF₂

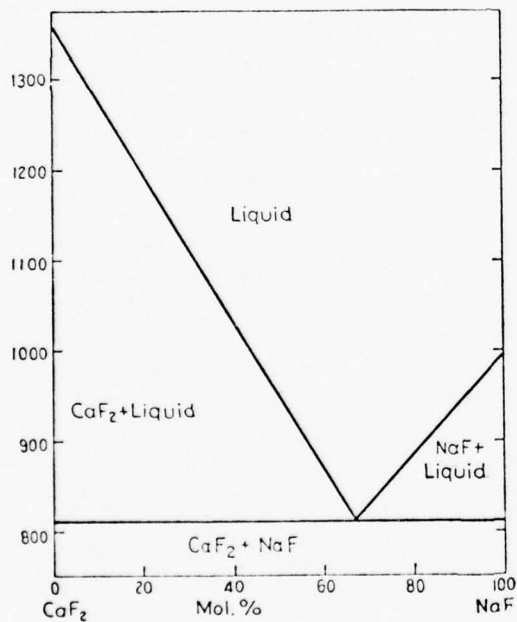


FIG. 1483.—System NaF-CaF₂.

P. P. Fedotieff and W. P. Iljinski, *Z. anorg. u. allgem. Chem.*, **129**, 101 (1923).

LiF-ZnF₂

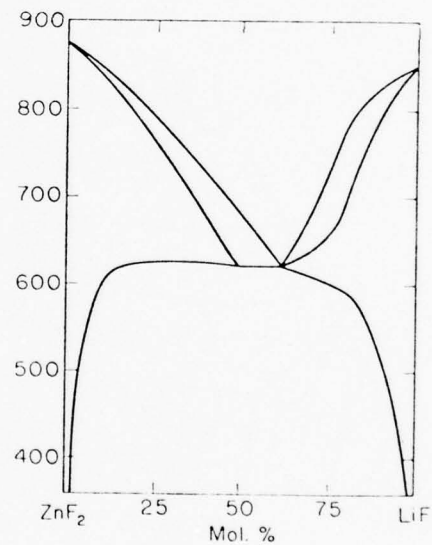


FIG. 1472.—System LiF-ZnF₂.

O. Schmitz-Dumont and Horst Bornfeld, *Z. anorg. u. allgem. Chem.*, **287**, 121 (1956).

Figure 3. Phase Diagrams of Fluoride Eutectic Salts (sheet 1 of 4)

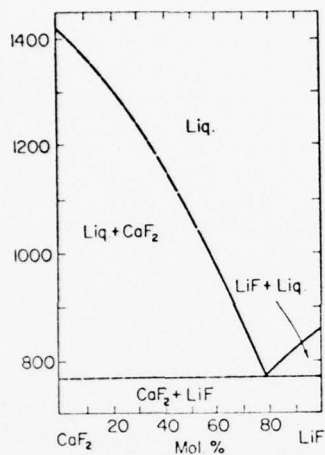
$$\text{KF-LiF-MgF}_2$$


FIG. 1470.—System LiF-CaF₂.

W. E. Roake, *J. Electrochem. Soc.*, 104, 661 (1957).

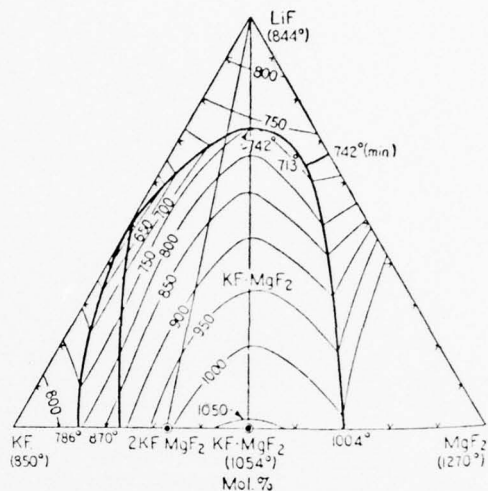


FIG. 1531.—System KF-LiF-MgF_2 .

A. G. Bergman and S. P. Parlenko, *Compt. rend. acad. sci., U.R.S.S.*, **31**, 818-19 (1941).

KF-LiF-NaF

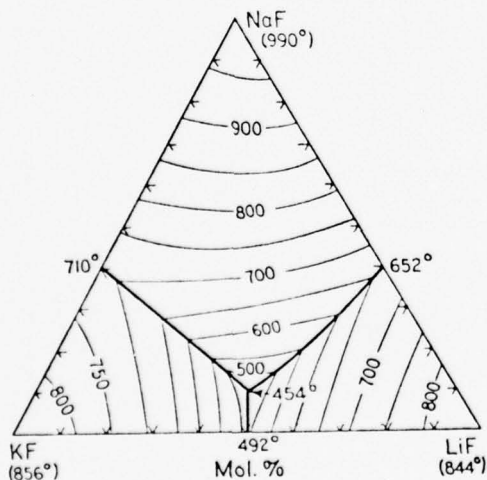


FIG. 1529.—System KF-LiF-NaF.

A. G. Bergman and E. P. Dergunov, *Compt. rend. acad sci., U.R.S.S.*, **31**, 754 (1941).

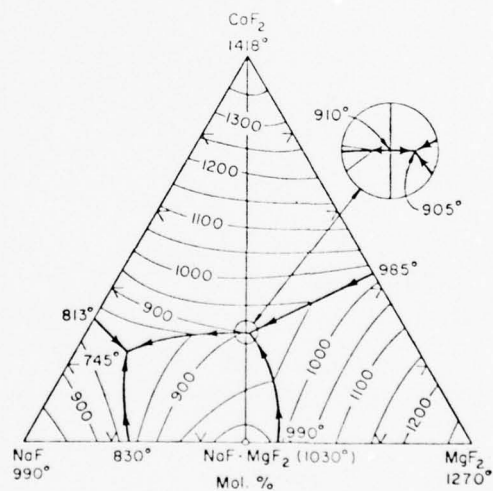
$$\text{NaF}-\text{CaF}_2-\text{MgF}_2$$


FIG. 1565.—System $\text{NaF}-\text{CaF}_2-\text{MgF}_2$; preliminary.

C. J. Barton, L. M. Bratcher, J. P. Blakely, and W. R. Grimes, Oak Ridge National Laboratory, Phase Diagrams of Nuclear Reactor Materials, R. E. Thoma, ed., ORNL-2548, p. 30 (1959).

NaF-MgF₂

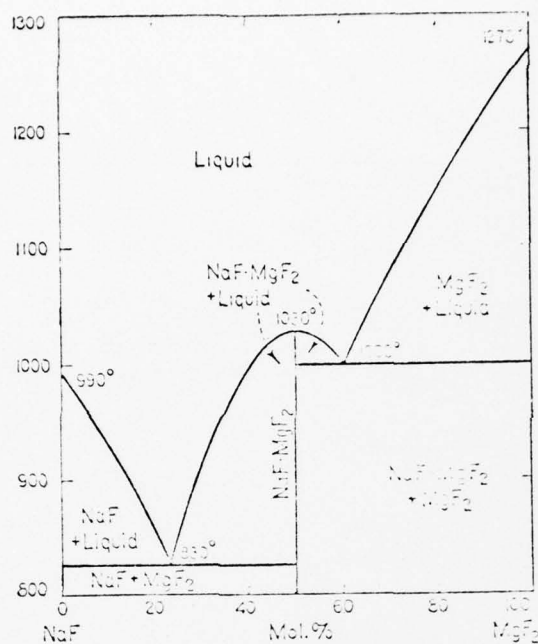


FIG. 1486.—System NaF-MgF₂.

A. G. Bergman and E. P. Dergunov, *Compt. rend. acad. sci., U.R.S.S.*, 31, 755 (1941).

LiF-NaF-MgF₂

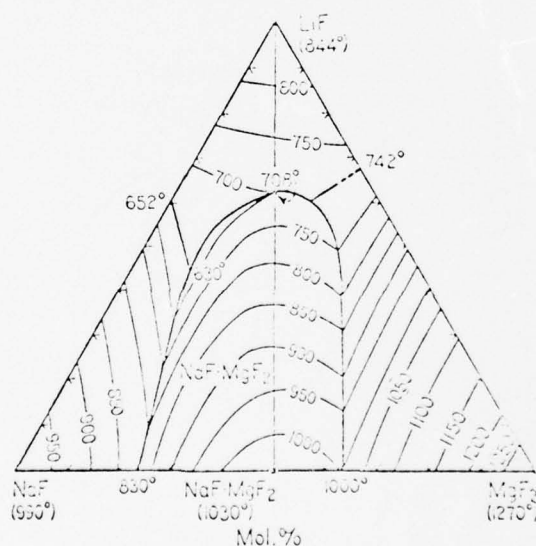


FIG. 1545.—System LiF-NaF-MgF₂.

A. G. Bergman and E. P. Dergunov, *Compt. rend. acad. sci., U.R.S.S.*, 31, 755 (1941).

Figure 3. Phase Diagrams of Fluoride Eutectic Salts (sheet 3 of 4)

KF-MgF₂

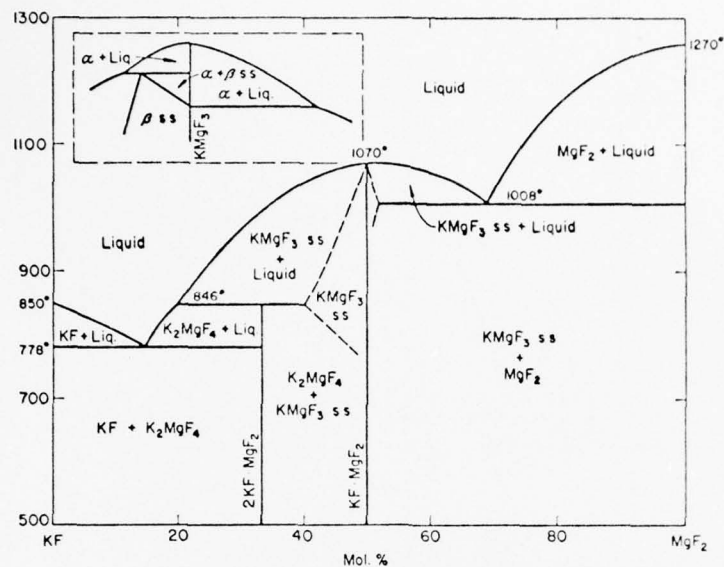


FIG. 1458.—System KF-MgF₂. Insert shows possible alternative for high-temperature region near KF·MgF₃.

R. C. DeVries and Rustum Roy, *J. Am. Chem. Soc.*, **75**, 2481 (1953).

KF-NiF₂

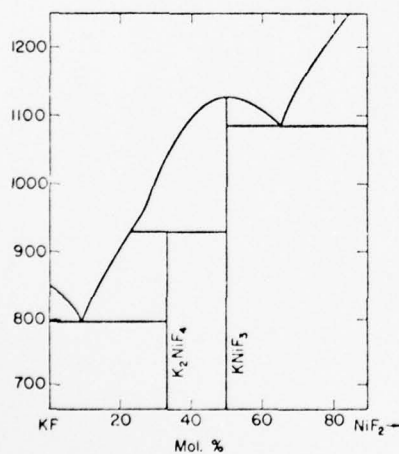


FIG. 1459.—System KF-NiF₂.

G. Wagner and D. Balz, *Z. Elektrochem.*, **56**, 576 (1952).

KF-ZnF₂

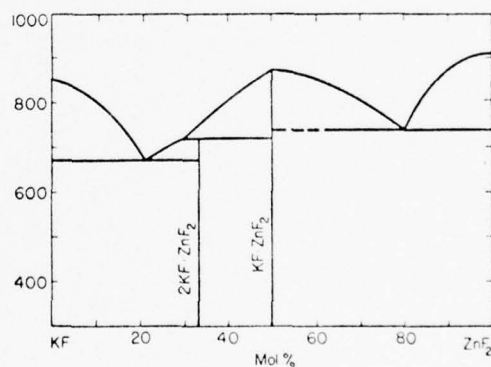


FIG. 1460.—System KF-ZnF₂, tentative.

C. J. Barton, L. M. Bratcher, and W. R. Grimes, Oak Ridge National Laboratory, Phase Diagrams of Nuclear Reactor Materials, R. E. Thoma, ed., ORNL-2548, p. 49 (1959).

See also O. Schmitz-Dumont and Horst Bornfeld, *Z. anorg. u. allgem. Chem.*, **287**, 122 (1956).

56716

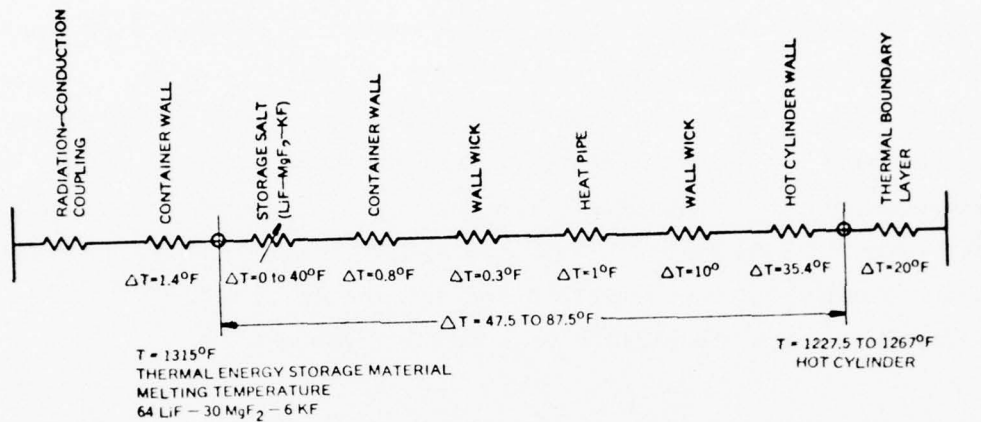


Figure 4. Temperature Distribution in the Thermal Energy Storage Unit for a VM Cooler with 64 LiF-30 MgF₂-6 KF as TES Material

56715

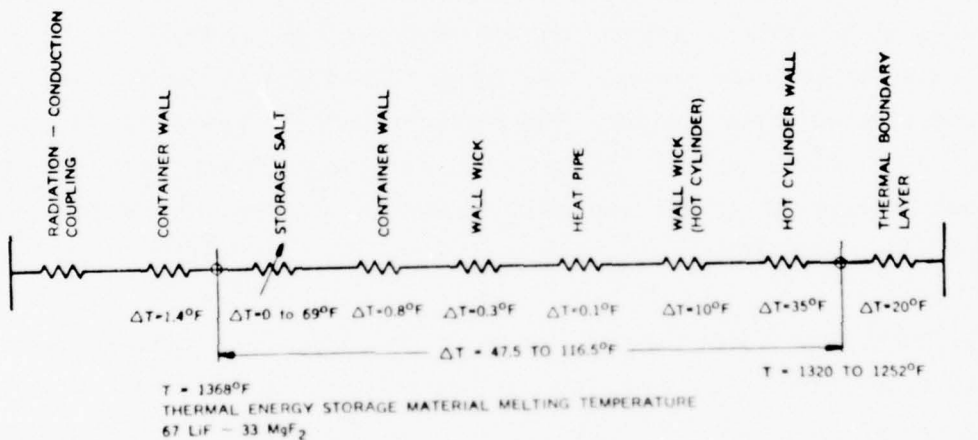


Figure 5. Temperature Distribution in the Thermal Energy Storage Unit for a Vuilleumier Cooler with 67 LiF-33 MgF₂ as TES Material

fusion which were given as 944 joules/gram in Ref. 2 and as 788 joules/gram (0.219 kWh/kg) in a communication by North American Philips Corporation. It appears now that the heat of fusion of the ternary salt of Ref. 2 was not a measured value but had been calculated with the assumption of "ideality," i.e., the heat of fusion of the ternary eutectic is the sum of the heat of fusion of its constituents when melting as a single salt at the eutectic temperature. The latent heat quoted by the second source was an ideal value based on the difference in thermal energy content of the salt at temperatures above and below the eutectic temperature and extrapolated to the eutectic temperature. The underlying assumption must have been that the eutectic salt increases its thermal energy in a step function at the eutectic temperature similar to a single component salt.

The test results of this program have shown that the heat of fusion of the ternary salt is only about 50 percent the heat of fusion calculated under the assumption of ideality. It should have been obvious that ideality was an inappropriate assumption when looking at the phase diagram of the salt shown in Figure 3. The phase diagram indicates clearly the formation of a double salt, KF-MgF_2 , and transition lines. While the instrumentation and general test setup of this program was not sophisticated enough for performing basic research on thermodynamic properties of binary and ternary salts, some general behavior and thermodynamic properties could be demonstrated quite clearly. The results which are presented in Section IV of this report proved the selection of the ternary salt without the availability of proven and well documented thermodynamic data to be a technical liability.

The ternary eutectic $\text{LiF-MgF}_2\text{-KF}$ is not available as a commercial salt. It had to be prepared by combining its constituents in a retort. Based on the molecular fraction of 0.64, 0.30, and 0.06 for LiF, MgF_2 , and KF,

-
2. "Summary and Selection of Inorganic Salts for Application to Thermal Energy Storage," by Alina Borucka, Report ERDA 59, June 1975.

respectively, the weight fractions of the eutectic are 0.4281, 0.4820, and 0.0899. The specific weight of the eutectic was given as 2.1233 gram/cm³.

Preliminary heat transfer calculations indicated that the losses from the thermal energy storage unit would be approximately 200 watts, if the unit is insulated with Flexible Min-K material. This predicted value proved to be correct for the steady state condition at 1300°F, as will be seen from the test data in Subsection 4.2.1. The thermal energy storage unit therefore had to be sized for a total power release of 1.2 kW for 1 hour of operation. This corresponds to a total energy storage requirement of 1.2 kWh or 4.32×10^6 joules. When the lower value of the heat of fusion of 0.219 kWh/kg or 0.465 kWh/liter (based on the liquid density at the melting point) was accepted, the total weight of the thermal energy storage material was calculated to be 5.480 kg and the required volume of the material 2.581 liter (157.481 in.³). Thus, the total material required for the eutectic salt was

LiF	2.346 kg
MgF ₂	2.641 kg
KF	<u>0.493 kg</u>
Total	5.480 kg

2.2.2 OPTIMIZATION OF THERMAL ENERGY STORAGE DEMONSTRATION UNIT

The thermal energy storage unit has as its purpose the storing of thermal energy in the form of fusion energy of a salt. It is expected that by using a thermal energy storage system, the overall weight of the power supply for a Vuilleumier cooler will be lighter and that the power system will have an equal or better reliability than a power supply which stores energy in electrical batteries. For achieving this goal, the overall structure containing the thermal energy storage material had to be made as small as possible so that, by itself, it will be light and will require the least

amount of insulation for containing the thermal energy with the lowest thermal losses. Thermal losses from the thermal energy storage unit are reflected in additional solar panel requirements as well as a larger thermal energy storage unit.

The requirement of testing the thermal energy storage unit in a 1-g environment imposed limitations on the design which would not exist if the unit could have been designed for exclusive space application and would not have to be tested in the laboratory.

The general lay-out of the thermal energy storage unit was presented in Figure 1. It was indicated that electric heaters would supply energy to the thermal energy storage salt and that thermal energy for the operation of the hot cylinder of the Vuilleumier cooler would be transferred from the thermal energy storage material by heat pipe action. Direct transfer from the salt to the hot cylinder could not be considered as the heat transfer area of the hot cylinder is very small relative to the required amount of thermal energy salt. Direct energy transfer would therefore not only result in a very high temperature differential, but would also encompass a large temperature variation during the extraction of the energy from the salt. The aim was to find an optimum configuration with respect to weight and thermal losses for the basic design of the unit.

2.2.2.1 Overall Configuration

Several parameters affect the weight and configuration of the thermal energy storage unit. The most important parameters appeared to be the thickness of the thermal energy storage salt, t_s , the heater diameter, D_H , and the wick thickness, t_w , which are indicated in Figure 6. For maintaining the most uniform temperature of the hot cylinder and the heat pipe, it is desirable to make the thickness, t_s , of the thermal energy storage salt as small as possible and to achieve a large surface area and a small depth across which heat flux occurs. The effect of the salt thickness on the

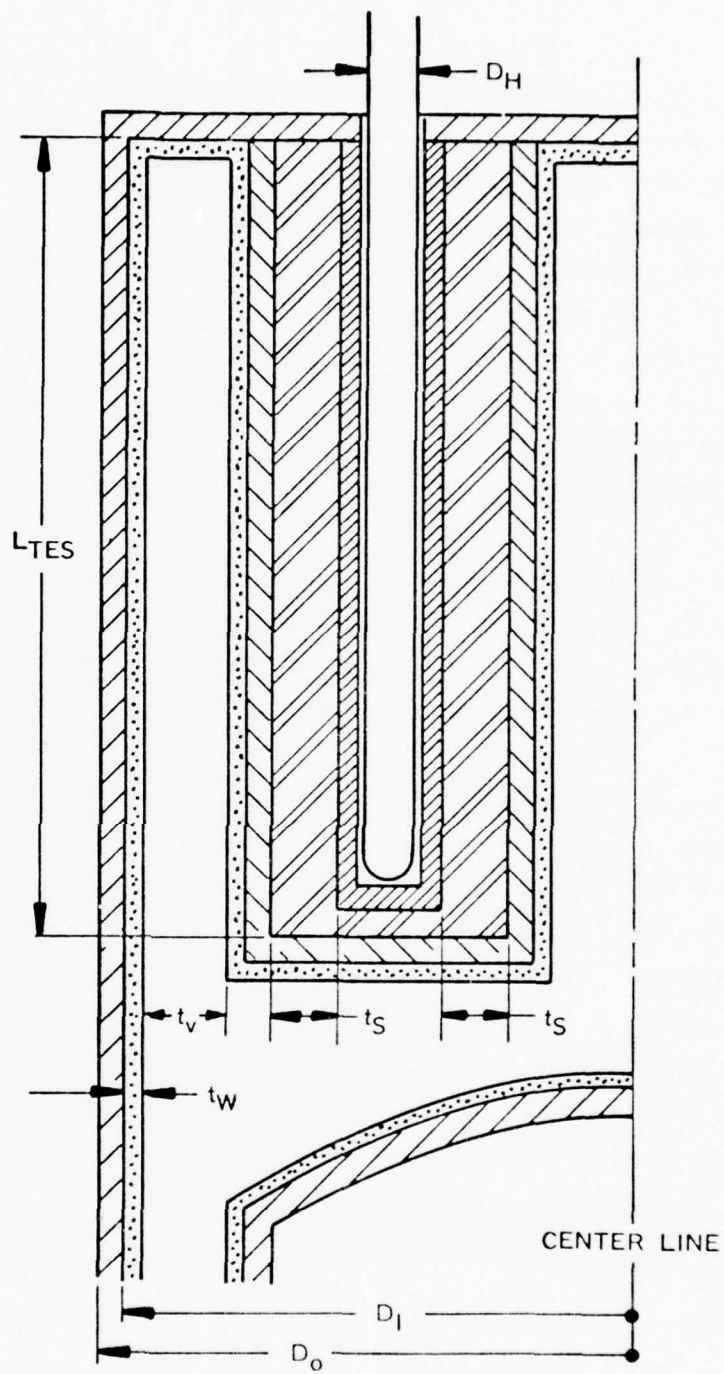


Figure 6. Parameters Investigated in the Optimization of the Thermal Energy Storage Unit.

length, L_{TES} , of the thermal energy storage unit is shown in Figure 7 for two designs which differ solely with respect to the size of the heater diameter, D_H , and the vapor flow area, A_V . A correlation of all the dimensional parameters of the unit are shown in Figure 8. The thermal losses for the various configurations are presented in Figures 9 through 16. It is quite obvious that, for the lowest losses, the thermal energy storage salt should have a thickness of about 0.8 inch. Figures 10, 12, 14, and 16 also indicate that, after a certain insulation thickness has been reached, additional insulation will only add weight to the unit without substantially further reducing thermal losses.

The results of the thermal loss calculations are summarized in Figures 17 and 18. They confirm that the vapor flow width has a minimal effect on the thermal losses and that, therefore, a minimal effort is required for optimizing on this parameter in the sizing of the unit.

Based on the parametric design study of the thermal energy storage unit, the heat loss from the unit appeared to be between 185 watts for an outer insulation diameter of 10 inches and 124 watts for an outer insulation diameter of 15 inches. These losses compare with the losses of a directly electrically heated hot cylinder of a Vuilleumier cooler of about 50 watts as shown in Figure 19 for the same type insulation. The design that evolved from the optimization study is shown in Figure 20. The length of the unit is about three times the diameter. In this design, the thermal load at the heater surface is only 1 watt/cm².

2.2.2.2 Insulation Design

Prior to optimizing the insulation of the TES demonstration unit by employing a superinsulation consisting of radiation shields between layers of conduction insulation, it was decided to use less expensive insulation made of two conduction insulation materials, Flexible Min-K and Cerafelt. The insulation layers exposed to the highest temperature were to be Flexible Min-K. For insulating the unit below 600°F, Cerafelt was chosen.

546598

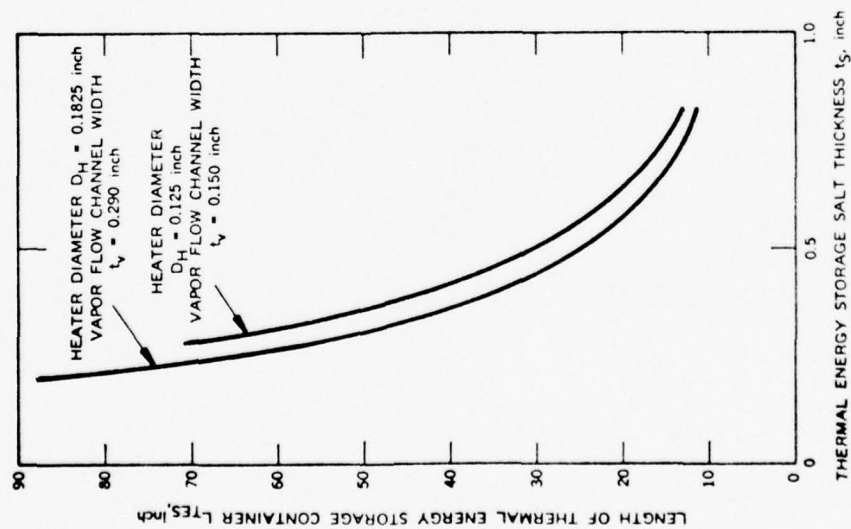


Figure 7. Effect of Thermal Energy Storage Salt Thickness on the Length of the Thermal Energy Storage Unit

546599

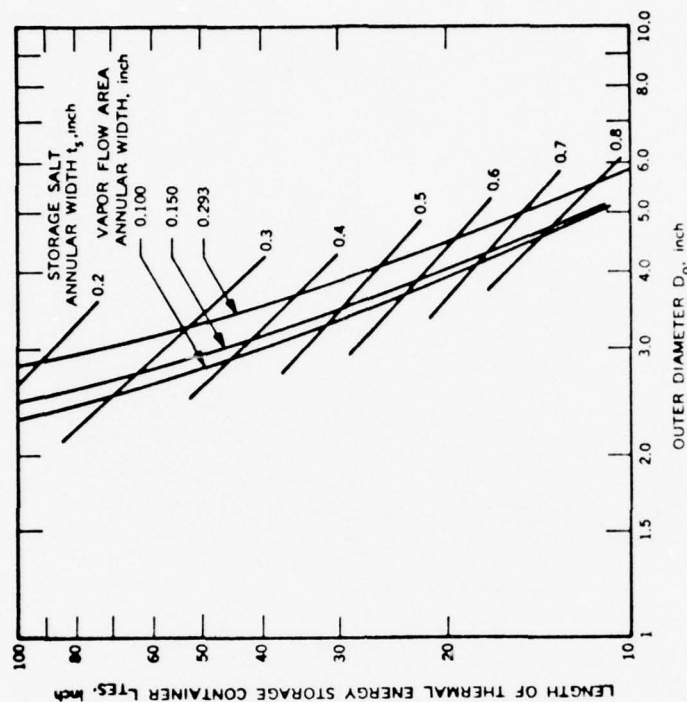


Figure 8. Correlation Between Primary Dimensions of 1-kW-Hr Thermal Energy Storage Unit (Required Thermal Energy Storage Material Volume $V_{TES} = 157.481 \text{ Inch}^3$)

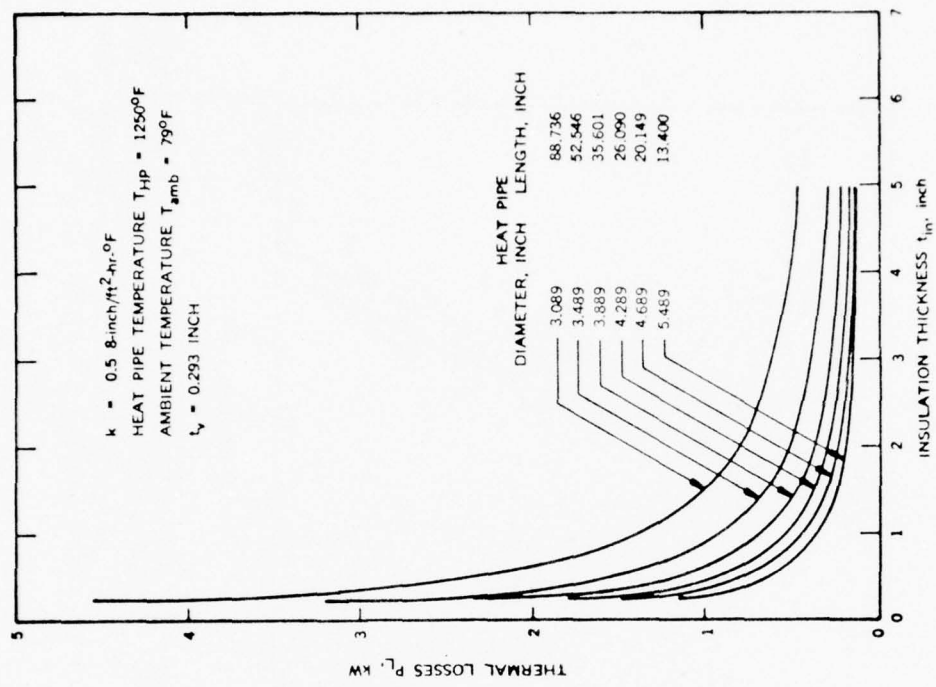


Figure 9. Thermal Losses from Thermal Energy Storage Heat Pipe (0.1825-inch Dia. Heater)

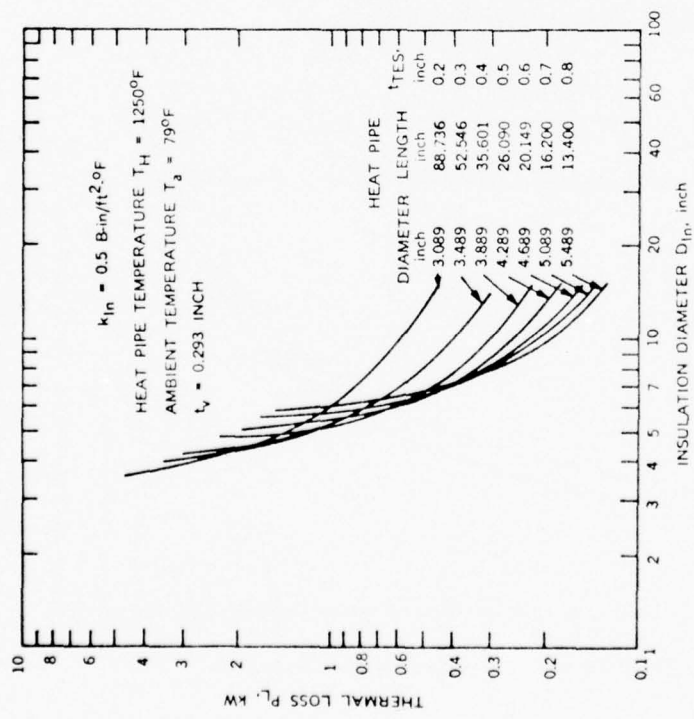


Figure 10. Power Losses from Thermal Energy Storage Heat Pipe (0.1825-inch Dia. Heater)

56704 A

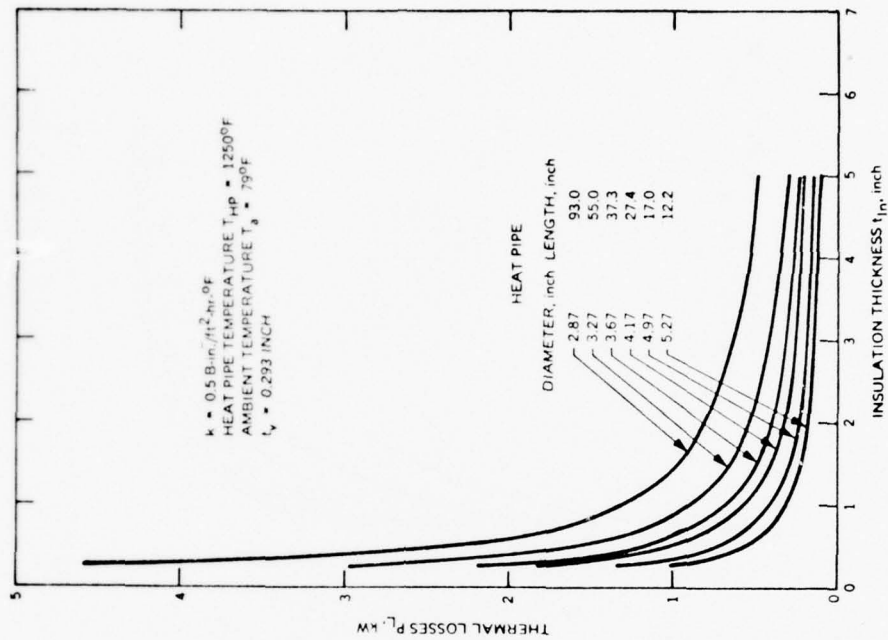


Figure 12. Power Losses from Thermal Energy Storage Heat Pipe (0.125-inch Dia. Heater)

56702

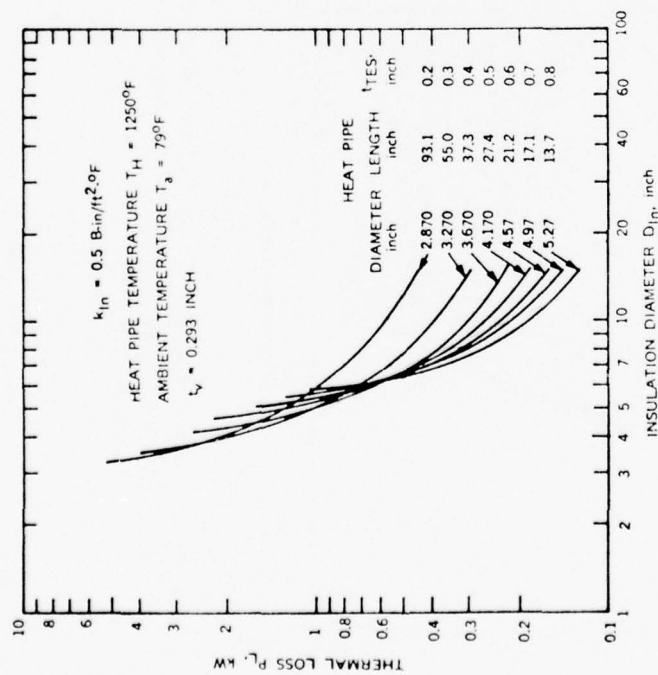


Figure 11. Thermal Losses from Thermal Energy Storage Heat Pipe (0.125-inch Dia. Heater)

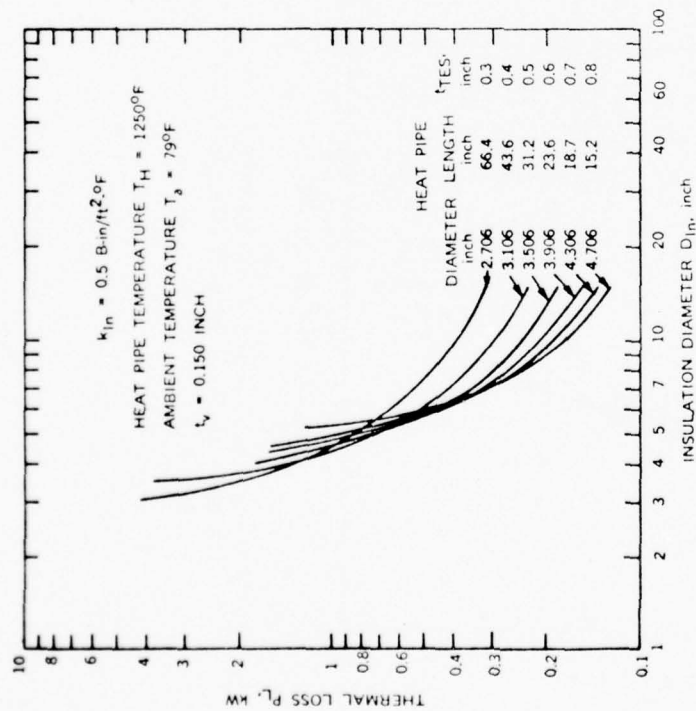


Figure 13. Thermal Losses from Thermal Energy Storage Heat Pipe (0.125-inch Dia. Heater)

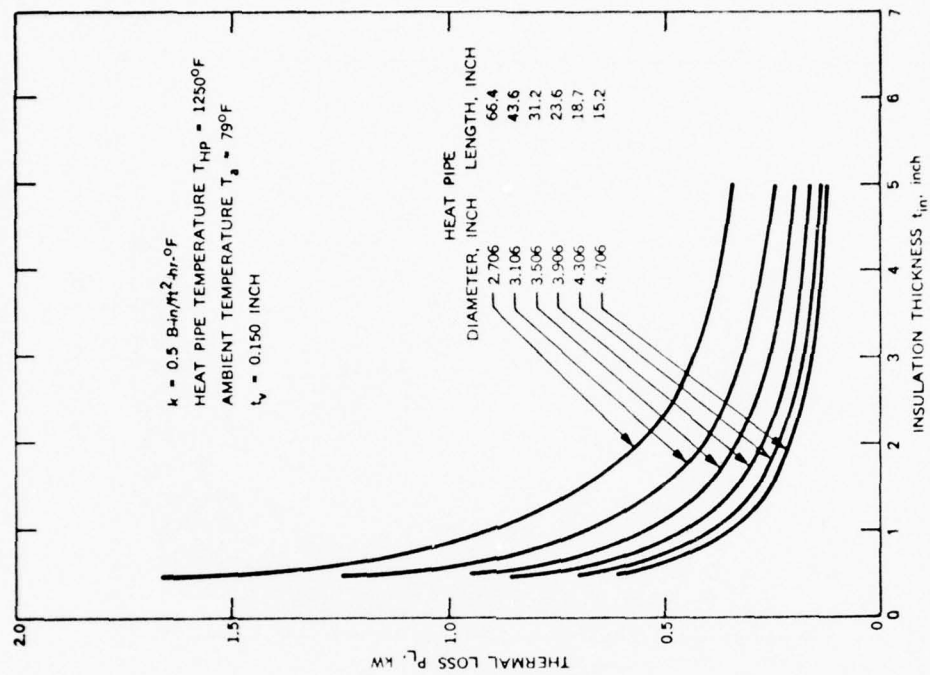


Figure 14. Power Loss from Thermal Energy Storage Heat Pipe (0.125-inch Dia. Heater)

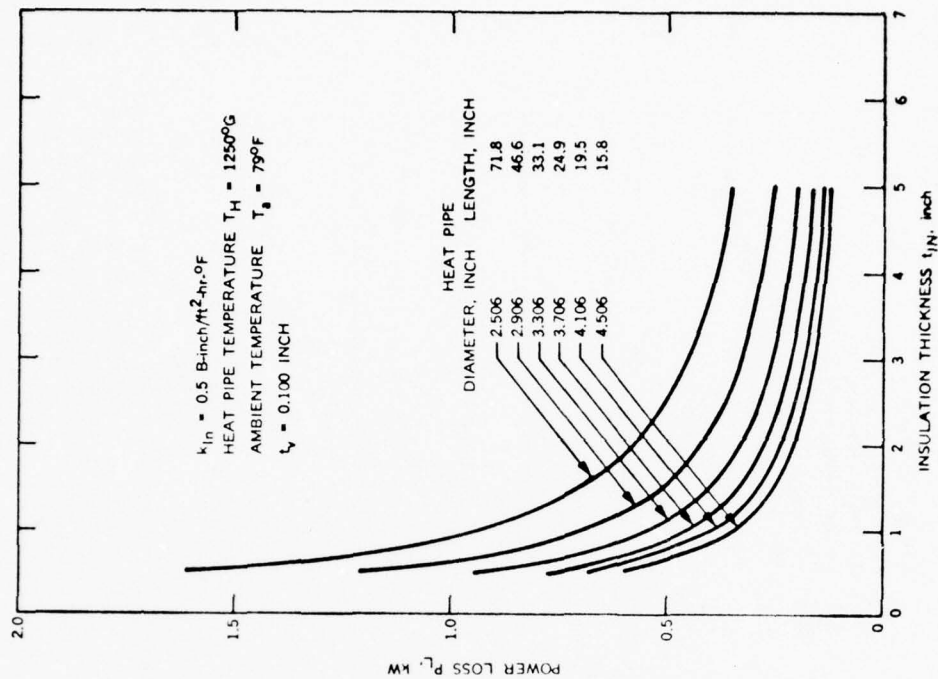


Figure 15. Thermal Losses from Thermal Energy Storage Heat Pipe (0.125-inch Dia. Heater)

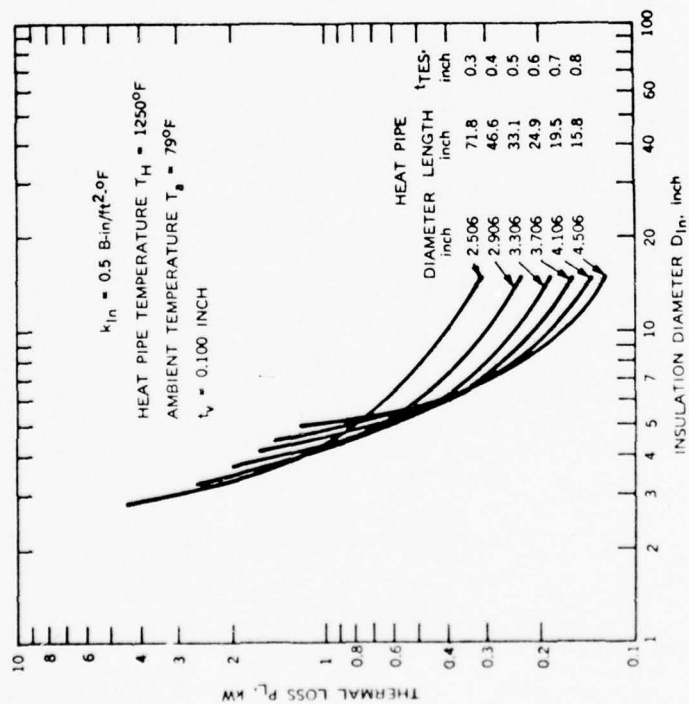


Figure 16. Power Loss from Thermal Energy Storage Heat Pipe (0.125-inch Dia. Heater)

56708

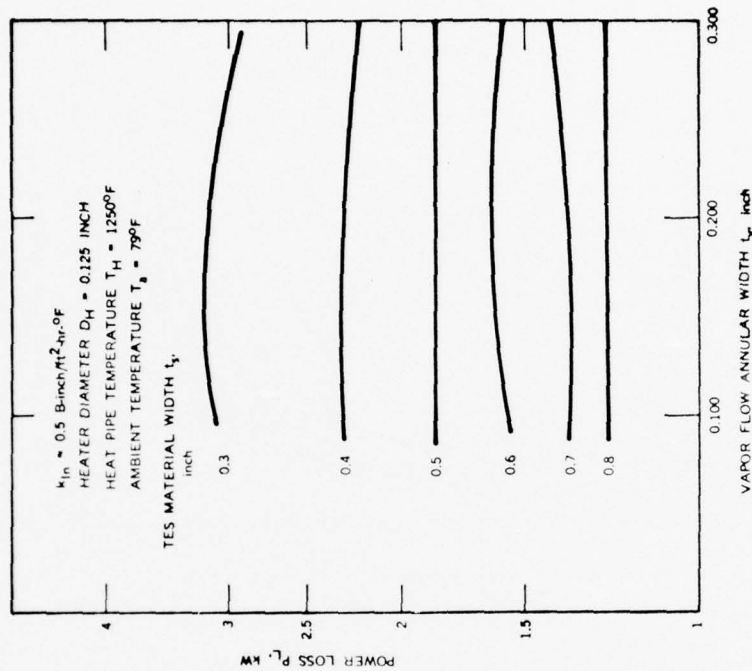


Figure 18. Effect of Vapor Flow Annular Width and Thermal Energy Storage Material Thickness on Thermal Loss of the Thermal Energy Storage Unit (Insulation Diameter $D_{in} = 15 \text{ Inch}$)

56709

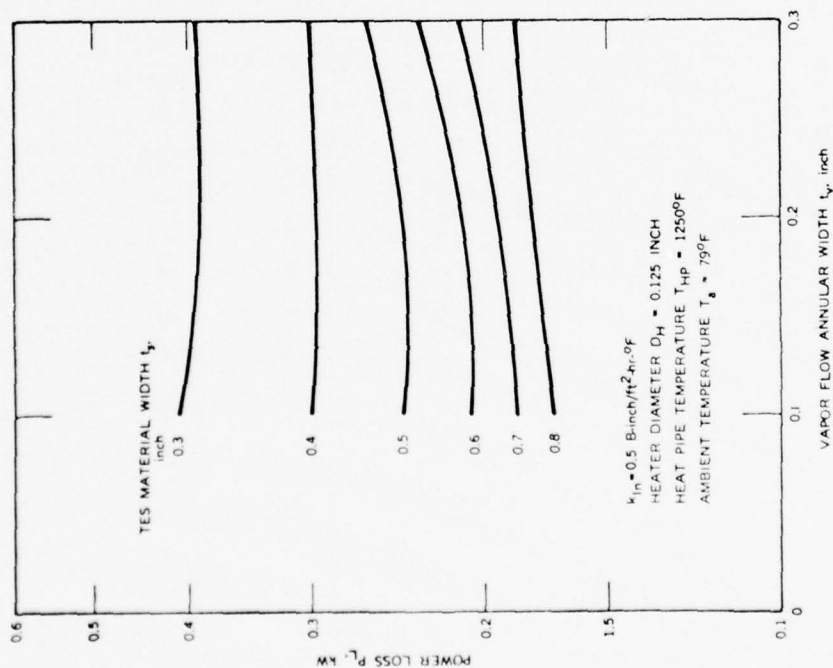


Figure 17. Effect of Vapor Flow Annular Width and Thermal Energy Storage Material Thickness on Thermal Loss of the Thermal Energy Storage Unit (Insulation Diameter $D_{in} = 10 \text{ Inch}$)

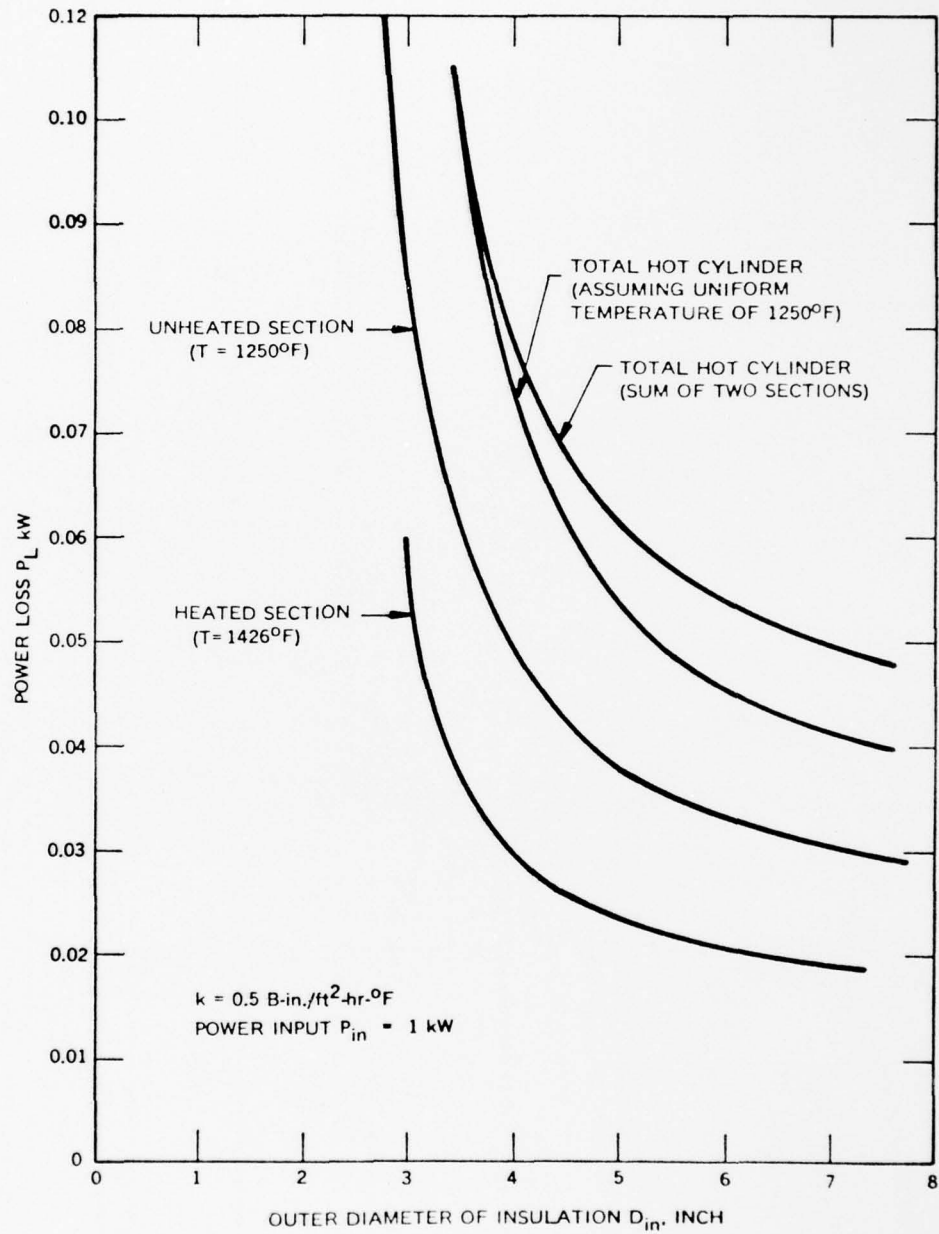


Figure 19. Power Losses from Hot Cylinder of VM Cooler

56721

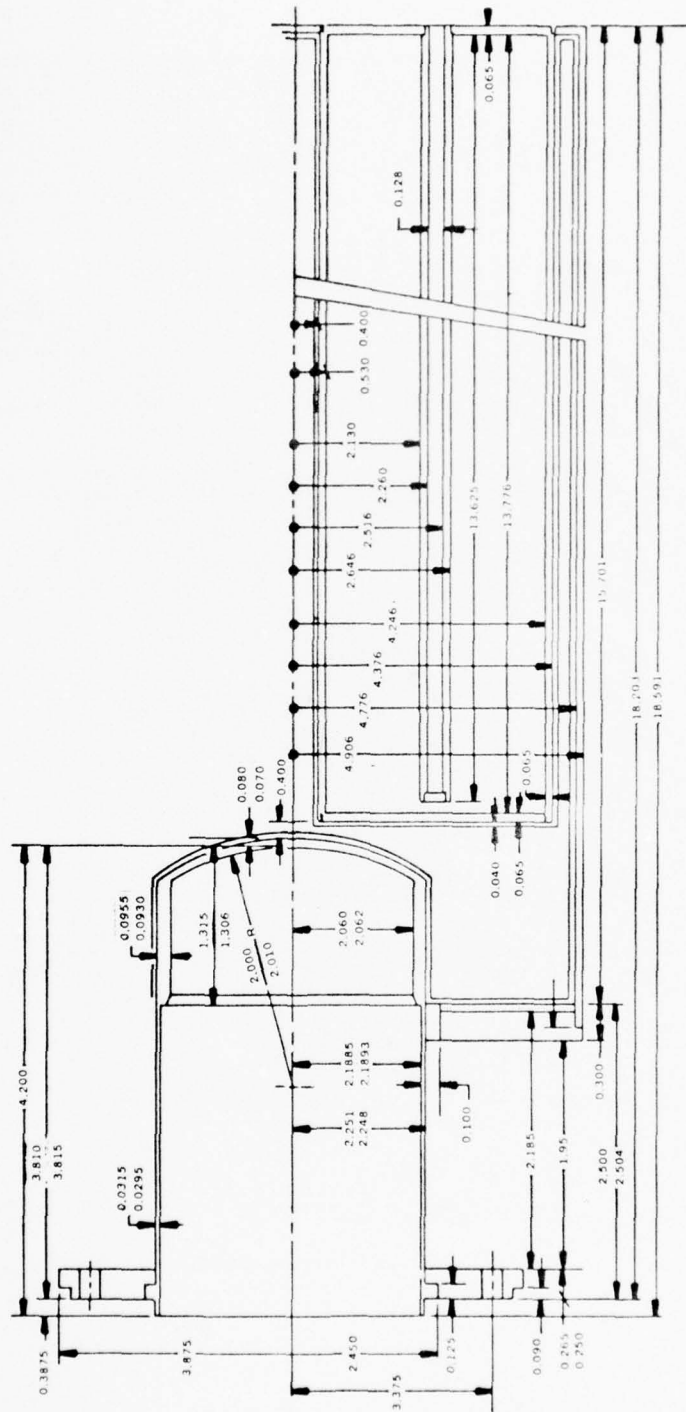


Figure 20. Optimum Design for a 1-kW-Hr Thermal Energy Storage Unit

For the final design of the thermal energy storage unit, the thermal losses as a function of insulation thickness and outer insulation diameter are shown in Figure 21. The temperature distribution through the insulation for three insulation thicknesses are presented in Figure 22. Based on these parametric studies, the amount of insulation material for each type and the total insulation weight were calculated as shown in Figure 23.

2.2.2.3 Heat Pipe Design

With the basic dimensions of the thermal energy storage unit established, the heat pipe parameters had to be determined. The analysis and heat pipe computer program that had been developed for the design of the 15-ft long heat pipe could not be used because of the substantial differences between the thermal energy storage unit and the heat pipe with respect to design and operation. The 15-ft long heat pipe had a distinct evaporator and condenser section which were separated by a relatively long adiabatic section. In the thermal energy storage unit, the adiabatic section is missing. Since the evaporator section constitutes the heat pipe, the flow rate of the vapor as well as of the fluid in the wick vary along the heat pipe. Furthermore, the vapor flow area of the TES unit is the combination of an annulus and a pipe, thus having a completely different hydraulic diameter than the 15-ft heat pipe. The vapor flow in the thermal energy storage unit has to account for "blowing," while the flow in the wick has to consider suction flow.

In Figures 24, 25, and 26, the pressure drops for three different vapor flow area designs are presented. In order for the heat pipe to operate satisfactorily, the total pressure drop cannot be larger than the capillary pressure or suction pressure available from the wick structure. In all three designs the elevation pressure drop is the highest while the pressure drop in the wick is the lowest. The elevation pressure drop is the dominating pressure drop and is entirely determined by the diameter of the thermal energy storage unit. As was indicated earlier, the diameter of the

56973

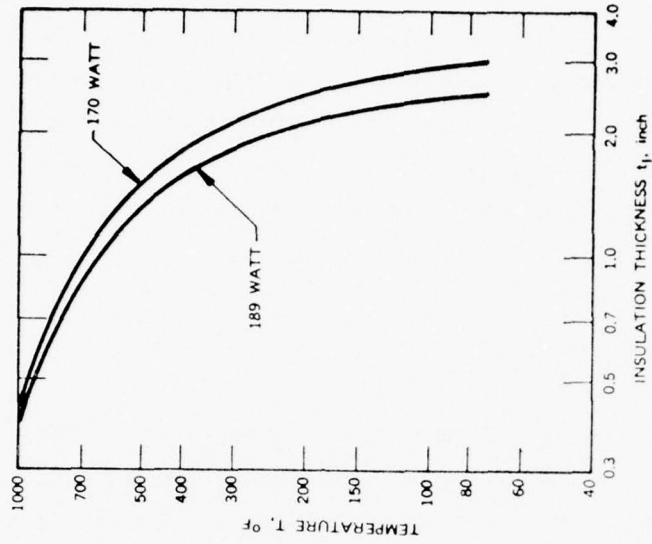


Figure 22. Temperature Distribution in Thermal Insulation of Thermal Energy Storage Demonstration Unit

56972

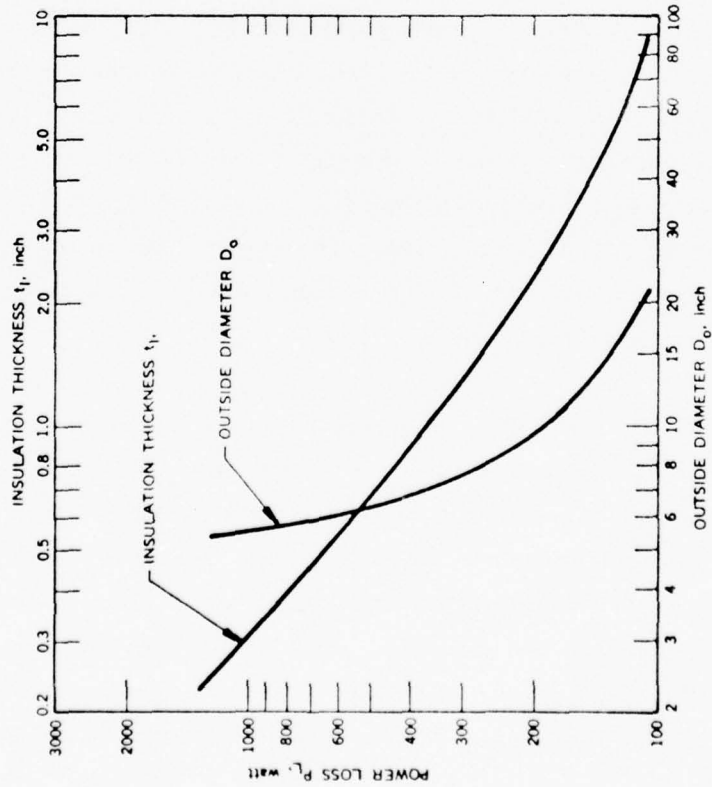


Figure 21. Power Loss as Function of Insulation Thickness of Final Thermal Energy Storage Demonstration Unit Design

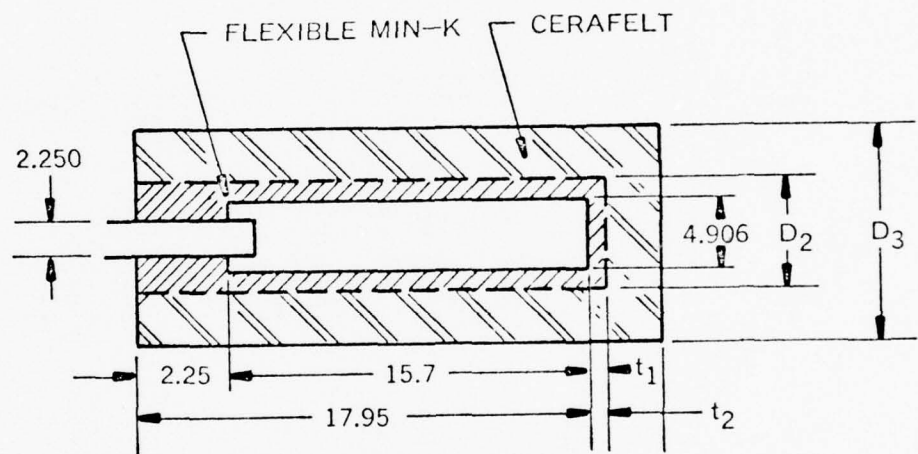


Figure 23. Insulation Design of Thermal Energy Storage Unit

56893

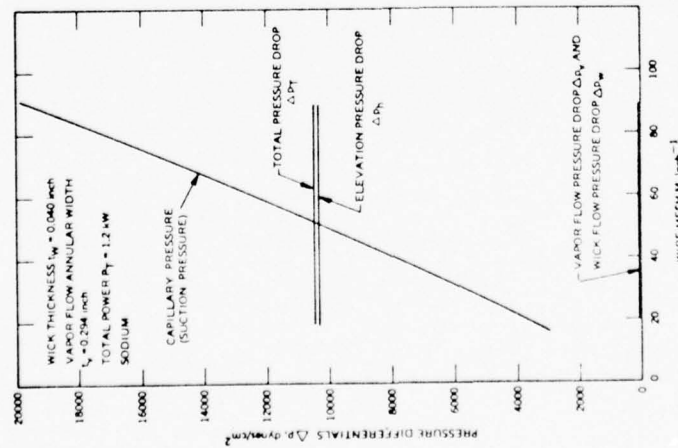


Figure 24. Pressure Drops and Available Suction Pressure for Various Wire Screens

56717

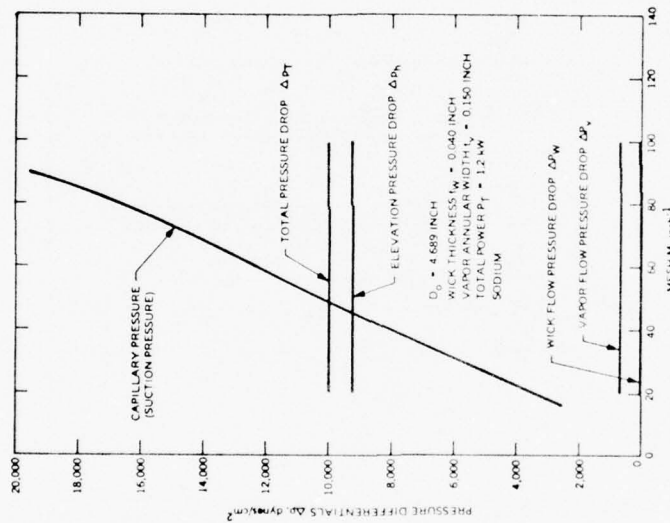


Figure 25. Pressure Drops and Available Suction Pressure for Various Wire Screens

56892

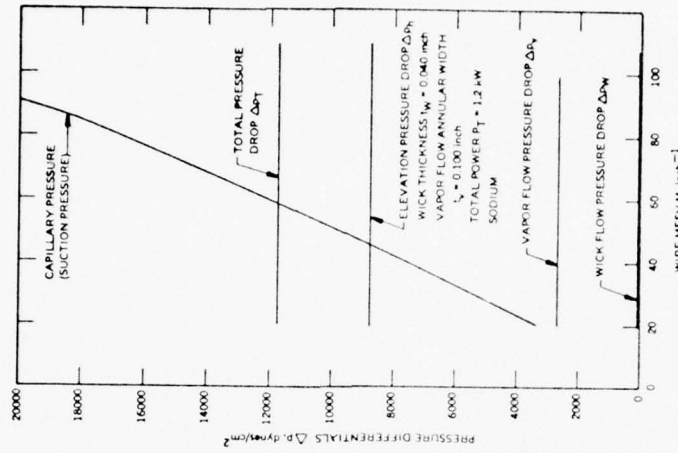


Figure 26. Pressure Drops and Available Suction Pressure for Various Wire Screens

unit was predicated on the lowest thermal losses from the unit. The optimum wick design was based on the calculations shown in Figure 27.

A bolting cloth with Mesh 70 was selected for the wick structure. This design would generate a suction pressure about 37 percent above that required. As indicated by the calculations, a finer mesh bolting cloth would apparently provide a larger safety margin. There is, however, an uncertainty whether the higher safety margin can actually be achieved because of limitations in maintaining a consistent wick structure with effective small pore sizes between the layers during the manufacturing process.

2.2.2.4 Total Weight of Optimum Thermal Energy Storage Unit

The total weight of the thermal energy storage unit is comprised of the weight of: (1) the container material, Inconel 600; (2) the wick filled with the sodium working fluid; (3) the insulation; and (4) the thermal energy storage material.

Container (Inconel 600)

Total Volume	47.48 inch ³
Specific Weight	0.302 lb/inch ³
Weight	14.34 lb

Wick with Sodium

Total Volume	18.70 inch ³
Wick Material	$M = 70 \text{ inch}^{-1}$, $D_W = 0.00375 \text{ inch}$
Specific Weight of Wick Material	0.302 lb/inch ³
Effective Volume Density	20.33 percent
Specific Weight of Sodium	0.0279 lb/inch ³

TES PROGRAM T3 K-1.62X10-3XM-.797 CM2

PROGRAM 2340-002-000
PARAMETRIC STUDY OF TES HEAT PIPE 22 JULY 1975

WORKING FLUID SODIUM,	22.991 GRAM/MOL		
OPERATING TEMPERATURE	1250.000 DEG.F		
POWER	1200.00 WATT		
HEAT PIPE DIAMETERS	4.776 INCH	4.376 INCH	.400 INCH
WICK LENGTH	14.620 INCH		

	PROPERTIES	FLUID	VAPOR
LATENT HEAT, JOULES/G		.401E 04	
SURFACE TENSION, DYN/CM		.134E 03	
VISCOSITY, G/SEC-CM		.195E-02	.106E-03
SPECIFIC GRAVITY, G/SEC3		.789E 00	.328E-04
PARTIAL PRESSURE, DYN/CM2			.112E 06
SONIC VELOCITY, CM/SEC			75656.06

WALL WICK THICKNESS .040 INCH

WICK AREA 3.871 CM2, VAPOR AREA 11.646 CM2, AREA RATIO 3.008
ELEVATION PRESSURE 9386.91 DYN/CM2, VELOCITY 784.044 CM/SEC

MESH WIRE IN-1, INCH	PERMEABILITY CM2	SUCTION DELP W DYN/CM2	DELP V DYN/CM2	DELP T DYN/CM2	SAFETY PERC.		
20	.0090	.148E-03	3630.	24.	836.	10247.	-64.57
30	.0065	.107E-03	5547.	33.	836.	10256.	-45.91
40	.0065	.854E-04	8046.	42.	836.	10264.	-21.61
50	.0055	.715E-04	10265.	50.	836.	10272.	-.07
60	.0045	.618E-04	12234.	57.	836.	10280.	19.01
70	.0037	.547E-04	14061.	65.	836.	10288.	36.68
80	.0037	.492E-04	16914.	72.	836.	10295.	64.30
90	.0035	.448E-04	19556.	79.	836.	10302.	89.83

Figure 27. Heat Pipe Design Calculations for Final Design of a 1-kW-Hr Thermal Energy Storage Unit

Effective Specific Weight of Wick	0.0836 lb/inch ³
Weight	1.564 lb

Thermal Energy Storage Material

Material (Molecular)	65 LiF - 30 MgF ₂ - 6 KF
Material (Weight)	42.81 LiF - 48.21 MgF ₂ - 8.99 KF
Heat of Fusion	99.43 watt-hr/lb
Specific Weight	0.0766 lb/inch ³
Energy Requirement	1200 watt-hr
Volume	157.48 inch ³
Weight	12.07 lb

Insulation

Material	Flexible Min-K and Cerafelt
Weight	7.96 lb (189 watt loss)
	8.81 lb (179 watt loss)
	10.59 lb (170 watt loss)

Based on the above tabulated weight values of the four major components of the thermal energy storage unit, the total weight of the unit and the specific power weights are as shown in Table 2.

TABLE 2. TOTAL WEIGHT OF THERMAL ENERGY STORAGE UNIT

Total Weight W_T (lb)	Power Loss P_L (watt)	Specific Weight W_T/E (lb/watt-hr)	Specific Energy E/W_T (watt-hr/lb)
35.93	189	29.94	33.40
36.78	179	30.65	32.63
38.56	170	32.13	31.11

The weight distribution for the entire thermal energy storage unit is shown in Table 3.

TABLE 3. WEIGHT DISTRIBUTION OF THE THERMAL ENERGY STORAGE UNIT

	<u>Weight (lb)</u>	<u>Percent of Total</u>
Thermal storage Material	12.07	32.82
Container Material	14.34	38.99
Wick		
Screen 1.148 lb		
Sodium 0.416 lb		
	1.56	4.24
Insulation	<u>8.81</u>	<u>23.95</u>
Total	36.78	100.00

The values in Table 3 indicate that the greatest impact on the weight of the thermal energy storage unit could be achieved by a reduction in the container weight. The container weight is primarily determined by the thickness of the walls, which in the optimized design was $t = 0.065$ inch. If by further investigation it could be established that thinner walls would be safe for containing the thermal energy storage material and the working fluid of the heat pipe, considerable savings in overall TES unit weight could be achieved.

The wick of the heat pipe contributes a surprisingly low value to the overall weight. Only 4.24 percent of the total weight is attributed to the wick, and the wick structure itself adds only 3.12 percent to the weight. The insulation material contributes a substantial amount to the overall weight, despite the fact that it has already been optimized by using two different materials according to the temperature distribution in the insulation. The effect of superinsulation on heat losses and weight is discussed in the next section.

2.2.2.5 Alternate Insulation

For practical reasons it was decided to employ Flexible Min-K insulation with a layer of Cerafelt for testing the thermal energy storage demonstration unit. The weight evaluation indicated that the insulation contributed about 24 percent to the total weight of the thermal energy storage unit. It was concluded that the weight of the unit and the thermal losses could be lowered by employing the insulating technique used for achieving the lowest heat losses from a resistojet.

The properties of high temperature thermal insulation materials as they have been reported in the literature are presented in Table 4. During the development of ion engines at XEOS, in-house work on the improvement of the insulation of ionizers was carried out. This brought about the results plotted in Figure 28. The performance of an insulation system, which was called Linde Super Insulation and was reported in the literature, has a characteristic shown in Figure 29. This insulation system is compared with a system which was applied to the ion engine and to a resistojet in a slightly different and easier applicable form. The construction of this insulation employs a nominal 0.020 inch thick Fiberfrax paper separated by 0.001 inch thick molybdenum foil. For this construction the Fiberfrax paper had an effective thickness of only 0.016 inch. Fiberfrax is an alumina-silica fiber composition which is processed to the Fiberfrax paper with a binder.

Using the thermal conductivity value determined from the apparent thermal losses of the resistojet, the thermal losses from the thermal energy storage unit were calculated as shown in Table 5 and plotted in Figure 30. For comparison, the thermal losses have also been calculated for an insulation with a thermal conductivity of only 9.7×10^{-3} B-inch/ft²-hr-°F. This insulation was mentioned in a paper as being available. The weight of the insulation as a function of the total thermal losses from the thermal energy storage unit are presented in Figure 31 with the weight of the

TABLE 4. PROPERTIES OF HIGH-TEMPERATURE THERMAL INSULATION MATERIALS

<u>Insulating Material</u>	<u>Maximum Service Temperature (°F)</u>	<u>Density (lb/ft³)</u>	<u>Thermal Conductivity at 1250°F (Btu/hr-ft °F)</u>
Thermoflex Refractory	2300	3.0	1.4×10^{-1}
Fiber Felt		24.0	6.4×10^{-2}
Micro-Quartz Felt	2000	3.0	9.5×10^{-2}
		6.0	6.9×10^{-2}
Dyna-Quartz Felt	2750	4.5	7.3×10^{-2}
		10.0	6.3×10^{-2}
Min-K 2000 (molded)	1800	20.0	2.9×10^{-2}
Copper flakes dispersed in fibrous quartz	1400	-	5×10^{-3}
Nickel flakes dispersed in fibrous quartz	1700	-	5×10^{-3}
Copper foil spaced by fibrous quartz paper	1400	-	5×10^{-4}
Nickel foil spaced by fibrous quartz paper	1700	-	5×10^{-4}
Stainless steel spaced by ZrO ₂	2000	-	3×10^{-4}
Titanium spaced by ZrO ₂ particles	2000	-	3×10^{-4}

56884

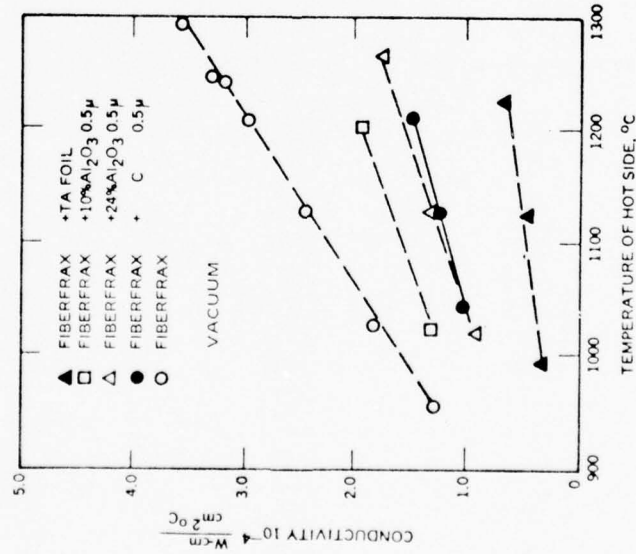


Figure 28. Conductivity of Various Combinations of Fiberfrax

56885

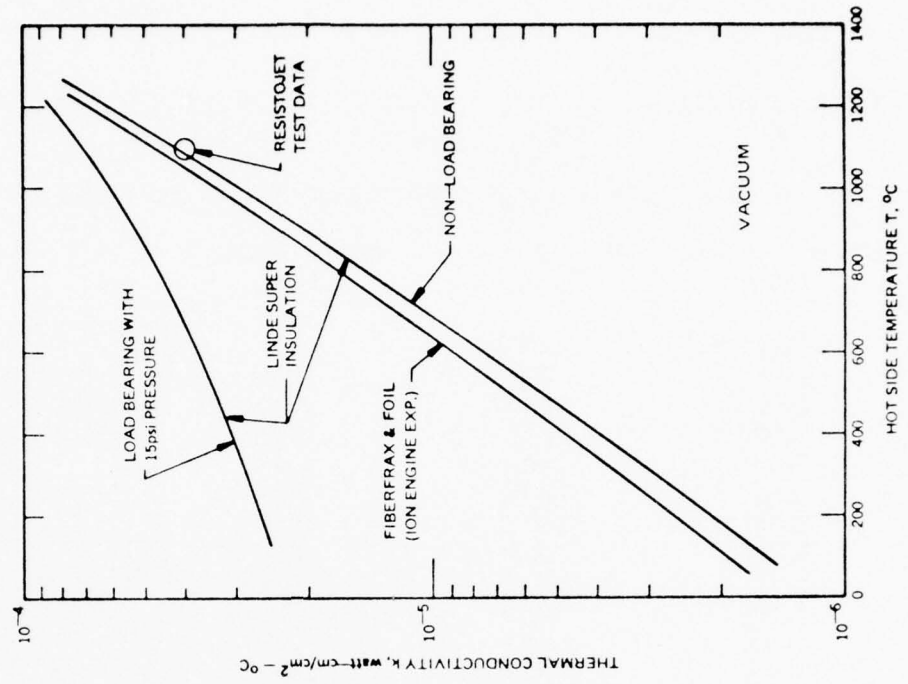


Figure 29. Thermal Conductivity of Super Insulation

TABLE 5. THERMAL LOSSES AS FUNCTION OF THERMAL CONDUCTIVITY OF INSULATION MATERIAL AND INSULATION THICKNESS

INNER DIAMETER D LENGTH L TEMPERATURE DIFFERENCE DELT
 INCH INCH DEGREE F
 4.906 15.701 1171.00
 HEAT TRANSFER COEFFICIENT, B-INCH/FT²-HR-DEG.F 9.71E-03

OUTER DIAMETER INCH	THICKNESS TI INCH	POWER LOSS KW
5.406	.250	.024
5.906	.500	.013
6.406	.750	.009
6.906	1.000	.007
7.406	1.250	.006
7.906	1.500	.005
8.406	1.750	.005
8.906	2.000	.004
9.406	2.250	.004
9.906	2.500	.004
10.406	2.750	.003
10.906	3.000	.003
11.406	3.250	.003
11.906	3.500	.003
12.406	3.750	.003

INNER DIAMETER D LENGTH L TEMPERATURE DIFFERENCE DELT
 INCH INCH DEGREE F
 4.906 15.701 1171.00
 HEAT TRANSFER COEFFICIENT, B-INCH/FT²-HR-DEG.F 2.78E-02

OUTER DIAMETER INCH	THICKNESS TI INCH	POWER LOSS KW
5.406	.250	.069
5.906	.500	.036
6.406	.750	.026
6.906	1.000	.020
7.406	1.250	.017
7.906	1.500	.015
8.406	1.750	.013
8.906	2.000	.012
9.406	2.250	.011
9.906	2.500	.011
10.406	2.750	.010
10.906	3.000	.009
11.406	3.250	.009
11.906	3.500	.009
12.406	3.750	.008

TABLE 5. THERMAL LOSSES AS FUNCTION OF THERMAL CONDUCTIVITY OF INSULATION MATERIAL AND INSULATION THICKNESS (Cont'd)

INNER DIAMETER D INCH	LENGTH L INCH	TEMPERATURE DIFFERENCE DELT DEGREE F
4.906	15.701	1171.00
HEAT TRANSFER COEFFICIENT, B-INCH/FT ² -HR-DEG.F 5.00E-01		
OUTER DIAMETER INCH	THICKNESS TI INCH	POWER LOSS KW
5.406	.250	1.229
5.906	.500	.653
6.406	.750	.460
6.906	1.000	.364
7.406	1.250	.306
7.906	1.500	.267
8.406	1.750	.239
8.906	2.000	.219
9.406	2.250	.202
9.906	2.500	.189
10.406	2.750	.179
10.906	3.000	.170
11.406	3.250	.162
11.906	3.500	.156
12.406	3.750	.150

STOP 0

!EDIT DCUN

EDIT HERE

*TY 1-9

1.000 4.906, 15.701, 1171.,
 2.000 .25, 15,
 3.000 0.00971,
 4.000 4.906, 15.701, 1171.,
 5.000 .25, 15,
 6.000 .0278,
 7.000 4.906, 15.701, 1171.,
 8.000 .25, 15,
 9.000 .5,

*

BEST AVAILABLE COPY

56711

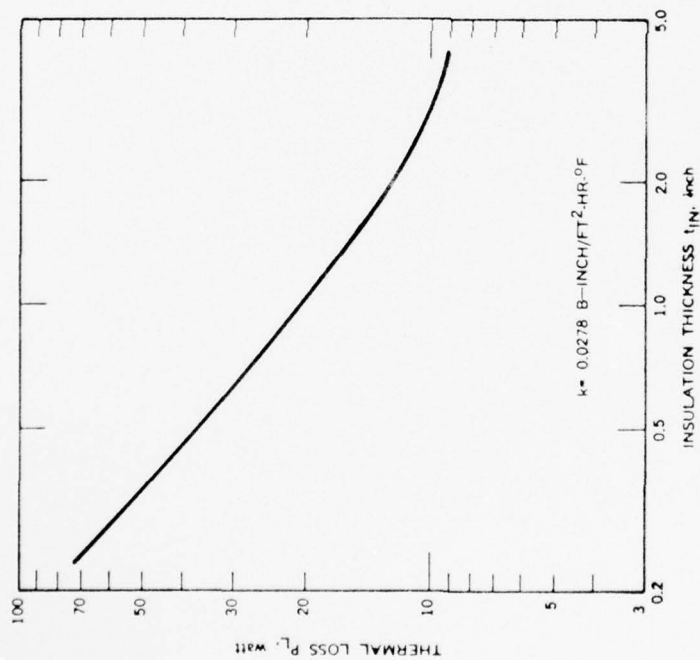


Figure 30. Effect of Insulation Thickness on the Total Loss of Thermal Energy from the Thermal Energy Storage Unit (Fiberfrax with Molybdenum Foil)

56712

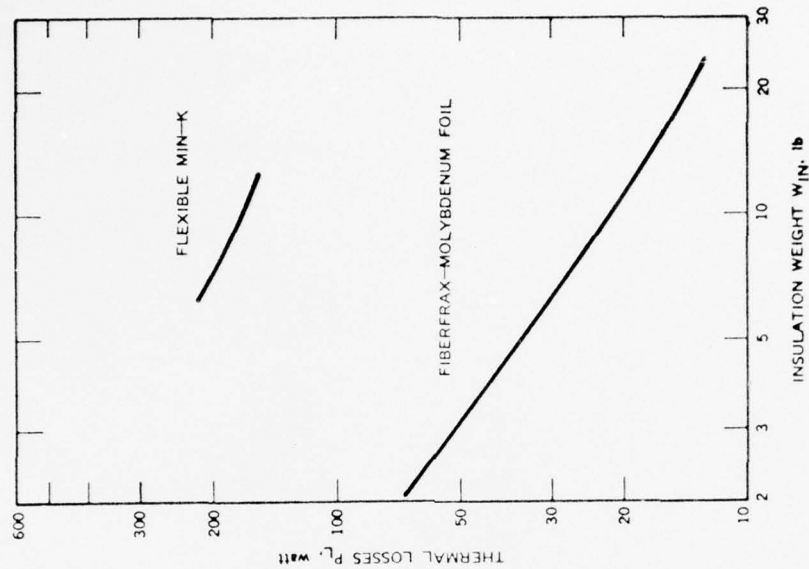


Figure 31. Thermal Losses as Affected by the Amount of Insulation

insulation composed of Flexible Min-K. While the losses are close to 200 watts for 8 pounds of Flexible Min-K, the Fiberfrax-Molybdenum foil system reduces the loss to less than 30 watts for the same weight.

The application of the Fiberfrax-Molybdenum foil system is much more costly. As the insulation has to be designed to minimize the heat flux along the metal foil, the seams of the insulation cannot be permitted to run perpendicular to the surfaces. Therefore, the insulation has to be cut to different widths for each layer, which has to be wrapped individually over the thermal energy storage unit. The use of this type of insulation would have contributed little to the demonstration of the thermal energy storage unit concept. In the discussion on the testing of the TES demonstration unit it will become clear that the relatively high thermal loss helped to produce a consistent and repeatable test condition for determining the operation of the TES unit.

2.2.3 FINAL THERMAL ENERGY STORAGE DEMONSTRATION UNIT DESIGN

When placing the order for the fabrication of the components of the optimized thermal energy storage demonstration unit, it was impossible to locate a vendor who was willing to fabricate the tubes to the design dimensions. The vendor who had formed the tubes for the 15-foot heat pipe was not able to manufacture the smallest of the five tubes, which has an inner diameter of 0.493 inch. He stated that his manpower was no longer available to perform this work, although he was willing to undertake the forming of the other four tubes. No other vendor could be found to even respond to the request for quote.

Because of the unexpected difficulties in locating a vendor for manufacturing the tubes, it became obvious that the thermal energy storage demonstration unit would have to be designed around standard tubes or pipes made of Inconel 600. In Figure 32 the available Inconel 600 pipes are shown. Pipes were selected from this stock sheet that permitted the

BEST AVAILABLE COPY

PIPE SIZE	O. D. IN INCHES	PIPE SCHEDULES														DBLE. E. H.
		5	10	20	30	STD.	40	60	E. H.	80	100	120	140	160		
1/8		.035 .1383	.049 .1863			.068 2447	.068 2447		.095 .3145							
1/4		.049 .2570	.065 .3297			.088 4248	.088 4248		.119 .5351							
3/8		.049 .3276	.065 .4235			.091 5676	.091 5676		.126 7388							
1/2		.065 5380	.083 6710			.109 8510	.109 8510		.147 1.088					.187 1.304	.294	
3/4		.065 6838	.083 8572			.113 1.131	.113 1.131		.154 1.474					.218 1.937	.308	
1		.065 8678	.109 1.404			.133 1.679	.133 1.679		.179 2.172					.250 2.844	.358	
1 1/4		.065 1.107	.109 1.806			.140 2.273	.140 2.273		.191 2.997					.250 3.765	.382	
1 1/2		.065 1.274	.109 2.083			.145 2.718	.145 2.718		.200 3.631					.281 4.859	.400	
2		.065 1.604	.109 2.601			.154 3.653	.154 3.653		.218 5.027					.343 7.444	.436	
2 1/2		.083 2.475	.120 3.531			.203 5.773	.203 5.773		.276 7.661					.375 10.01	.552	
3		.083 3.022	.120 4.078			.216 7.576	.216 7.576		.300 10.75					.438 14.32	.600	
3 1/2		.083 3.472	.120 4.973			.226 9.109	.226 9.109		.318 12.50						.636	
4		.083 3.915	.120 5.613			.237 10.79	.237 10.79	.281 12.66	.337 14.98			.438 19.00		.531 22.51	.674	
4 1/2						.247			.355						.710	
5		.109 6.349	.134 7.770			.258 14.62	.258 14.62		.375 20.78			.500 27.04		.625 32.96	.750	
6		.109 7.585	.134 9.289		.250 17.02	.280 18.97	.280 18.97		.432 28.57			.562 36.39		.718 45.30	.864	
7						.301			.500						.875	
8		.109 9.914	.148 13.40	.250 22.36	.277 24.70	.322 28.55	.322 28.55	.406 35.64	.500 43.39	.500 50.87	.593 60.63	.718 67.76	.812 74.69	.906	.875	
9						.342			.500							
10		.134 15.19	.165 18.70	.250 28.04	.307 34.24	.365 40.48	.365 40.48	.500 54.74	.500 64.33	.593* 76.93	.718 89.20	.843 104.1	1.000 115.6	1.125		
11						.375			.500							
12		.165 22.18	.180 24.16	.250 33.38	.330 43.77	.375 53.52	.406* 73.15	.562 73.15	.500 88.51	.687* 107.2	.843 125.5	1.000 139.7	1.125 160.3	1.312		
14			.250 36.71	.312 45.68	.375 54.57	.375 63.37	.438 84.91	.593 84.91	.500 106.1	.750 130.7	.937 150.7	1.093 170.2	1.250 189.1	1.406		
16			.250 42.05	.312 52.36	.375 62.58	.375 82.77	.500 107.5	.656 107.5	.500 136.5	.843 164.8	1.031 192.3	1.218 223.5	1.437 245.1	1.593		
18			.250 47.39	.312 59.03	.437 82.06	.375 104.8	.562 138.2	.750 138.2	.500 170.8	.937 208.0	1.156 244.1	1.375 274.2	1.562 308.5	1.781		
20			.250 52.73	.375 78.60	.500 104.1	.375 122.9	.593 166.4	.812 166.4	.800 208.9	1.031 256.1	1.280 296.4	1.500 341.1	1.750 379.0	1.968		
24			.250 63.41	.375 94.62	.562 140.8	.375 171.2	.687 238.1	.968 238.1	.500 296.4	1.218 367.4	1.531 429.4	1.812 483.1	2.062 541.9	2.343		

UPPER FIGURES
Wall Thickness
in inches

LOWER FIGURES
Wt. per Ft.
in pounds

*12" - Sch. 40S : .375 WALL
49.56 WT. PER FT.

*10" - Sch. 80S : .500 WALL
54.74 WT. PER FT.

*12" - Sch. 80S : .500 WALL
65.42 WT. PER FT.

Figure 32. Available Inconel 600 Pipes

manufacture of the thermal energy storage demonstration unit with some small variations in the optimum design. The most appropriate pipe sizes for satisfying the design requirements were:

3/8" nominal	0.674" O.D. x 0.091" wall
2" nominal	2.375" O.D. x 0.154" wall
2-1/2" nominal	2.875" O.D. x 0.302" wall
4" nominal	4.500" O.D. x 0.237" wall

Since a replacement pipe for the largest of the five tubes was not available, it still had to be fabricated from available sheet metal.

Figure 33 shows the modified design that evolved from incorporating standard pipes. This design can be compared with the original design which was shown in Figure 20. Because the smallest pipe had a larger internal diameter than in the original design, the vapor flow passage in the center of the TES unit was larger than required. This displaced some of the TES material which had to be compensated for by lengthening the unit approximately 2 inches. The lengthening of the unit resulted in a 3 percent increase in total weight as given in the following weight distribution:

<u>Design</u>	<u>Weight, lb</u>	<u>Percent</u>
<u>Original</u>		
TES material	12.07	32.82
Container material	14.34	38.99
Wick - screen material	1.15 lb	
- sodium	<u>0.42 lb</u>	
Insulation	<u>8.81</u>	<u>23.95</u>
Total	36.79	100.00

Technical drawing of a building section showing dimensions in feet and inches. The drawing includes a cross-section of a building with a curved roof and a detailed view of the roof structure. Dimensions are provided for various parts of the building, including the roof, walls, and floor. The drawing is oriented vertically on the page.

Dimensions (in feet and inches):

- Overall width: 4.200
- Overall height: 20.599
- Roof height: 20.211
- Roof slope: 15.634, 15.784
- Roof thickness: 0.065, 0.126
- Roof structure dimensions: 4.906, 4.776, 4.156, 4.026, 2.599, 2.469, 2.197, 2.067, 0.623, 0.493
- Roof structure dimensions (continued): 1.315, 1.306, 2.000 R, 2.010, 0.080, 0.070, 0.400
- Roof structure dimensions (continued): 0.0315, 0.0295, 0.0935, 0.0930
- Roof structure dimensions (continued): 2.251, 2.1885, 2.248, 2.1893, 2.060, 2.042
- Roof structure dimensions (continued): 0.040, 0.065, 0.065
- Roof structure dimensions (continued): 0.090, 0.285, 0.230
- Roof structure dimensions (continued): 2.500, 0.300, 2.504
- Roof structure dimensions (continued): 0.125, 0.100, 2.185, 1.95
- Roof structure dimensions (continued): 3.375, 2.450, 3.875, 3.810, 3.815

Figure 33. Final Design for a 1-kW-Hr Thermal Energy Storage Unit

Modified

TES material		12.07	31.89
Container material		15.17	40.08
Wick - screen material	1.32 lb		
- sodium	<u>0.48 lb</u>		
Insulation		<u>8.84</u>	<u>23.28</u>
Total		37.88	100.00

The heater well in the modified design had a slightly larger width. The original design called for a gap of only 0.128 inch. The modified design resulted in a gap of 0.136 inch. With the maximum heater diameter of 0.130 inch, this design was expected to operate in the radiation heat transfer mode. Heat transfer from the heater to the walls of the well solely by radiation heat transfer had been assumed in the original heat transfer calculations and in the selection and sizing of the heaters. Any heat transfer by conduction had been considered a bonus in the operation of the heater, as it would slightly decrease the heater operating temperature.

When compared with the original design, the modified design resulted in a 3 percent increase in weight. The heater surface was slightly larger because of the greater length of the unit. The design modification required for using standard - though still not easily available -Inconel 600 tubes for the fabrication of the TES unit appeared to be acceptable.

2.2.4 HOT CYLINDER DESIGN

Prior to machining of the hot cylinder, the design was evaluated for maximum stresses and their location. This was deemed important as the hot cylinder was to become an integral part of the thermal energy storage unit. The pertinent dimensions and tolerances of the hot cylinder, as shown in Hughes Aircraft Company Drawing X3180095, are repeated in Figure 34. When using the relations given in Roark: Formulas for Stress and Strain, and the stress concentration factors given by Peterson: Stress Concentration

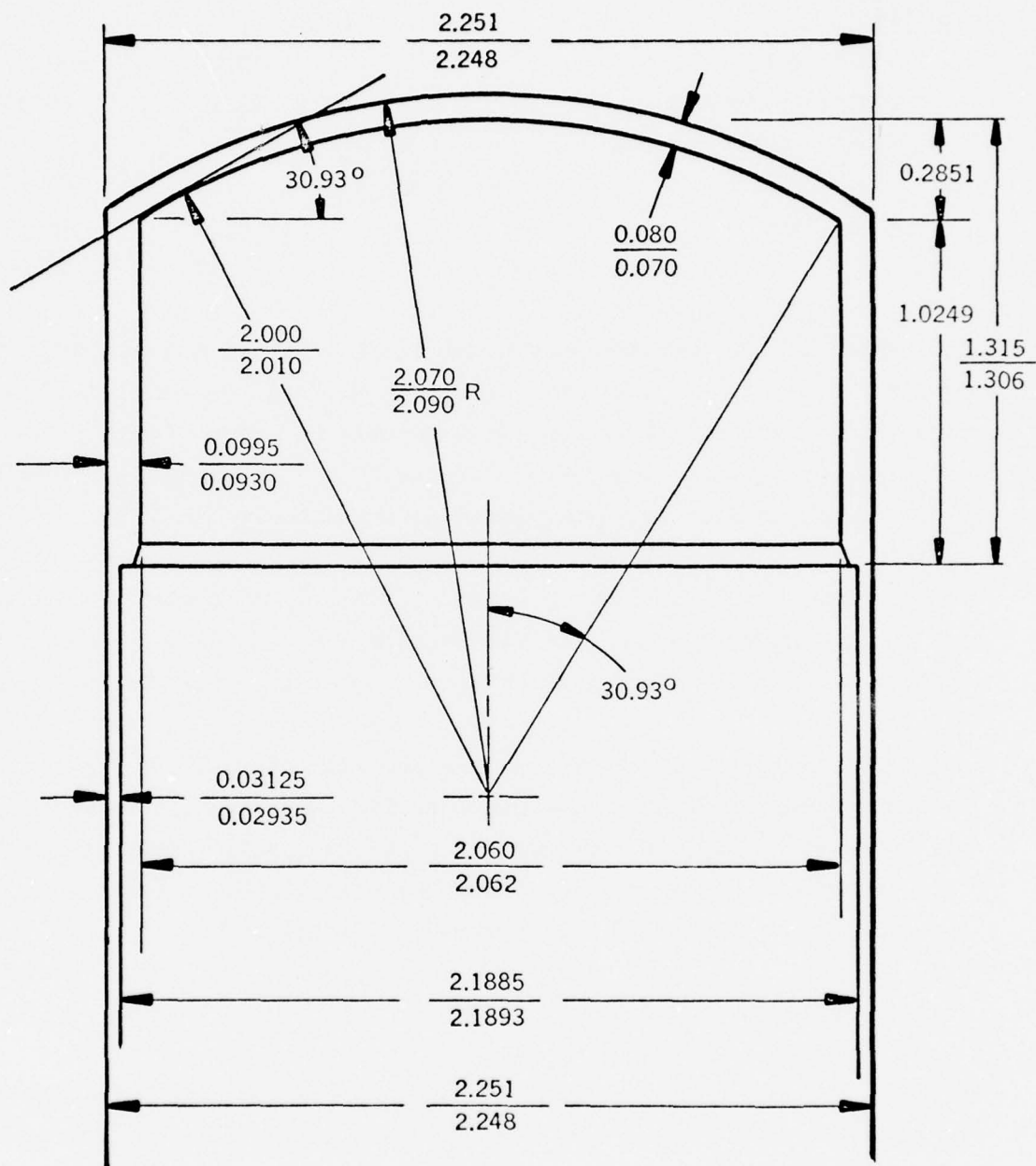


Figure 34. Original Hot Cylinder Design

Factors, stresses as high as 157,000 psi with the lower limit of the plate thickness of 0.070 inch were calculated. The calculations took into account the curvature of the end plate which attaches to the cylinder under an angle of 30.93 degrees as shown in Figure 34. When using a simplified approach for calculating maximum stresses by matching of moments and deflections of a curved plate with a cylinder, stresses as high as 132,000 psi were calculated.

Data given by the Carpenter Technology Corporation for René 41 (Vacumeltrol 41) were correlated with the Larson-Miller parameter

$$P_{L-M} = (460 + T) \times (C + \log_{10} t) \times 10^{-3}$$

where:

T = temperature, °F

t = time, hours

The best fit was found by making the constant C equal to 20. The correlation with the original data is shown in Figure 35. For an operating temperature of 1250°F and an operating lifetime of 5000 hours and 20,000 hours, the Larson-Miller parameters are 40.53 and 41.55, respectively. Based on the correlation of Figure 35, the maximum allowable stresses for rupture are 55,000 and 69,000 psi, respectively. For structural stability and maximum allowable distortion, the allowable stresses should be kept below these values.

For comparison, the Larson-Miller parameter correlation with the rupture stress for Inconel X750 and Inconel 718 are shown in Figures 36 and 37. The constant C is 17.5 for Inconel alloy X750 and 25 for Inconel alloy 718. The Larson-Miller parameters for the two lifetimes are tabulated below.

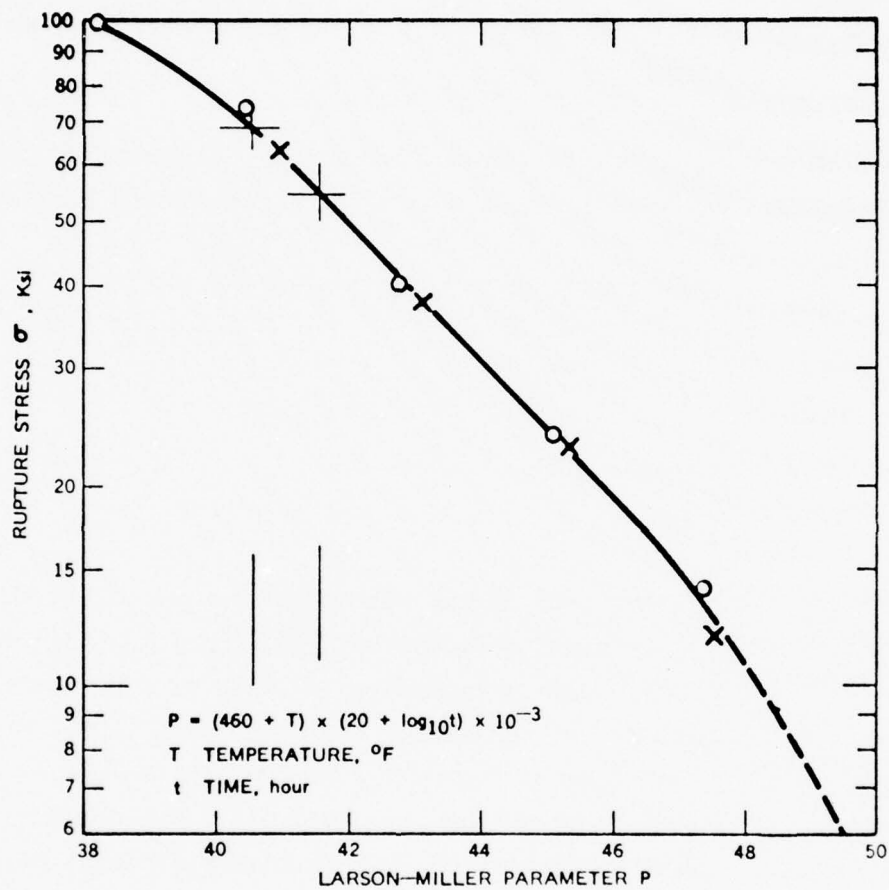


Figure 35. Rupture Stress of René 41 (Carpenter Vacumeltrol 41)
(Technical Data, Carpenter Technology Corporation 6/70)

56693

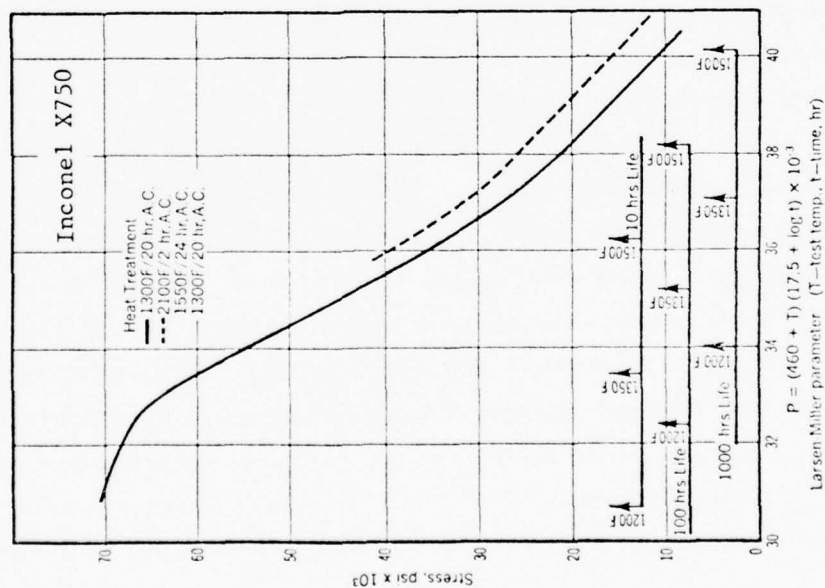


Figure 36. Life of cold-rolled, annealed and aged sheet.

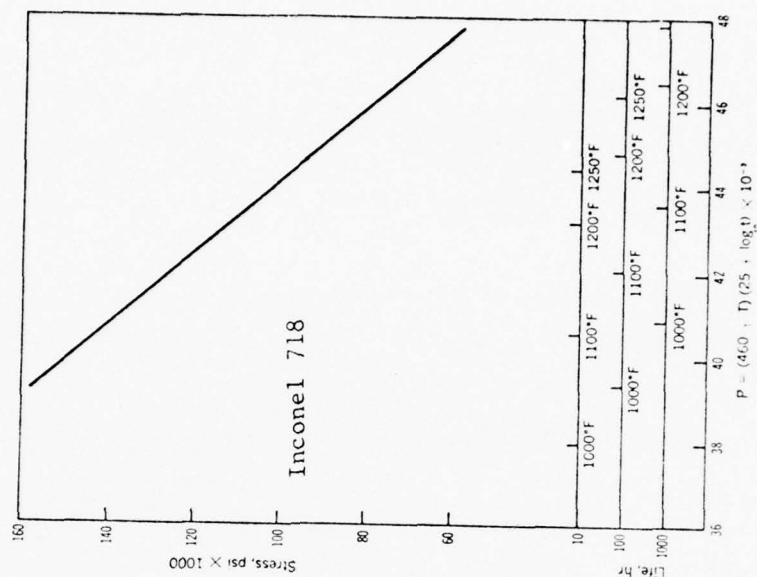


Figure 37. Larson-Miller parameter plot of rupture life of cold-rolled sheet, 0.025-0.250-in. (Annealed and aged in accordance with AMS 5598). In the Larson-Miller parameter, P , T is temperature, $^{\circ}\text{F}$, and t is time, hr.

Larson-Miller Parameters

	<u>Inconel X750</u>	<u>Inconel 718</u>	<u>René</u>
5,000 hours	36.25	49.08	40.53
20,000 hours	37.28	50.11	41.55

The maximum allowable stresses for the various materials are given in the following tabulation.

Maximum Allowable Stresses

	<u>Inconel X750</u>	<u>Inconel 718</u>	<u>René</u>
5,000 hours	33,000 psi	50,000 psi	69,000 psi
20,000 hours	24,000 psi	25,000 psi	55,000 psi

When the maximum allowable stresses for rupture (this does not consider the maximum allowable stresses for structural stability) were compared with the calculated maximum stresses in the hot cylinder under the stated operating conditions, it was felt that it would be of value to ascertain whether modifications could be made in the design without affecting the operating characteristic of the hot cylinder.

The most obvious improvement was the increase in the plate thickness and the tightening of its tolerance. The results of the parametric study are shown in Figure 38. It is interesting to note that just the tolerance of the plate thickness permits the maximum stress to vary between 130,000 and 96,000 psi. Without increasing the cylinder wall thickness, which was 0.0955 inch in the original design, the plate thickness should be at least 0.092 inch. With this plate thickness, the maximum stresses are equal at 68,000 psi. A slight increase of the cylinder wall thickness would bring the maximum stresses down to the allowable stress for 20,000 hour operation with René 41.

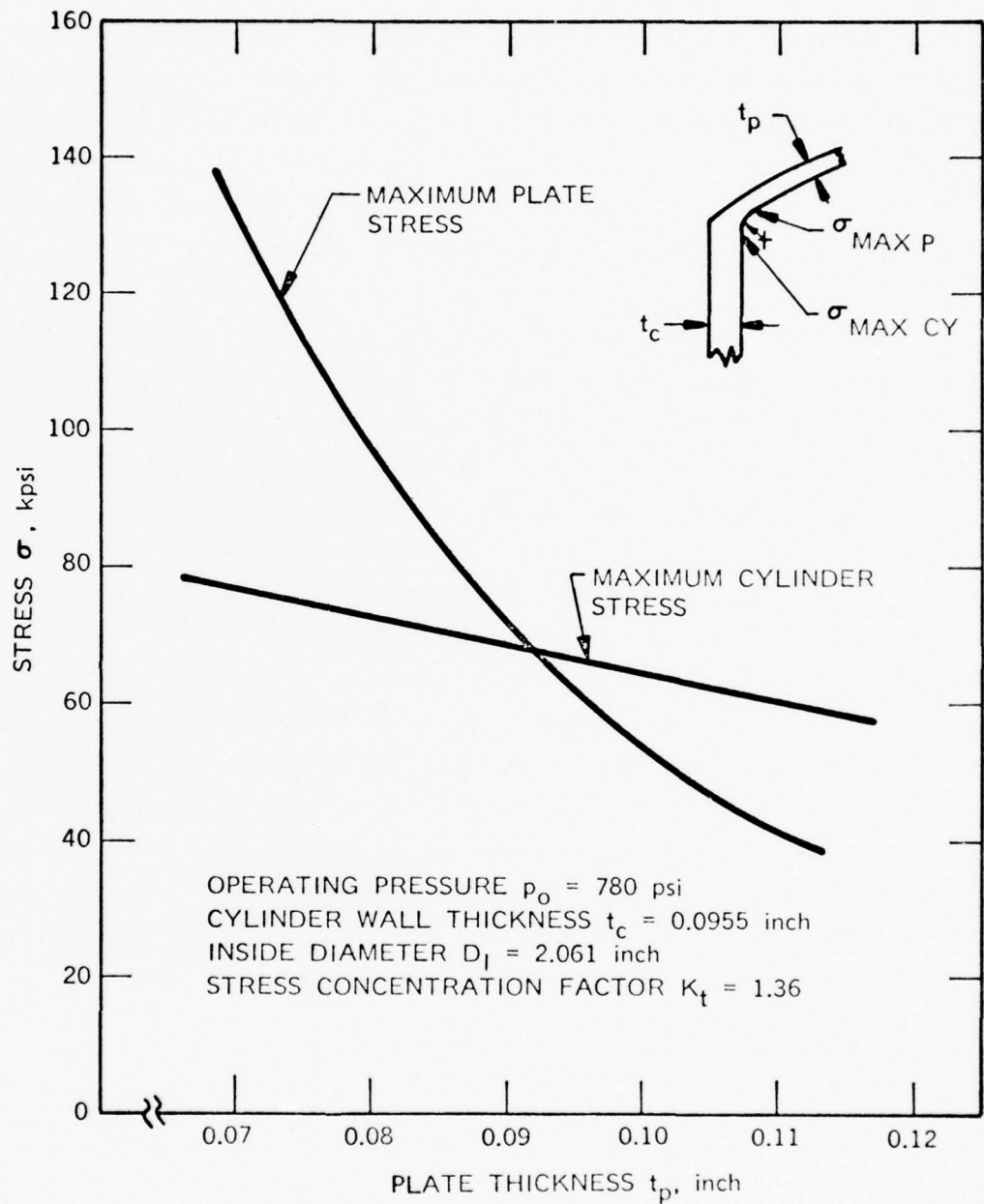


Figure 38. Effect of Plate Thickness on the Maximum Stresses in the Hot Cylinder of the AFLIR Vuilleumier Cooler

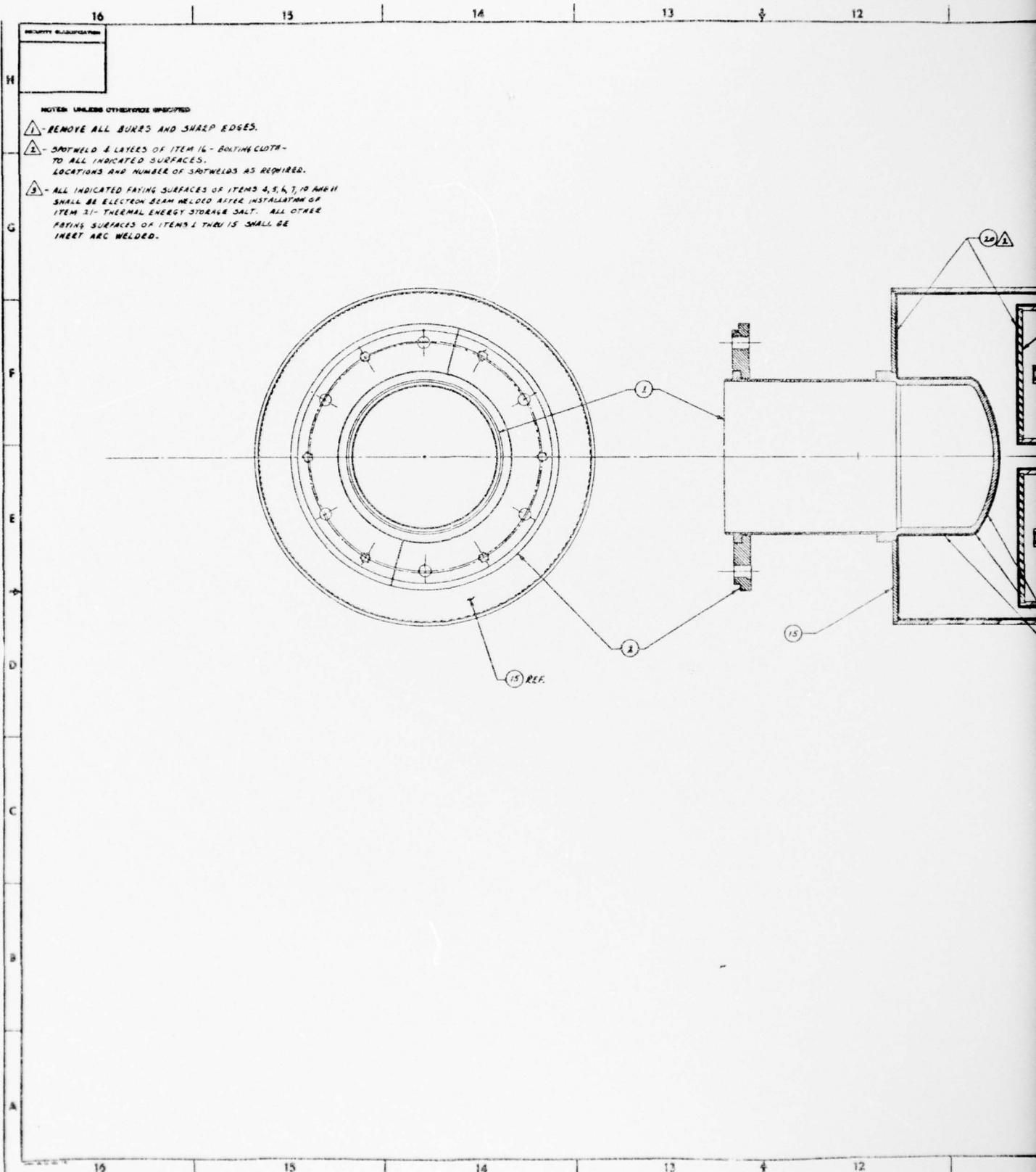
When the manufacture of the hot cylinder was investigated, it became apparent that the availability of material in the most desirable sizes was very limited and that the cost of the material was relatively high. Since the difficulties in obtaining the material increase with the diameter, it became obvious that the hot cylinder should be designed for the smallest bar diameter. The original design called for a bar stock diameter of at least 3.875 inches. This size was needed for machining the hot cylinder with the mounting flange as a single unit.

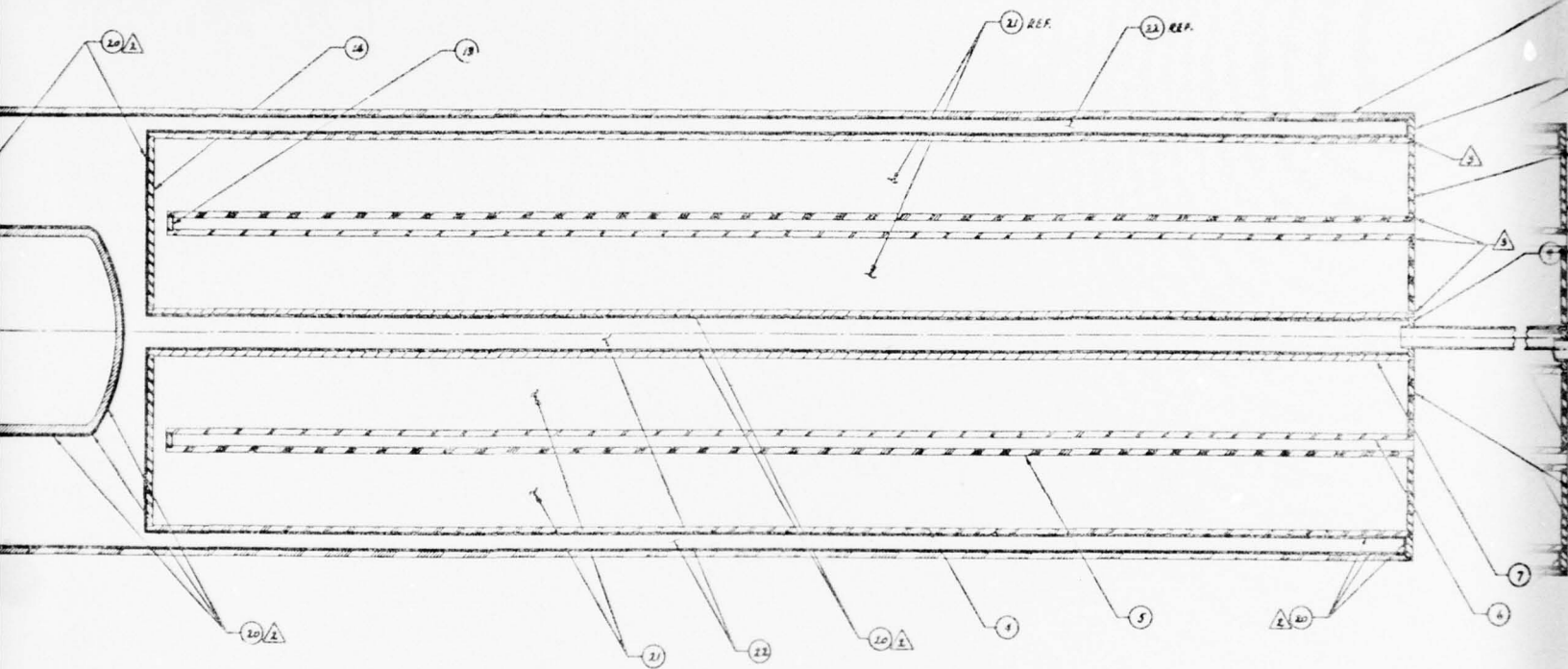
A considerable saving in material and machining could be achieved by designing the hot cylinder with the smallest mounting flange possible. Calculations indicated that, for a very conservative allowable bearing stress of 20,000 psi and a shear stress of 15,000 psi, the flange diameter had not to be larger than 2.292 inches, and the thickness of the flange not more than 0.029 inch. A hold-down ring with the diameter equal to that of the original flange, made of plate material, could be used for securing the hot cylinder to the cooler body. Such design modification appeared to be especially useful if René 41 was to be used, as the machinability of that material is considered extremely poor. The proposed and accepted design of the hot cylinder is presented in Figure 39 with the detailed design of the TES demonstration unit. This change did not require modifications to the cooler. All design changes assured better dimensional stability and easier fabrication of the hot cylinder. Furthermore, the material selection became less critical and made the use of Inconel 718 possible without reservations for the present application.

2.3 SPECIAL HEAT TRANSFER CONSIDERATIONS

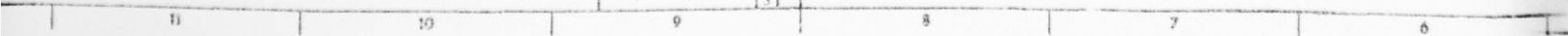
2.3.1 EFFECT OF VOLUMETRIC CHANGE OF THERMAL ENERGY STORAGE MATERIAL

With the specific design of the thermal energy storage demonstration unit established, the secondary effect associated with the volumetric change of the thermal energy storage material during melting and solidification was





707485



2

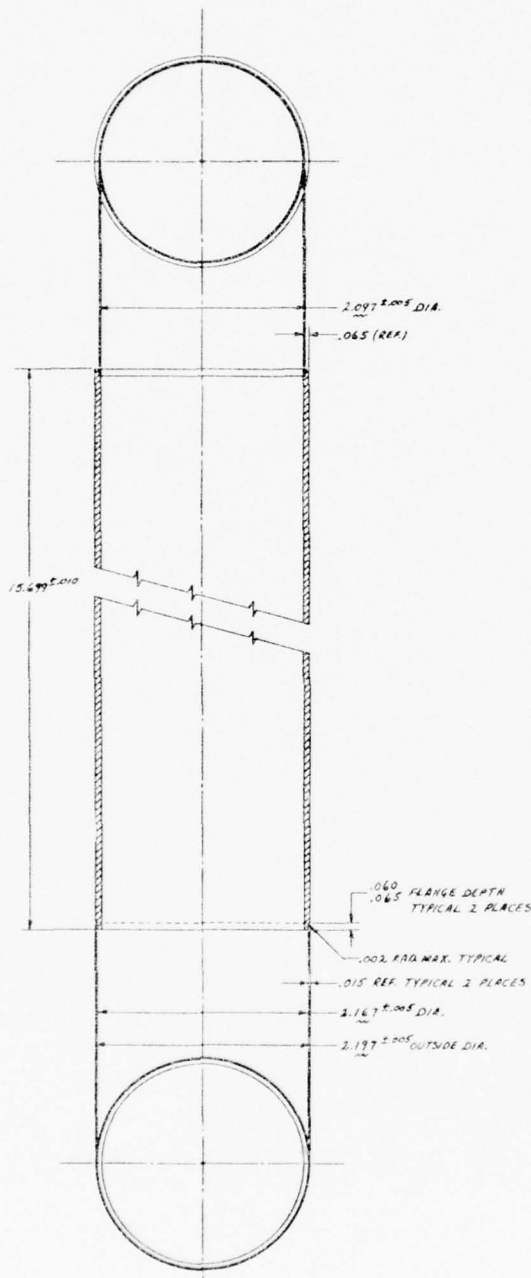
[illegible]

Figure 39. (Sheet 1 of 3) 57/58

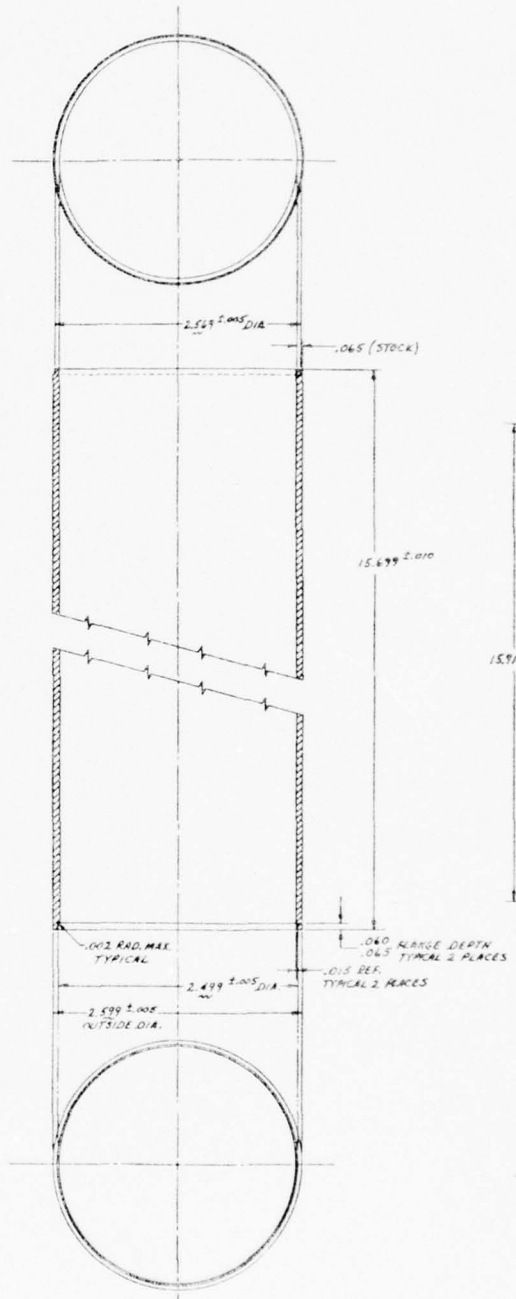
16
15
14
13
4
12
11

SECURITY CLASSIFICATION

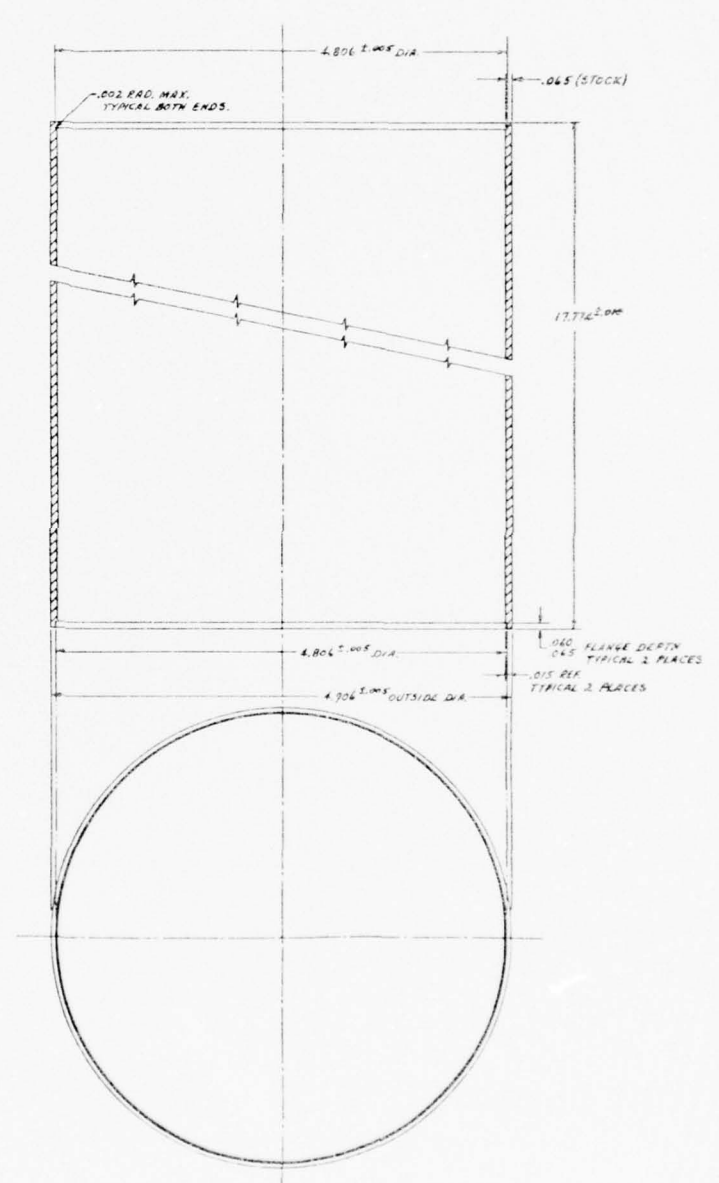
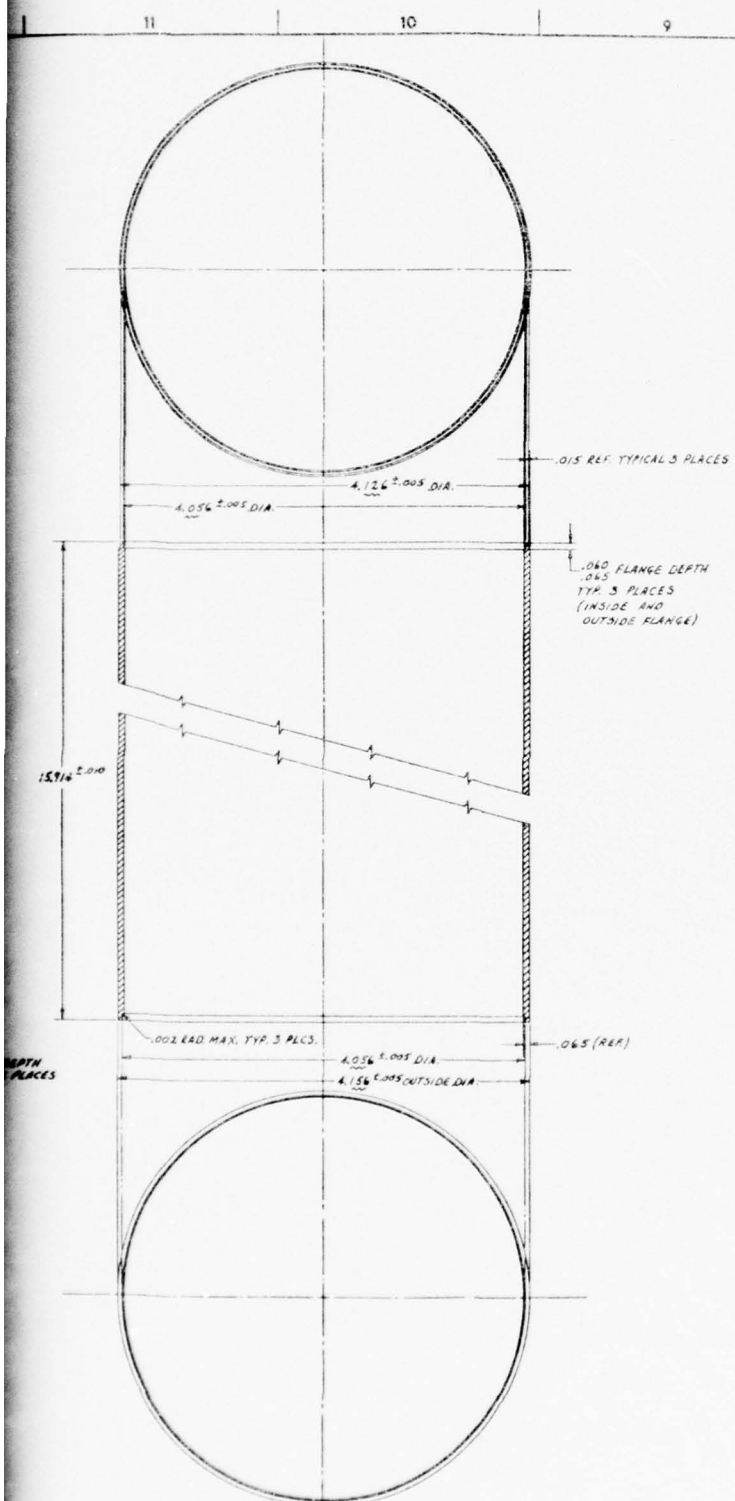
NOTES: UNLESS OTHERWISE SPECIFIED



ITEM 6 - TUBE NO. 4 - ONE REQ'D. ①
MAT'L. REF: INCONEL 600



ITEM 5 - TUBE NO. 3 - ONE REQ'D. ①
MAT'L. REF: INCONEL 600



707485

2

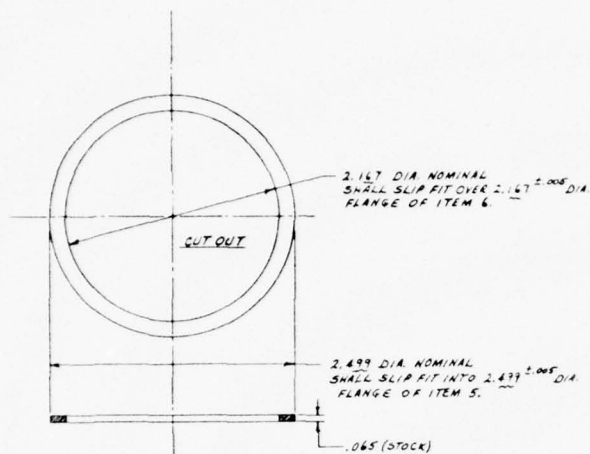
6 5 4 3 2 1



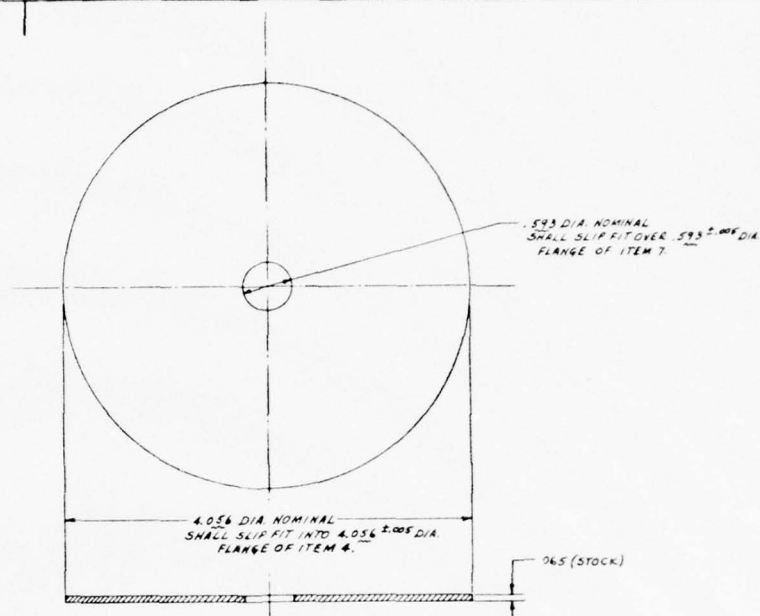
59/60

13

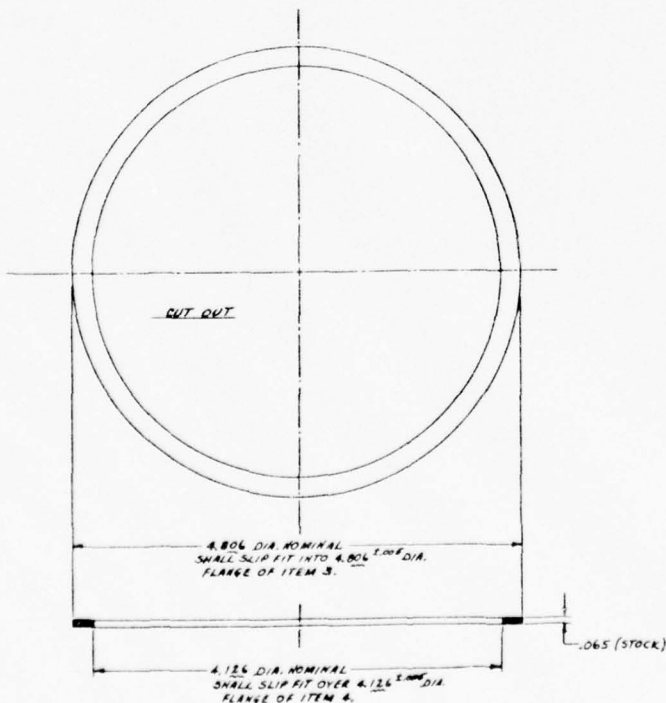
	16	15	14	13	↓	12	11
H	SECURITY CLASSIFICATION						
	NOTES: UNLESS OTHERWISE SPECIFIED						
G							
F							
E							
→							
D							
C							
B							
A							
	16	15	14	13	↓	12	11



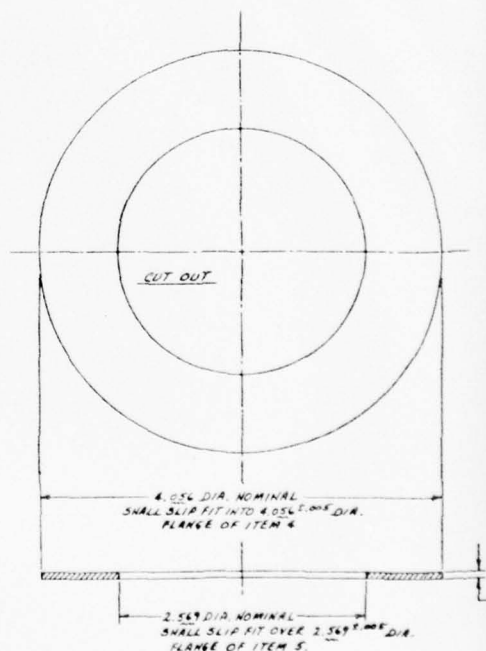
ITEM 13 - RING NO. 5 - ONE REQ'D. Δ
MAT'L REF: INCONEL 617



ITEM 14 - RING NO. 6 - ONE REQ'D. Δ
MAT'L REF: INCONEL 617



ITEM 12 - RING NO. 4 - ONE REQ'D. Δ
MAT'L REF: INCONEL 617



ITEM 11 - RING NO. 3 - ONE REQ'D. Δ
MAT'L REF: INCONEL 617

Figure 39. S F

707485

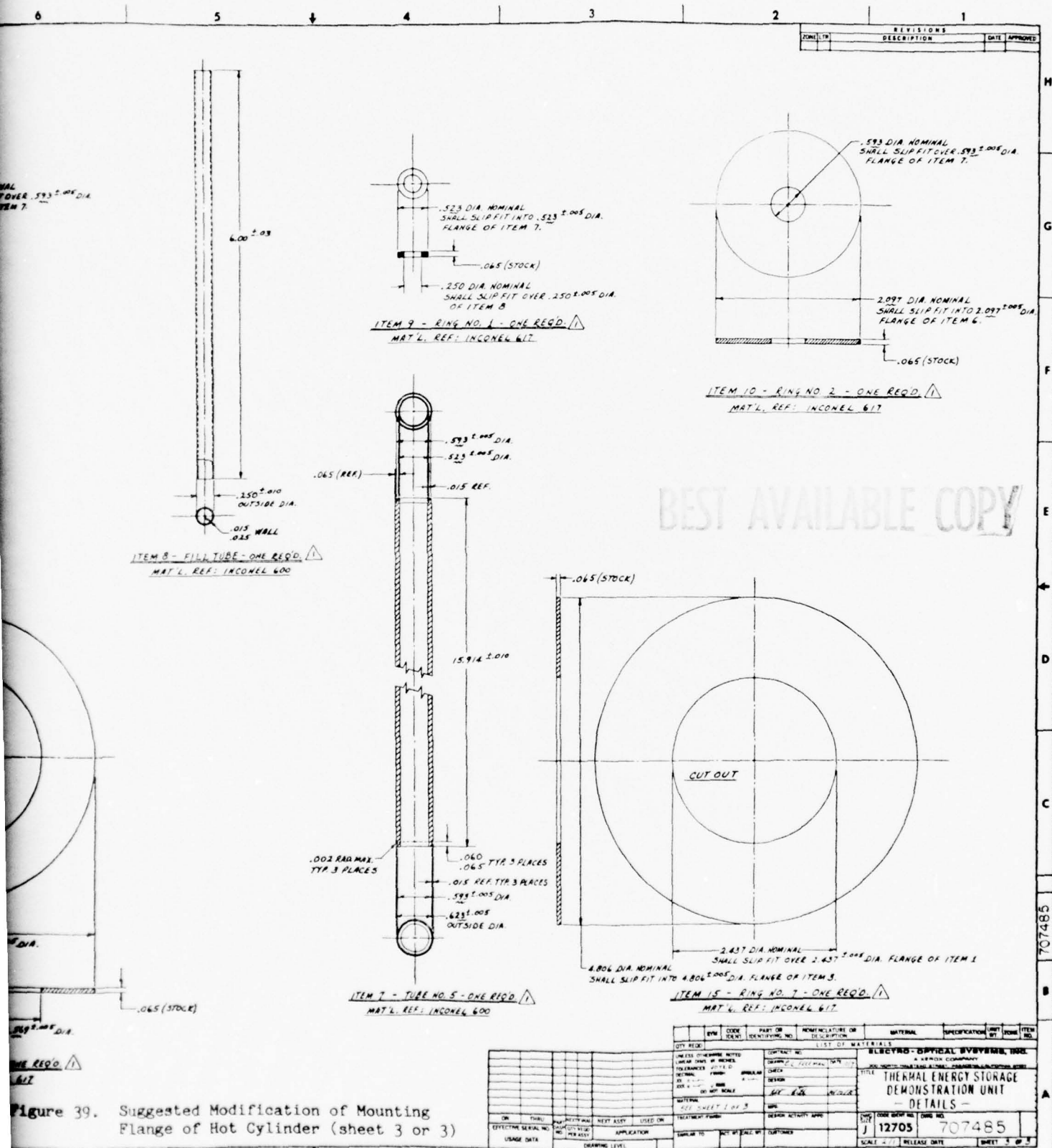


Figure 39. Suggested Modification of Mounting Flange of Hot Cylinder (sheet 3 or 3)

investigated. In the solid state the thermal energy storage material occupies only 76.1 percent of the liquid volume. The container volume of the thermal energy storage unit had to be designed for the largest volume, i.e., the volume of the liquid material. During extraction of the stored thermal energy, the salt contracts and voids form at that time, so that the TES material will no longer be in contact with the entire container wall as shown in Figures 40, 41, and 42. For a 24 percent volumetric void, a 20 percent surface detachment will occur. In the worst case the temperature drop across the thermal energy salt could increase by about 20 percent for a total of $\Delta T = 50^{\circ}\text{F}$. Even with this temperature drop the operating temperature of the hot cylinder would still be above 1200°F .

2.3.2 COOLING OF HOT CYLINDER DURING PERFORMANCE TESTING

For evaluating the thermal energy storage demonstration unit performance, the hot cylinder was cooled with a flow of air simulating the heat extraction from the hot cylinder wall by helium during operation of the Vuilleumier cooler. The arrangement for testing the thermal energy storage demonstration unit is shown in Figure 43. A plug shown in Figure 44 was machined from stainless steel that provided a 0.020-inch flow pass along the hot cylinder wall. The predicted heat transfer as function of flow rate is shown in Figures 45 and 46. With the 0.020 inch flow passage, the design power is extracted at a flow rate of 8.2×10^{-3} lb/sec (3.72 g/sec). At this flow rate the flow is well in the laminar flow regime, and the heat transfer varies relatively little with flow rate, i.e., the total heat transfer changes by only 5 percent for a flow rate variation of about 24 percent.

The length of the flow gap is $L = 1.025$ inch. With a flow gap of only $t = 0.020$ inch, the entrance regime is very short compared to the entire flow length. For evaluating the Nusselt number, the relation given by Eckert and Drake in Heat and Mass Transfer, 2nd Edition, p. 197, is used.

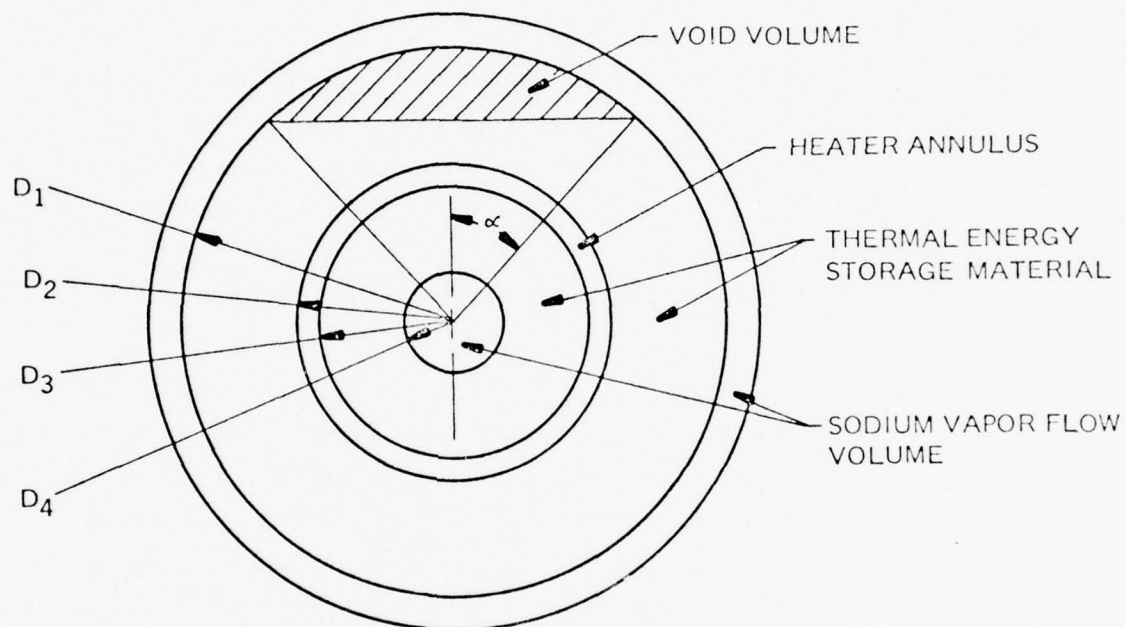


Figure 40. Configuration of Thermal Energy Storage Demonstration Unit

56887

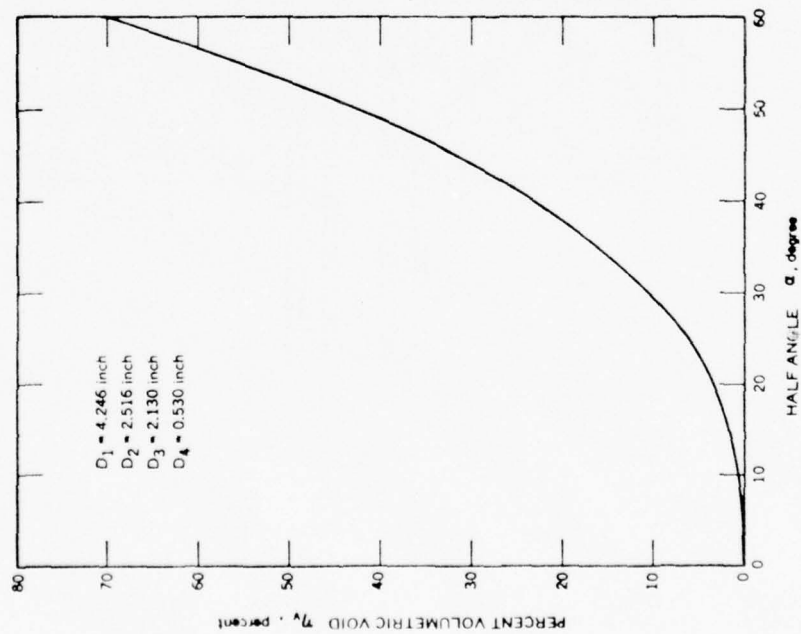


Figure 41. Volumetric Void as a Function of Half Angle for Thermal Energy Storage Demonstration Unit

56886

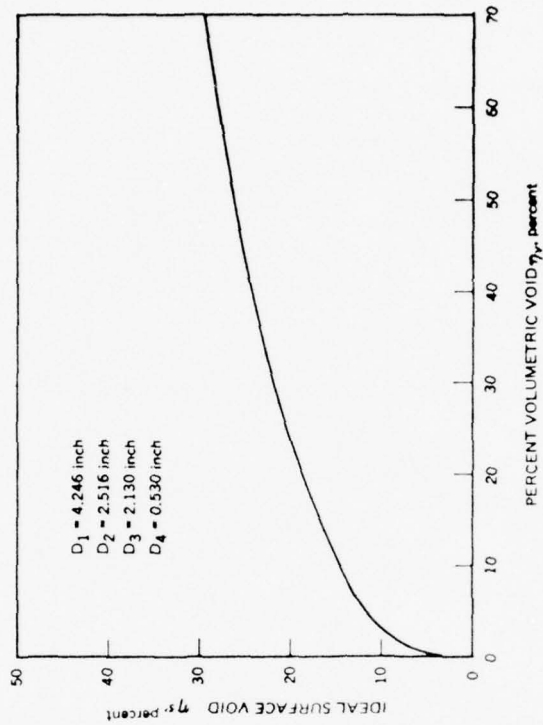


Figure 42. Volumetric Void and Surface Void Relation for Thermal Energy Storage Demonstration Unit

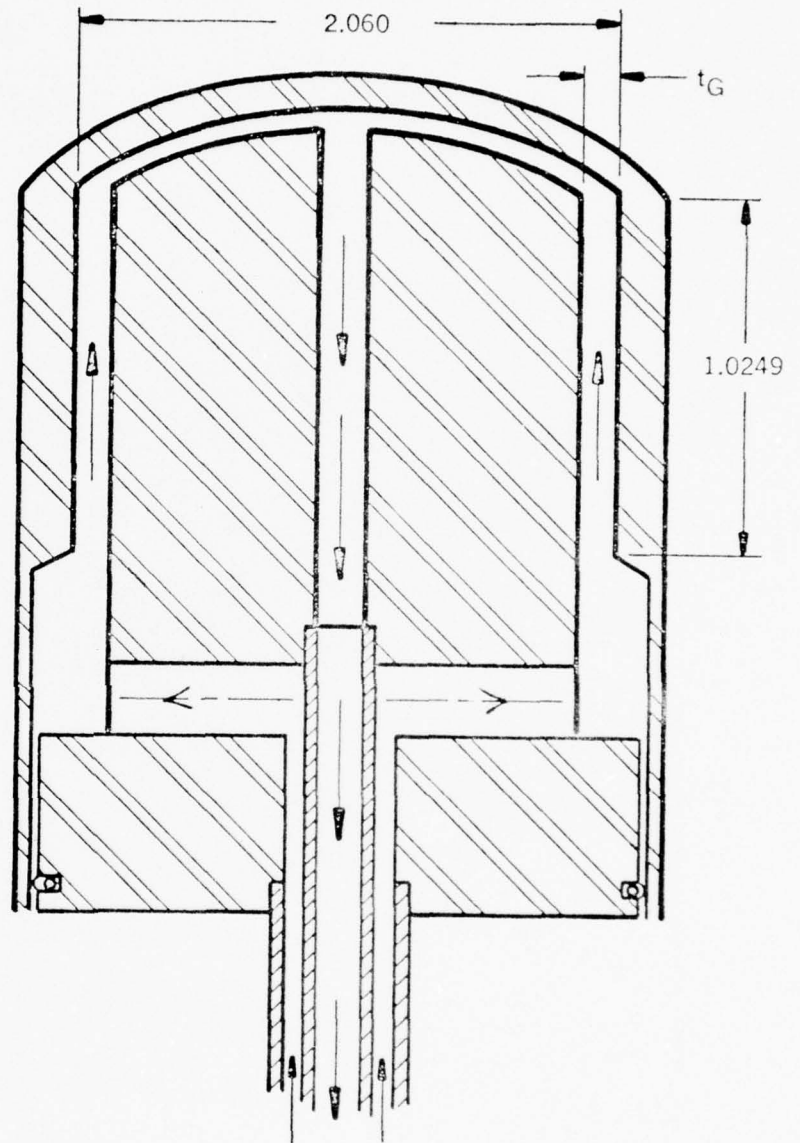


Figure 43. Gas Flow for Performance Testing of Thermal Energy Storage Demonstration Unit

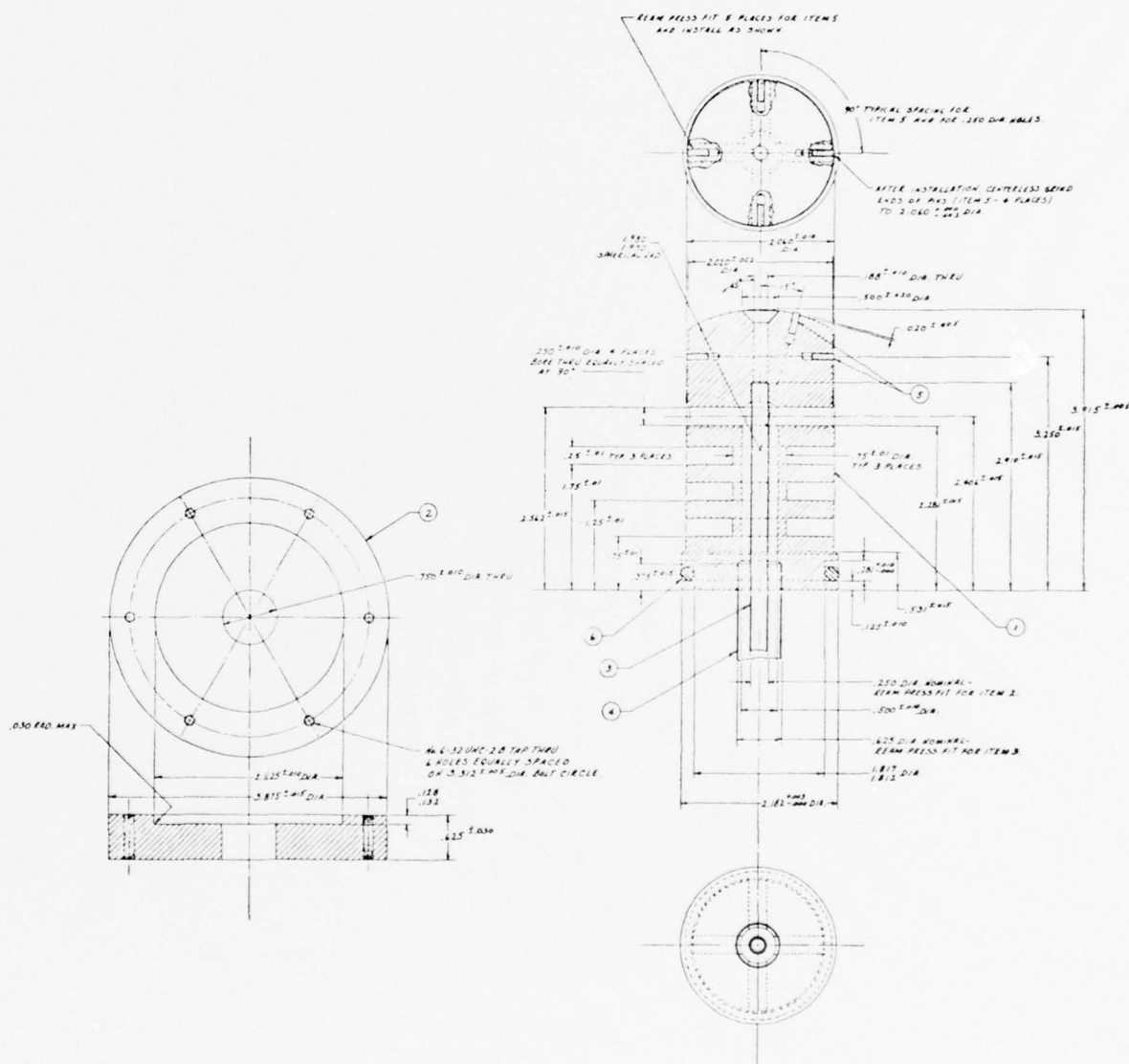


Figure 44. Flow Test Insert - Thermal Energy Storage Demonstration Unit

56633

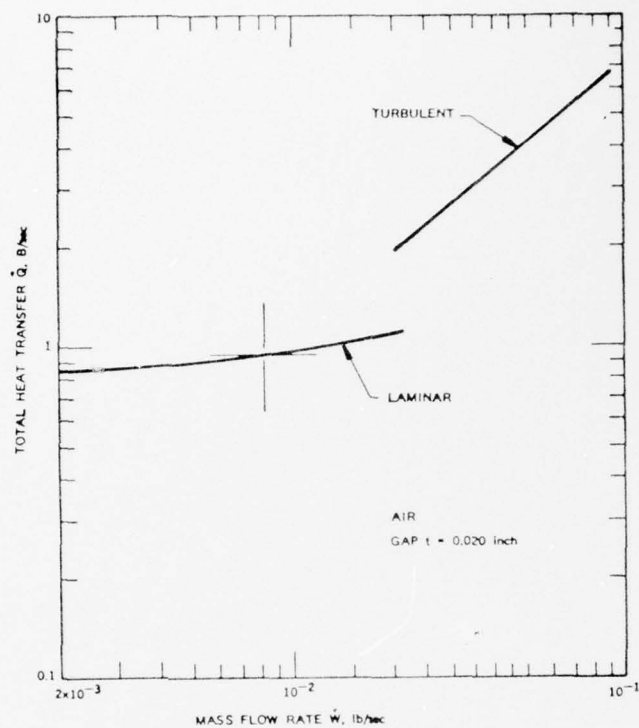


Figure 45. Total Heat Transfer from the Hot Cylinder to the Cooling Air

14600

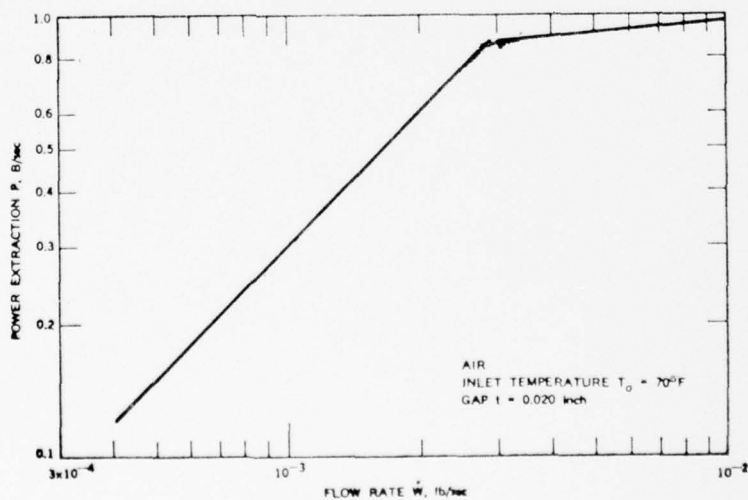


Figure 46. Power Extraction from the Hot Cylinder as Function of Flow Rate

The non-dimensional parameter $1/(Re_d Pr d/x)$ is about 0.05 so that the average effective Nusselt number is about 5 for the case under consideration. As shown by the correlation given by Eckert and Drake, Prandtl and various other literature sources, the heat transfer is not entirely dependent on the Nusselt number but is also a function of several additional parameters. Inlet conditions, roughness factors, and surface conditions are contributing parameters which, however, could not be expressed mathematically for inclusion in the heat transfer calculation.

The final temperature of the air that cools the hot cylinder of the Vuilleumier cooler and has an inlet temperature of 70°F, is shown in Figure 47. The calculated pressure drop along the flow pass is shown in Figure 48. With the expected pressure drop being approximately 1 psi, it was possible to arrange the flow metering system to operate in the choked orifice configuration. With the additional pressure drops in the lines and the fittings leading to and from the flow insert, the total back pressure was estimated to be not higher than 10 psig. The sonic orifice was therefore selected to operate with an upstream pressure of about 50 psia or 35 psig.

For spanning the entire range of flow rates which might be desirable for testing with shop air supply, two sonic orifices were calibrated, No. 55-1 and No. 47. Orifice No. 55-1 permitted lowering the flow rate to less than 0.7 g/sec of air, while with orifice No. 47, the upstream pressure was about 69 psig at the design flow rate of 8.2×10^{-3} lb/sec. The orifices were calibrated with a Wet Test Meter (American Meter Company Model AL 22), which has a maximum deviation of ± 1 percent from the calibration, and with a 1/4 percent Bourdon tube type pressure gage (Glassco).

In Figure 46 two regimes are indicated. Below 1.36 g/sec the amount of energy extracted from the hot cylinder will be equal to the heat capacity of the air between the inlet temperature and the operating temperature of

56682

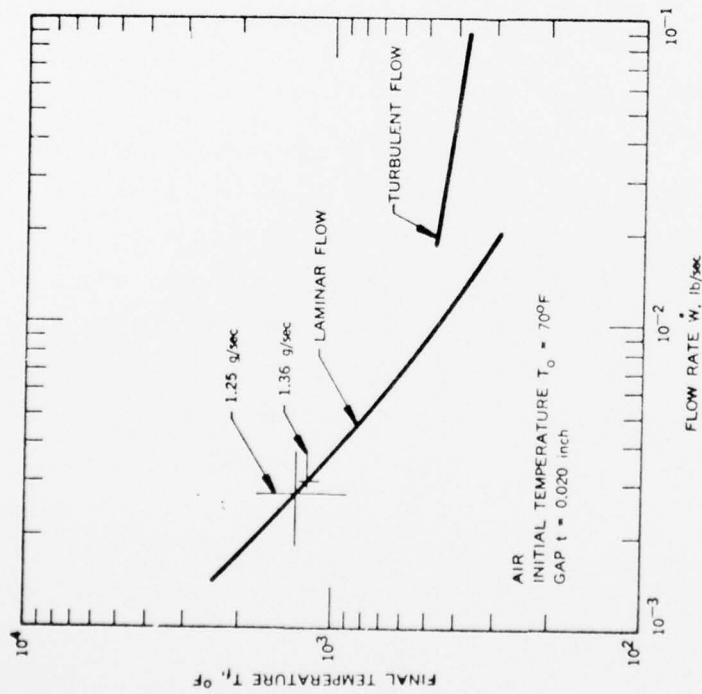


Figure 47. Final Air Temperature as Function of Flow Rate Through the Hot Cylinder

56681

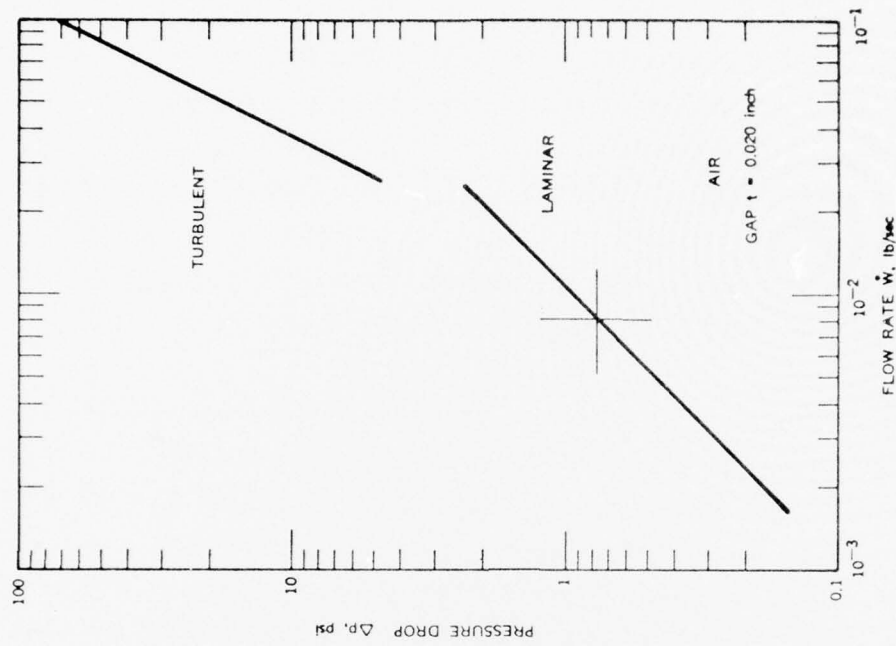


Figure 48. Pressure Drop Along the Heat Transfer Path of the Hot Cylinder of the Vuilleumier Cooler

hot cylinder, as the air will be heated to the operating temperature of the hot cylinder when flowing through the flow gap. Above 1.36 g/sec the cooling air will not reach the operating temperature of the hot cylinder. For this regime the power extraction is determined by the heat transfer to the cooling air under laminar flow conditions.

A testing problem was anticipated for the case when trying to raise the extraction rate to about twice the design rate. As can be seen from Figure 45, a heat transfer rate corresponding to 120 to 200 percent of the design extraction rate lies in a regime in which the flow is unstable for the 0.020-inch gap. Although the 0.020-inch gap is equal to the gap of the hot cylinder when mounted on the Vuilleumier refrigerator, it was anticipated to increase the gap by remachining the flow insert at a later date. This would have permitted testing at heat transfer rates above the design rates for the device. The correlations in Figure 49 indicate that, with a flow gap of 0.100 inch the hot cylinder can be tested from 50 percent of the design heat transfer without change in flow regime; i.e., the entire flow regime is turbulent. Very consistent test data should have been possible with this gap configuration. The pressure drops that were anticipated for that configuration are shown in Figure 50.

56678

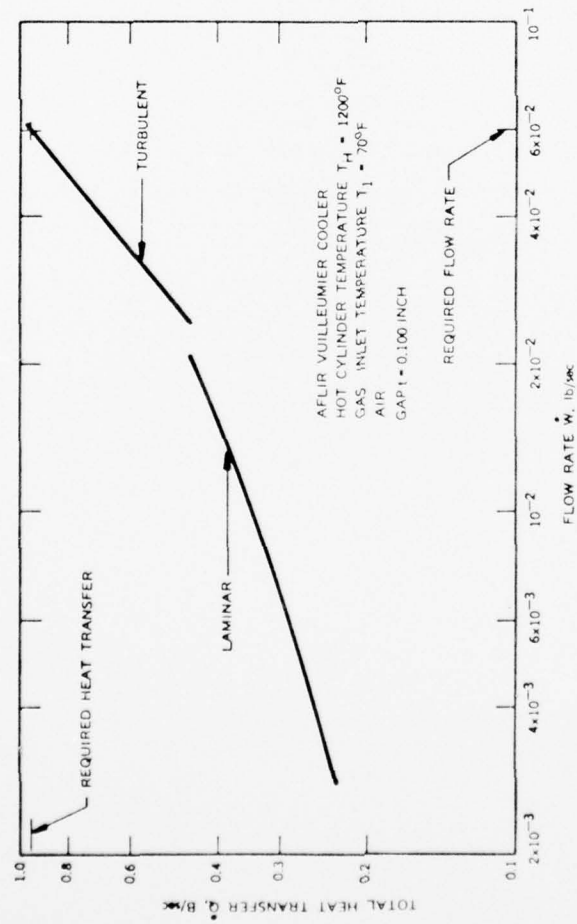


Figure 49. Flow Rate Requirement for Cooling Hot Cylinder of Vuilleumier Cooler During Thermal Energy Storage Unit Performance Test

56677

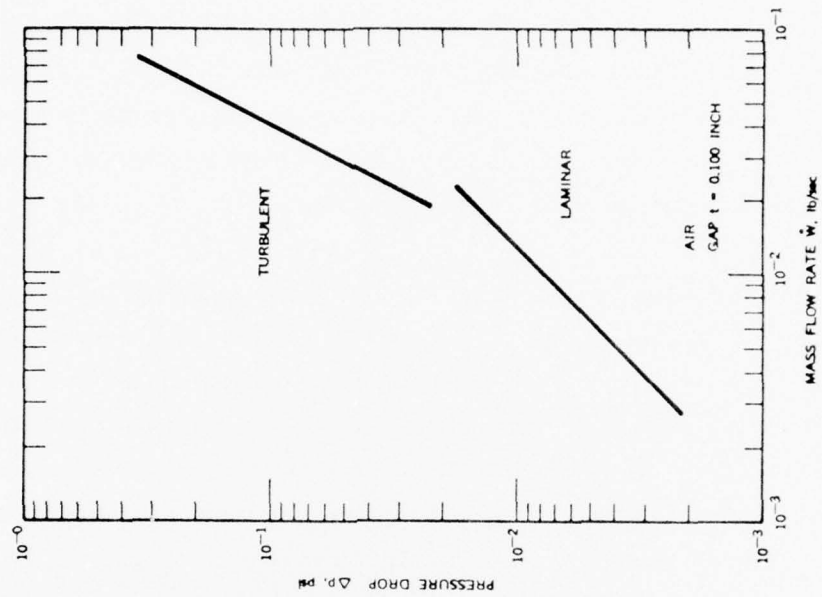


Figure 50. Pressure Drop Along the Heat Transfer Path of the Hot Cylinder of the Vuilleumier Cooler

SECTION III

FABRICATION OF THERMAL ENERGY STORAGE DEMONSTRATION UNIT

3.1 MACHINING AND INITIAL ASSEMBLY

The thermal energy storage unit was fabricated from Inconel 600 sheet metal and Inconel 600 pipes according to the availability of material and the capability of manufacturers to form the required components. Figure 51 shows the machined parts in an exploded view of the thermal energy storage demonstration unit with the hot cylinder and the hold down flange. The four smaller of the five tubes were machined from pipes, while the largest was roled from 0.065-inch Inconel 600 sheet metal. The same material was used for machining the seven flanges shown.

As indicated in a prior section of this report, the original TES design had to be modified to permit manufacture of the tubes from available Inconel 600 pipes because the tube forming vendor did not want to bid on forming the smallest of the five required tubes.

The cost of manufacturing the four tubes from standard pipes instead of from sheet metal was not lower, as one might have expected. Material cost was considerably higher because only thick-walled pipes, Schedule 40, are being manufactured and stocked by the suppliers. The cost of the pipes is based primarily on the material weight of Inconel 600, which is relatively expensive.

The hot cylinder of the Vuilleumier cooler was machined from Inconel 718, 2½-inch diameter bar stock. The inside of the hot cylinder was first rough machined removing the major amount of material. The final dimensions were obtained by the Elox process. The split hold-down flange was fabricated from stainless steel.

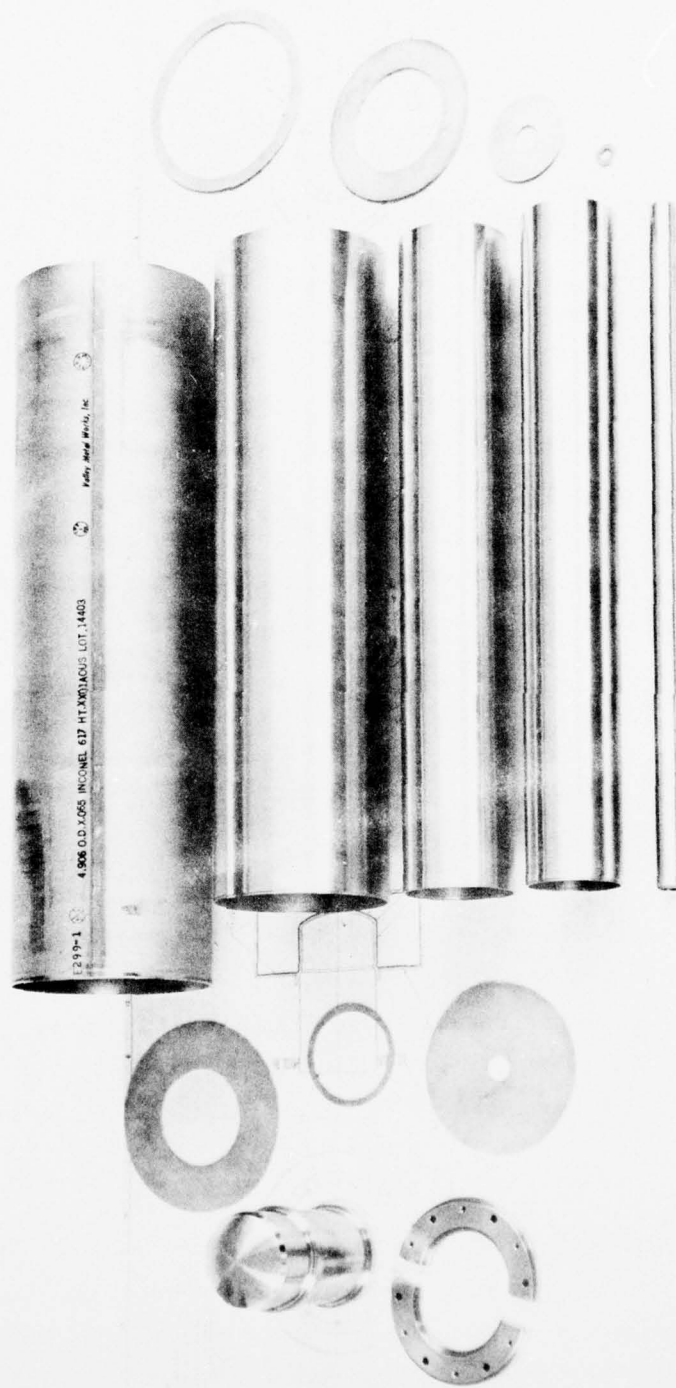


Figure 51. Exploded View of Thermal Energy Storage Demonstration Unit

The assembly of the thermal energy storage unit was initiated by electron beam welding all joints required for forming the container of the thermal energy storage material. Since the heater well walls are part of the thermal energy storage material container, the placement of the six electric heaters had to be included in the initial assembly of the unit. The six electric heaters were first wound tightly over a 2-inch diameter tube and then transferred as a unit over the inner surface of the heater well. The outer tube of the heater well was then slipped over the heaters. The installation of the heaters proved to be more difficult than had been anticipated. The 1/8-inch diameter heaters could not be wound uniformly enough to be easily accommodated even in the 0.132 inch nominal wide well.

With the thermal energy storage material container mechanically assembled and the heaters in place, the remaining welds were completed. At this stage of the assembly, the joints were checked with a helium leak detector. One joint was found faulty and had to be redone. This joint had to be welded with the heaters in place in the heater well. The extensions of the six heaters caused the electron beam to be deflected and to wander away from the joint. During weld repetition, the heater ends were shielded, thus preventing the interaction of the heater ends with the electron beam.

The thermal energy unit as it appeared at this stage of the manufacturing process and prior to its filling with the thermal energy storage material is shown in Figure 52.

3.2 LOADING OF THERMAL ENERGY STORAGE UNIT WITH TES MATERIAL

3.2.1 EVALUATION OF LOADING PROCEDURES

During the initial design of the thermal energy storage demonstration unit, it was planned to fill the unit with the thermal energy storage salt by first casting it in a casting form made of Mullite tubing. The Mullite tubing was acquired early in the program with the selected tube sizes

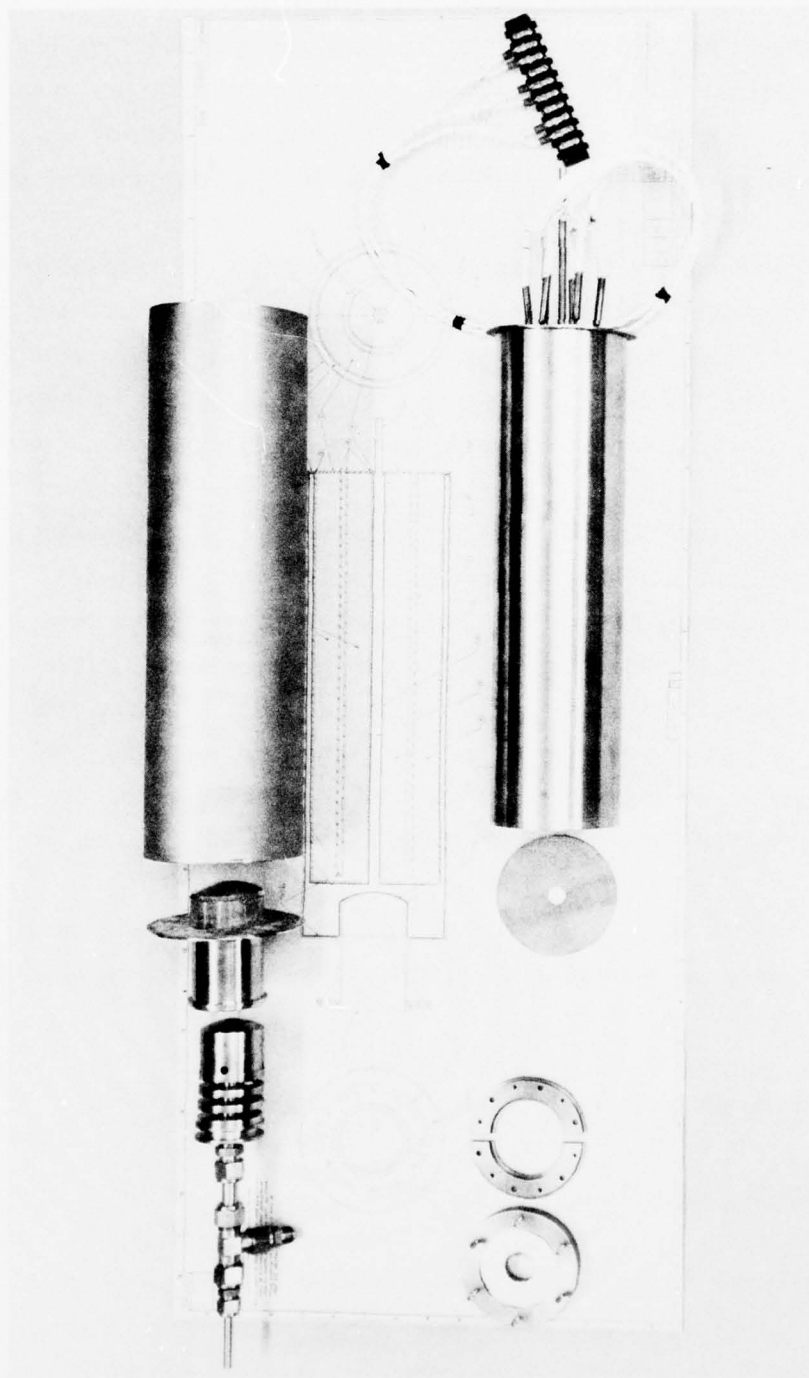


Figure 52. Thermal Energy Storage Unit Prior to Loading with Thermal Energy Storage Material

reflecting the optimum thermal energy storage unit design. When the initial thermal energy storage unit design had to be modified to reflect the availability of material, no standard Mullite tubing could be found that would permit the casting of the thermal energy storage salt to the desired sizes.

When several alternatives to filling the unit with its thermal energy material were considered, the melting of the ternary salt directly in the unit was investigated. The correct amount of the three reagent grade, chemically pure salts, LiF, MgF_2 , and KF, which are available in powder form would be poured into the unit in their correct combination and the six heaters would be used for melting the mixture directly in the unit.

To evaluate the casting process, a small container was made of Inconel 600 tubing. The volume of the container was sized to hold 100 grams of the eutectic mixture in powder form which occupies about three times the volume of the eutectic in solid form. One hundred grams of the salt mixture in powder form was measured to occupy 92 milliliters.

The container was surrounded by a shell heater which was controlled with a variac. Two thermocouples were placed at the bottom and along the side of the container. The output of the thermocouples was read on a digital voltmeter and also continuously displayed on a chart recorder. The results of a typical melt are shown in Figure 53, indicating the smallest rate of increase in temperature at 1310°F during the melting process. After the rate of increase in the temperature had increased again for 6 minutes the heaters were shut off.

After melting the mixture of the three components of the eutectic, LiF, MgF_2 , and KF, the occupied volume of the container was only one-third of its total volume. Successive additions of the powder mixture to the initial melt should have made it possible to fill the container with

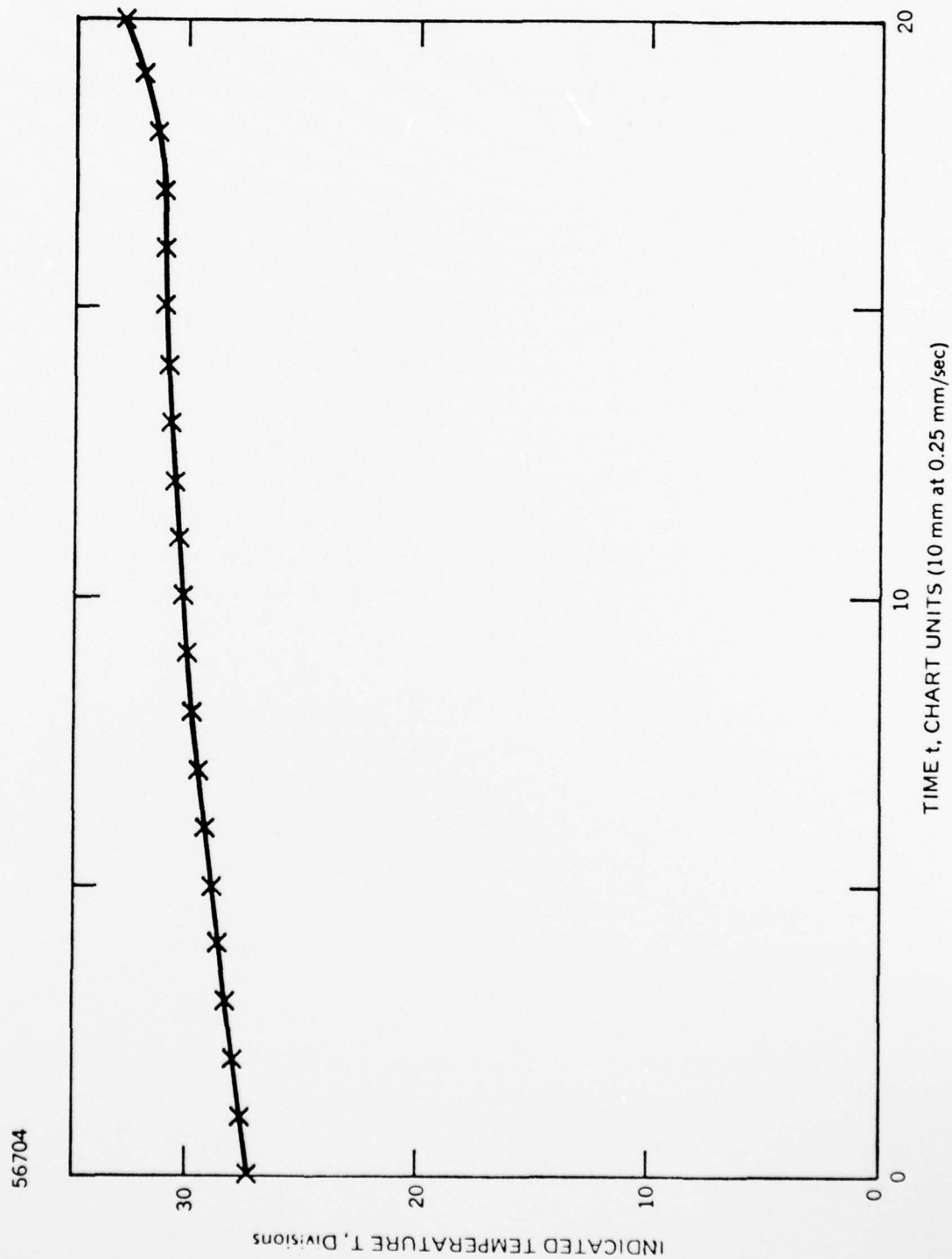


Figure 53. Temperature of Thermal Energy Storage Material Capsule During Melt-down

300 grams of eutectic salt. This proved to be correct. However, during the filling process, the surfaces of the container at the upper edges were considerably contaminated.

Inspection of those surfaces indicated that if welding would have been intended without danger of inclusion of contaminants remachining would have been required. The test indicated the need for rework of the TES unit after filling with the TES material, if the unit would have been filled by casting the material in the unit itself.

As the risk of damaging the hardware by the above outlined filling approach appeared to be high, it was decided to perform the casting in a casting fixture as had originally been intended.

3.2.2 CASTING OF TES MATERIAL

For the casting of the thermal energy storage salt, a casting fixture was machined from graphite (grade AGSX) which was secured from Union Carbide Corporation. The casting fixture was sized for casting one-third of the total thermal energy storage salt in each heat in a brazing retort. The casting fixture design is shown in Figures 54 and 55, while the finished machined parts of the fixture are shown in Figure 56.

The retort could be heated with an inert gas or in a hydrogen atmosphere. An argon atmosphere was selected for the casting to prevent any chemical reaction with the three salts, LiF, Mg_2F , and KF. The temperature was raised to $1350^{\circ}F$, which is about $40^{\circ}F$ above the melting temperature of the ternary eutectic, and was held at this temperature for about 1 hour to ensure full melting.

A total of four casts were made to account for a possible failure of a cast and to assure sufficient amount of salt available for filling the TES unit.

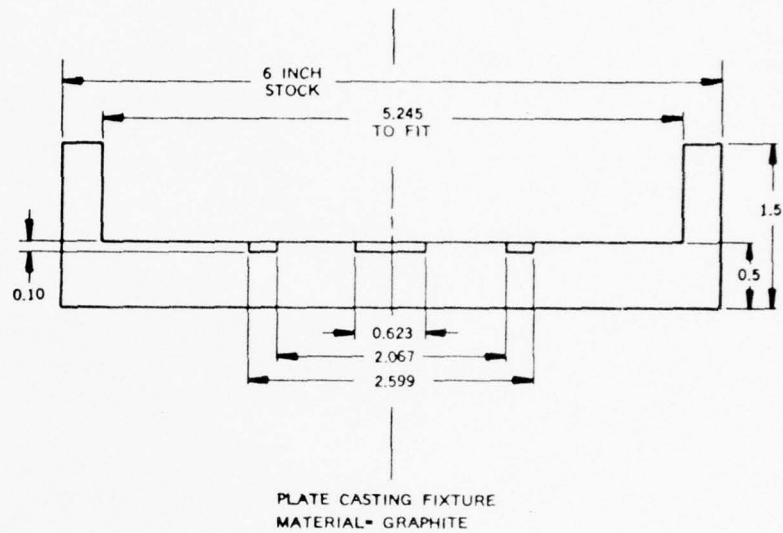


Figure 54. Bottom Plate of Casting Fixture SK2340-004-1
Material: Graphite

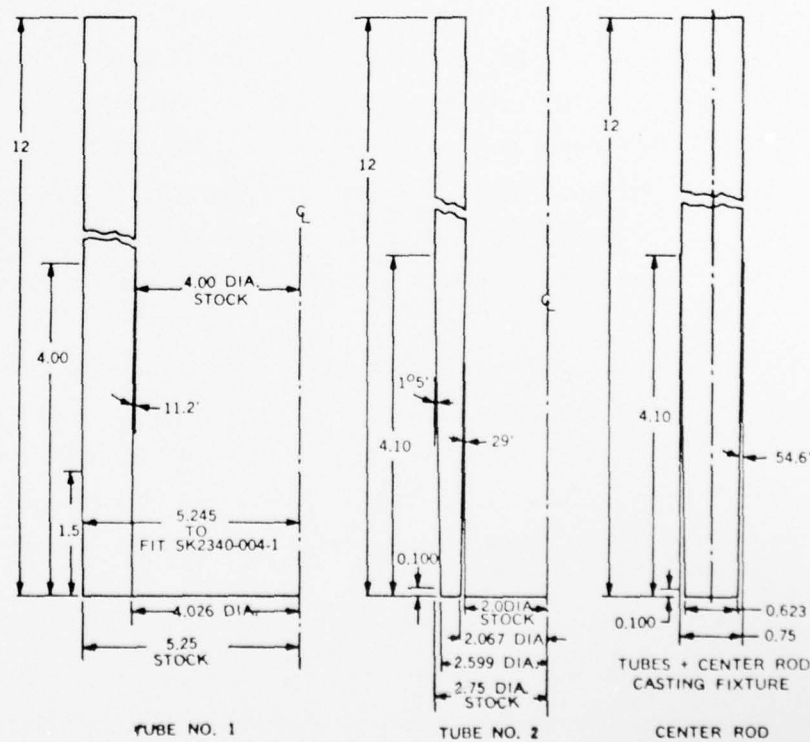


Figure 55. Tubes and Center Rod of Casting Fixture SK2340-004-1

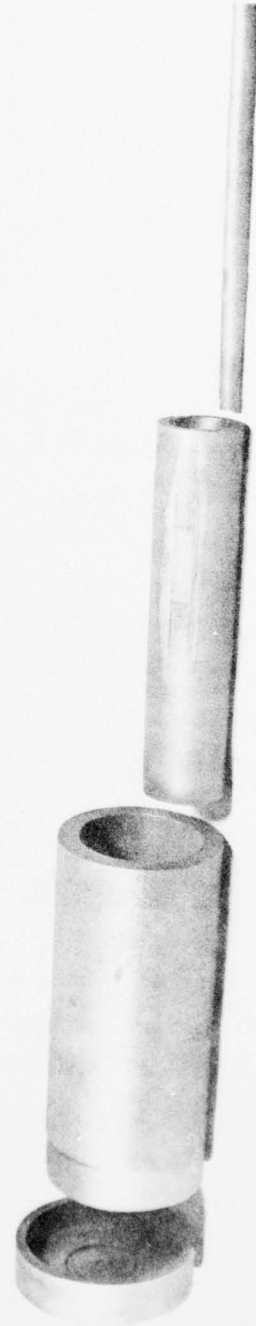


Figure 56. Casting Fixture (Exploded View)

after the casting. This proved to be a very prudent precaution as the cast turned out to be short by several grams. Furthermore, the resulting pieces of the salt showed voids in the center. The salt appeared to have solidified from the bottom as well as from the top, leaving the center portion full of voids between a large solid bottom piece and a small solid top piece. This could have been avoided by forcing cooling to proceed from the bottom of the cast, which may have been achieved by forcing the inert gas around the bottom of the test fixture during cool-down and by partially insulating the top part by increasing the thickness of the graphite.

The casting process of the thermal energy storage material in this project varied from the process used by General Electric in an earlier program for casting single solid pieces. At General Electric, the material was cast in a vacuum with shell heaters surrounding the single tube. After the material had become molten, the casting fixture was lowered with the heaters remaining in place. Thus, the lower portion of the fixture was cooled while the upper portion remained hot and no voids could form. This was a relatively expensive casting process as a vacuum chamber was contaminated by the very corrosive vapors of the salt and had to be thoroughly cleaned after its use.

3.3 FINAL ASSEMBLY OF THE THERMAL ENERGY STORAGE DEMONSTRATION UNIT

After the thermal energy storage demonstration unit had been loaded with the cast TES material, the final two welds of the container were completed. Unfortunately, at this stage of the manufacturing process it was not possible to leak check the final two welds. Following the two welds, wicking material, consisting of several layers of bolting cloth of 70 mesh, was applied to the inner surface of the outer tube of the TES unit. On the outer surface of the storage container, the flanges, and the hot cylinder. The distribution of the wick material is shown in Figure 57. Wherever wicking material was covering a heat transfer surface, the thickness of

AD-A040 895

XEROX CORP/ELECTRO-OPTICAL SYSTEMS PASADENA CALIF
THERMAL ENERGY STORAGE DEMONSTRATION UNIT FOR VUILLEUMIER CRYOG--ETC(U)

F/G 10/2

FEB 77 R RICHTER

F33615-75-C-2045

UNCLASSIFIED

2340-I-1

AFAPL-TR-76-110

NL

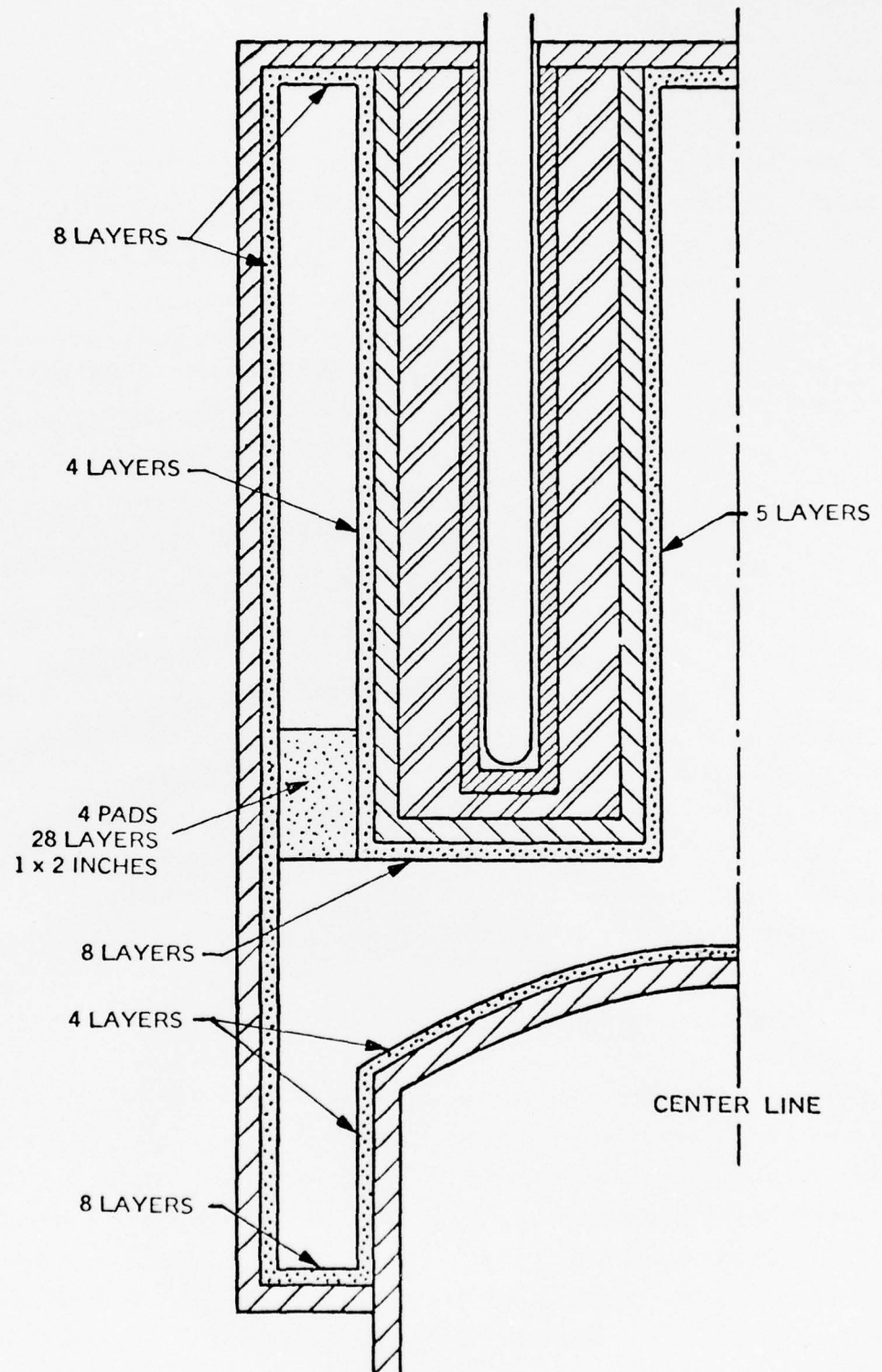
2 OF 2

AD
A040895



END

DATE
FILMED
7-77



56684 A

Figure 57. Distribution of Wick Material Consisting of Mesh 70 Bolting Cloth

wick was made not larger than four layers of bolting cloth. All other surfaces were covered with eight layers of bolting cloth. The appearance of the thermal energy storage unit with all internal surfaces covered with the wicking material is shown in Figure 58. The locations of the eight pads which bridge the outside wick with the wick of the TES container are evident in this picture.

The assembly of the thermal energy storage unit was completed with the welding of the outer tube to the hot storage container. The completed thermal energy storage demonstrated unit is shown in Figure 59.

Sixteen nickel-chromium versus nickel-aluminum thermocouples were placed on the inside and the outside of the thermal energy storage unit. The locations of these thermocouples are shown in Figure 60. The outside thermocouples were attached to the surfaces by spot welding stainless steel ribbons to the Inconel over the thermocouple naked junctions. The thermal energy unit was then wrapped with five layers of 3/8-inch Flexible Min-K insulation and one layer of 1/2-inch 8 pound weight Cerafelt insulation. The insulation was completed with one wrap of aluminum foil. The predicted thermal losses for the thermal energy storage demonstration unit with this type of insulation are shown in Figure 61. The completely insulated TES unit ready for filling of its heat pipe with sodium is shown in Figure 62.

3.4 FILLING OF HEAT PIPE WITH WORKING FLUID

Based on the modified thermal energy storage demonstration unit design, the theoretical total wick volume was calculated to be 27.383 inches³. For a wick constructed of a 70 Mesh wire screen, woven with a 0.00375 inch diameter wire, the void volume that is filled with sodium comprises 79.67 percent of the total wick volume. Thus, a sodium volume of 21.82 inches³ was indicated for filling the heat pipe section of the thermal energy storage unit. At the operating temperature of 1250°F, the specific weight of sodium is 0.7896 g/cm³, which determined the total weight of the fill to

37626

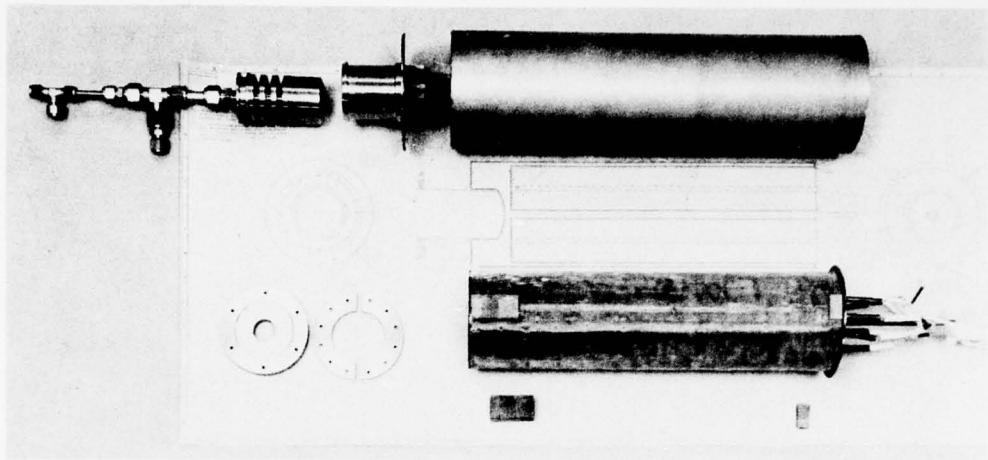


Figure 58. TES Demonstration Unit after Application of Wicking Structure and Prior to Final Welding

4765

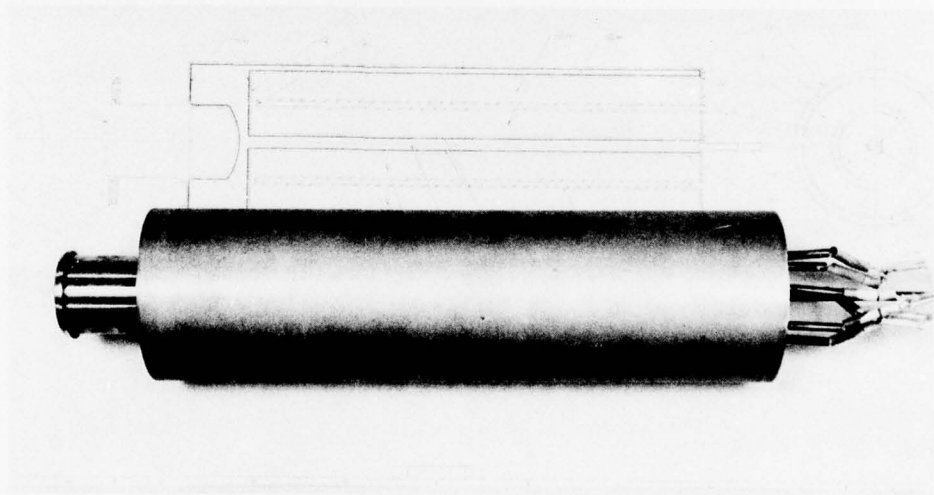


Figure 59. Completed Thermal Energy Storage Demonstration Unit

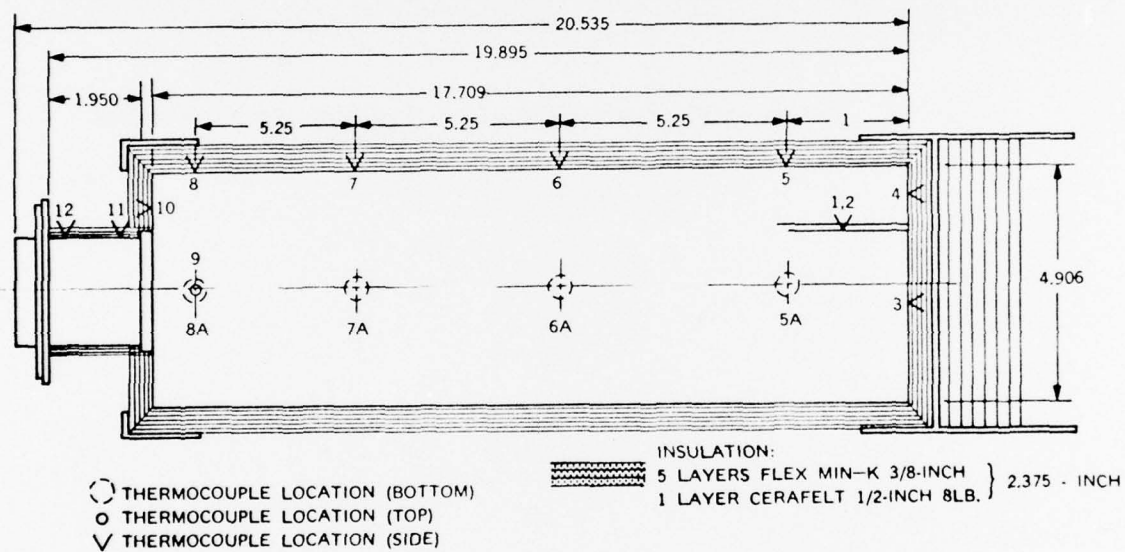


Figure 60. Insulation and Thermocouple Locations of Thermal Energy Storage Demonstration Unit for Vuilleumier Cooler Application

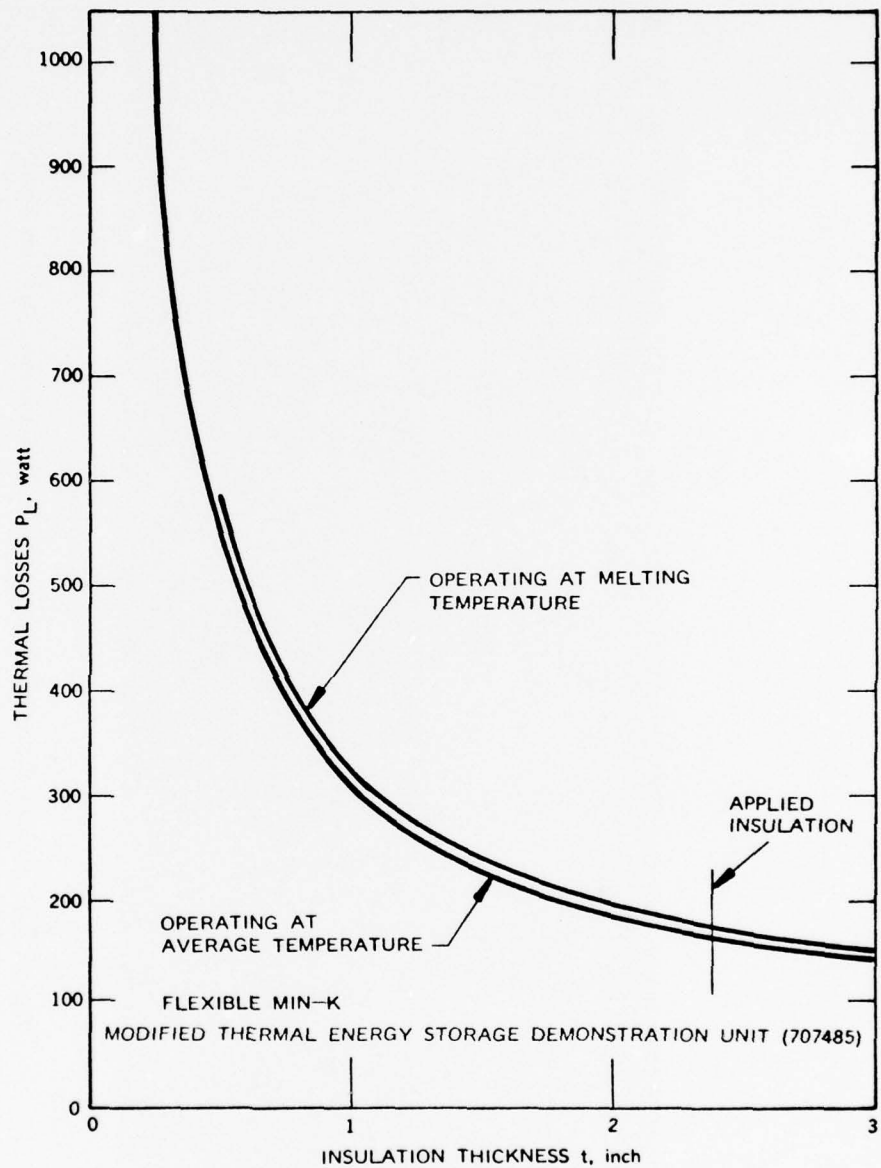


Figure 61. Predicted Thermal Losses from Thermal Energy Storage Demonstration Unit

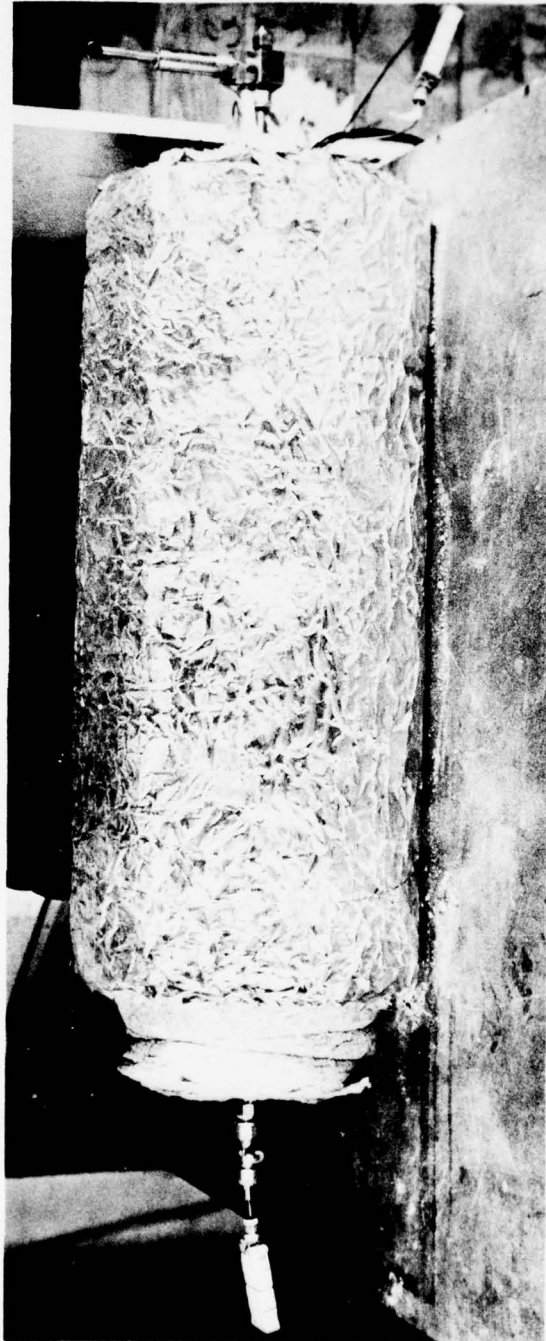


Figure 62. Fully Thermally Insulated TES Demonstration Unit

be 282.3 grams. Since the sodium was to be filled at a temperature of 320°F, at which the specific weight of the sodium is 0.913 gm/cm³, a calibrated fill volume of 18.523 inches³ was needed.

A fill volume was built from a stainless steel tube which had an O.D. of 1.250 inch, a wall thickness of 0.065 inch, and a length of 18.801 inch. The tube was weighed prior to and after filling it with sodium. The total amount of sodium in the tube was slightly more than 282.3 grams (i.e., 284.8 grams) because of the additional volume in the 1/4-inch tubes at the top and the bottom of the fill volume. After transferring the sodium into the thermal energy storage unit, the weight of the fill volume indicated that the heat pipe section had been filled with 281.1 grams of sodium.

It was attempted to fill the heat pipe section fairly accurately with the calculated required amount of sodium, although realistically the exact amount of sodium needed could not be verified until the thermal energy storage unit had been operated. Of all the individual wick volumes which comprise the total volume of the sodium, the eight layers of screen on the inner surface of the outer tube is the largest. Its calculated volume is 15.631 inches³ comprising 57.1 percent of the total calculated wick volume alone. As it is difficult to achieve a perfect wick of consistent void volume with bolting cloth, the required amount of sodium for filling the the wick without surplus or dryness in certain areas has to be established by testing the heat pipe.

With the filling of the heat pipe with the working fluid the fabrication tasks were completed and the thermal energy storage unit was ready for testing.

SECTION IV
TESTING OF THERMAL ENERGY STORAGE DEMONSTRATION UNIT

4.1 TEST SETUP

With completion of its fabrication the Thermal Energy Storage Demonstration Unit was integrated into the test setup which is shown in Figure 63. The thermal energy storage demonstration unit had been supplied with six individual heaters grouped in sets of two. The two heaters in each set were operated in parallel with each other, with their power being controlled by a variac. The average resistance of each heater was 18 ohms, so that at an applied voltage of 110 volts the power input was about 672 watts per heater for a possible total power input of about 4000 watts with all six heaters. Thus, even with only two heaters operating, it was possible to charge the thermal energy storage unit within one hour.

The three variacs could be adjusted and their power output determined by three sets of 1 percent full scale accurate ammeters and voltmeters. For controlling the temperature of the thermal energy storage unit, a temperature controller was used to turn off the power to the unit if the preset temperature was exceeded and to turn on the power when the temperature of the unit dropped below a preselected temperature.

While the temperature of all sixteen thermocouples could be determined from the output of a digital voltmeter, twelve of the temperatures were recorded continuously on a 24 point chart recorder. The gas flow for cooling the hot cylinder was controlled by the upstream pressure of a sonic orifice, and by observing the pressure downstream of the orifice to assure that, at all times during a test, sonic conditions at the orifice would exist. The pressures were measured with 1/2 percent accurate Bourdon pressure gages which can be seen in Figure 64.

5762

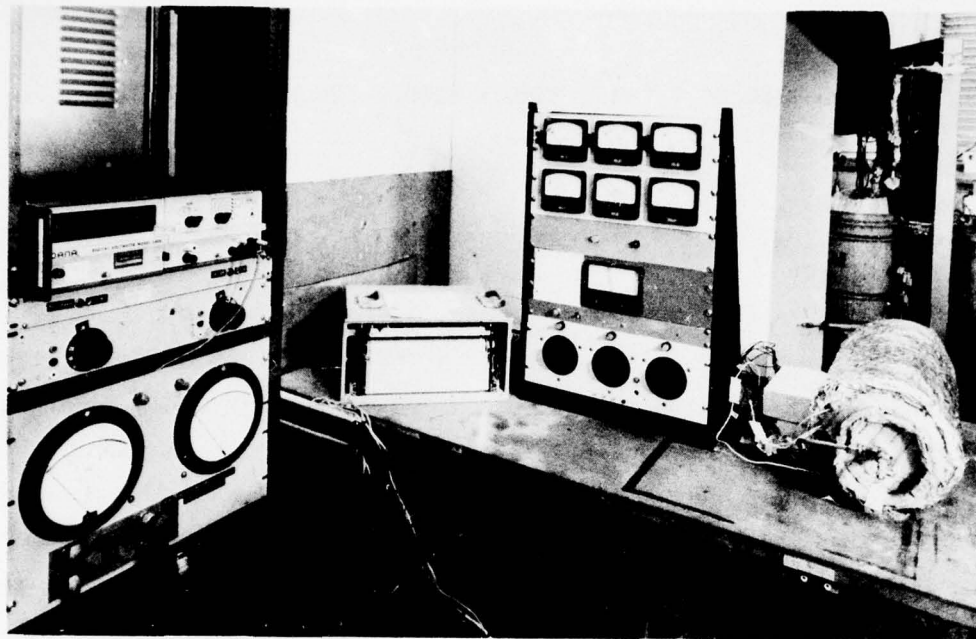


Figure 63. Thermal Energy Storage Demonstration Unit Test Setup
(View I)

5761



Figure 64. Thermal Energy Storage Demonstration Unit Test Setup
(View II)

4.2 INITIAL TESTING

After completion of the test setup and the instrumentation of the thermal energy storage unit, testing of the unit was initiated. The first objective was to measure the steady state thermal losses from the unit as a function of the operating temperature, and to determine the effective thermal capacity of the unit, $(W c_p)_{\text{eff}}$.

4.2.1 STEADY STATE THERMAL LOSSES AND THERMAL CAPACITY

4.2.1.1 Time Constant and Steady State Thermal Losses

The thermal energy storage unit comprises the main structure, the wick material, the heat pipe working fluid, sodium, and the thermal energy storage salt. The effective thermal capacities of the four components are:

Structural Material (Inconel)	1.865 B/ ^o F	27.80%
Thermal Energy Storage Salt	4.459 B/ ^o F	66.48%
Sodium	0.190 B/ ^o F	2.88%
Wick Material	<u>0.193 B/^oF</u>	<u>2.83%</u>
Total	6.707 B/ ^o F	100.00%
	7.076 x 10 ³ joules/ ^o F	

During the solidification of the thermal energy storage salt, a total amount of thermal energy of 4.32×10^6 joules was expected to be released. It was predicted that the temperature of structural components of the thermal energy storage unit would decrease from 1275^o to 1235^oF, while the average temperature of the thermal energy storage salt would decrease from 1310^o to 1270^oF. The contribution of the sensible heat of the thermal energy storage unit would therefore be

$$\begin{aligned} E_{\text{sensible}} &= 4.459 \times 40 + 2.248 \times 50 = 290.76\text{B} \\ &= 0.307 \times 10^6 \text{ joules} \end{aligned}$$

This compares with the assumed total latent heat of the thermal energy storage salt of

$$E_{\text{latent}} = 4.32 \times 10^6 \text{ joules.}$$

The contribution of the sensible heat would thus be only 6.63 percent of the total thermal energy released.

The steady state heat losses from the thermal energy storage unit were to be obtained by correlating the power input with the steady state temperature of the unit. For predicting the time that would be required to bring the unit to steady state conditions, the time constant for the system had to be estimated.

The thermal losses at the average operating temperature of 1250°F of the thermal energy storage unit were calculated to be about 180 watts. These losses are slightly higher than those shown in Figure 21. Thermal losses from the fill valve, which was to be left on the unit until the operation of the unit had been verified, and the heat losses at the hot cylinder end had to be added to the calculated losses. The effective time constant was estimated from the calculated thermal capacity of $7.076 \times 10^3 \text{ j/}^\circ\text{F}$ and the predicted thermal losses at the operating temperature, i.e., 180 watt at $T = 1250^\circ\text{F}$, to be $t = 46.25 \times 10^3 \text{ sec}$ or 12.85 hours.

This indicated that the unit would require about two days to reach its steady state temperature at each test point. The test results are shown in Figure 65. Because of the long time constant, the plotted values are not absolutely accurate, as it would have required a considerably longer time than was available to obtain true steady state data. The process was speeded up by establishing the temperature loss correlation, estimating the losses at a given temperature, and adjusting the input power of the heaters to equal these losses when a given temperature was reached.

56685

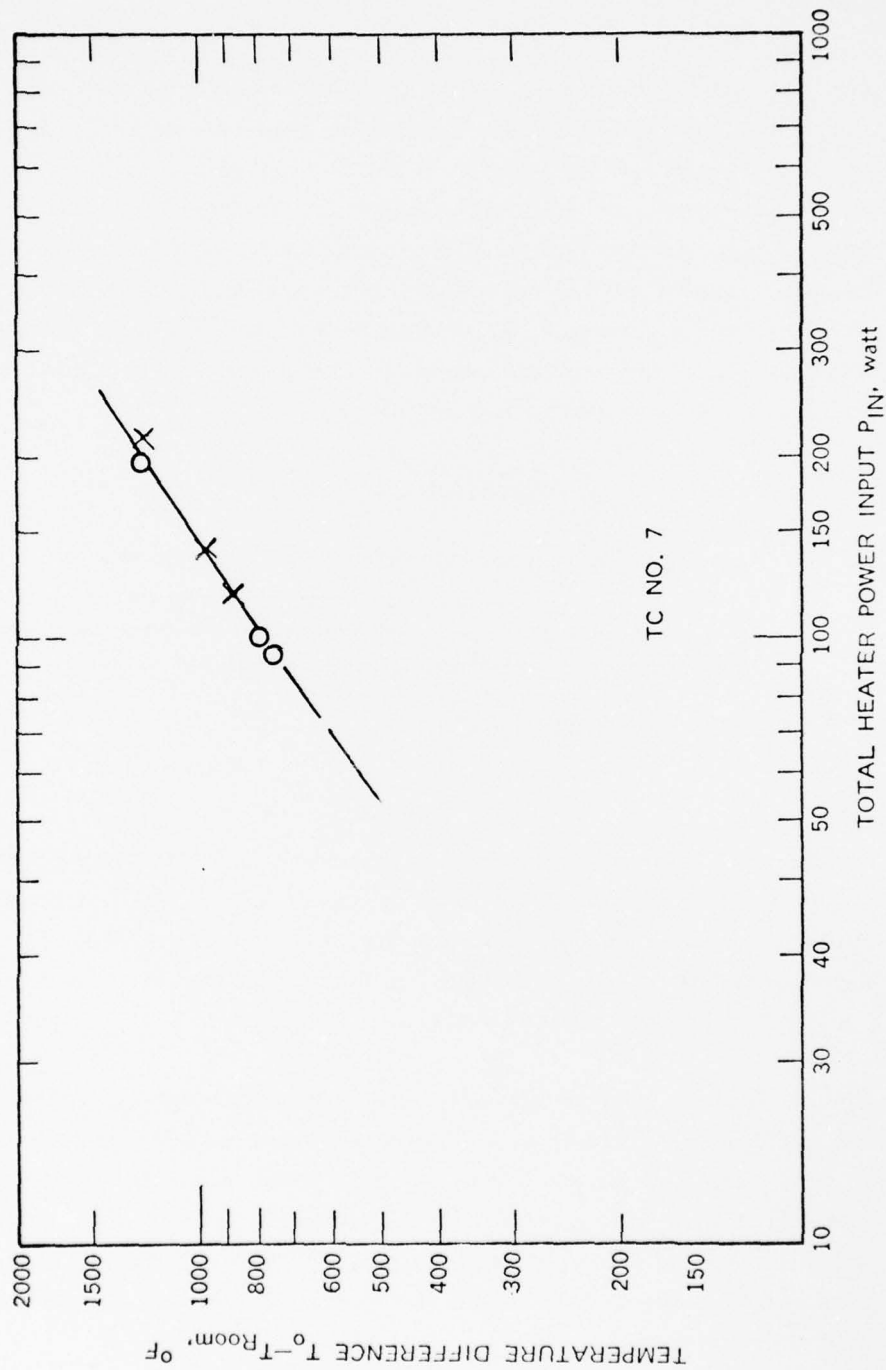
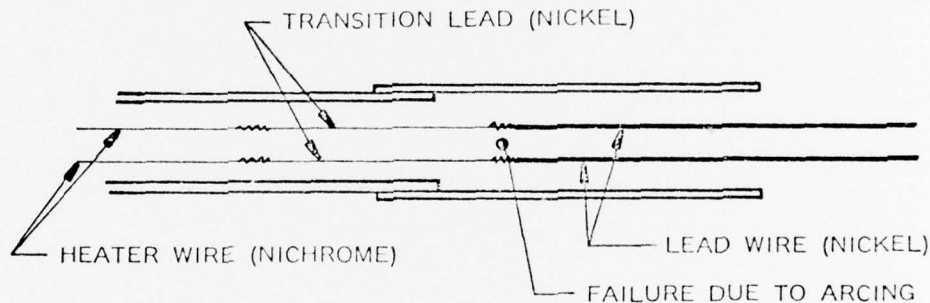


Figure 65. Energy Loss from Thermal Energy Storage Demonstration Unit (Insulation: 5 Layers 3/8-inch Flex Min-K, 1 Layer 1/2-inch 8 lb Cerafelt, 1 Sheet Aluminum)

During these initial tests, one of the three heater sets was used to supply the steady state power while the other two sets were employed to raise the temperature level. When the power of the two sets of heaters was raised for an average power output per heater of 162 watts (this compares with a design power output of 672 watts), three heaters failed almost simultaneously. Inspection of the heaters indicated that all three heaters had failed in the very same mode. Arcing between the two wires of each heater had occurred at the location where the transition wire had been welded to the lead wire, as shown in the sketch below.

56949



The heater vendor was contacted. Upon reviewing the heater design, the responsible manager conceded that a "human error" had occurred in the manufacturing process. It was felt that the remaining three heaters would not survive the planned testing, and that it would be appropriate to replace all heaters immediately with new heaters.

All six heaters were pulled out of the well after removing the insulation. New heaters from a different vendor were ordered and shipped from the east. Although the new heaters had the same power capacity as the original heaters, their power loading was considerably higher than that of the original heaters because each heater was only 29 inches long. This compared with the 70 inch length of the original heaters. Each heater was

bent into a hair pin and pushed into the heater well of the thermal storage unit. After replacing the insulation, testing of the thermal energy storage unit was continued.

During testing of the thermal energy storage unit, two of the six heaters of the second set of heaters failed by shorting internally to a dead short, although remaining isolated from the sheath. The vendor of the heaters was contacted who explained the failure by an accumulation of moisture at the cold end of the heater (i.e., the non-heated extension of the lead wires) where the short between the two lead wires occurred. He asked for the return of all six heaters for repair without charge. It was agreed that the heaters would be returned after completion of testing with the remaining four heaters. Since each heater had a capacity of over 1700 watts, ample capacity remained for continuing testing. The steady state heat loss data were found not to vary substantially from the original test data; indicating that the insulation was the same as before. The heat loss could be expressed as a function of temperature by

$$P_L = A(\Delta T)^n$$

where

P_L = power loss, watt

$A = 3.318 \times 10^{-3}$

$n = 1.546$

ΔT = temperature difference $T_o - T_{room}$, $^{\circ}F$

4.2.1.2 Thermal Capacity

With the correlation of the thermal losses against the operating temperature known, the effective thermal capacity of the thermal energy storage unit could be determined by the relation

$$(c_p W)_{eff} = \frac{(P_{in} - A \times (\Delta T)^n - P_{out}) dt}{dT}$$

where

$(c_p W)_{\text{eff}}$ = Effective sensible heat of the entire unit

P_{in} = Power input supplied by the electric heaters

P_{out} = Power extracted through the hot cylinder by cooling gas flow

A, n = Constants determined from steady state energy losses from the thermal energy storage unit

ΔT = Temperature difference between thermal energy storage unit temperature and ambient temperature

This relation was computerized to permit calculation of the effective thermal capacity, thermal losses, and power output. The required input data were the electrical power input and operating temperature of the unit at given time intervals.

Below and above the eutectic temperature of the thermal energy storage material the effective thermal capacity was expected to be relatively constant showing only a slight increase with increasing temperature. At the eutectic temperature, the effective heat capacity should, in the ideal case, approach infinity, as thermal energy is either stored or absorbed without increase in temperature. The computer program was expanded to also permit calculation of the energy extracted from or stored by the thermal energy storage material and the structural material of the thermal energy storage unit, and the total thermal energy extracted as a function of the temperature or the thermal energy storage unit.

4.2.2 TEST DATA EVALUATION

4.2.2.1 Sensible Heat Capacity

After the initial tests, which provided the correlation between the temperature of the thermal energy storage unit and the thermal losses from

the unit, the unit was heated to a temperature that was assumed to be below the eutectic temperature of the thermal energy storage material. The maximum measured heater well temperature was 1303°F with a power input of 214 watts. Thus, no storage of thermal energy in form of latent heat of fusion should have occurred and all energy that would be released due to thermal losses from the unit through the insulation would be the total sensible heat of all materials of the unit. By determining the temperature of the unit as a function of time and applying the relation shown on page 42 it should be possible to verify the calculated thermal capacity of the unit, which must be known for evaluating the thermal capacity of the thermal energy storage material.

The measured correlations between thermal energy storage temperature and time are shown in Figures 66 and 67. The plotted test results immediately indicated that the temperatures do not correlate in the expected manner. Due to the higher thermal losses at the higher temperatures, a steeper drop in temperature at the beginning of the cooling cycle would have been predicted if the unit had a relatively constant thermal capacity. On the other hand the data indicated a much larger thermal capacity at the higher temperature. When the data were reduced, the thermal capacity was found to increase with temperature as shown in Figure 68.

In Figure 69, the temperatures of the thermal energy storage unit are shown as they were measured during the heating of the unit. The appearance of the heating curve is very similar to the appearance of the cooling curves, indicating that the effective thermal capacity of the unit is the same whether measured during cooling or during heating.

The test data made it appear that the effective thermal capacity of the thermal energy storage unit increased with increasing temperature. At the average operating temperature of $T = 650^{\circ}\text{F}$, the effective thermal capacity of the unit appeared to be $7.22 \times 10^3 \text{ joules}/^{\circ}\text{F}$. This compared with the predicted effective thermal capacity of $7.1 \times 10^3 \text{ joules}/^{\circ}\text{F}$, a variation of 1.7 percent. The abnormal behavior was evident from the cooling curves as

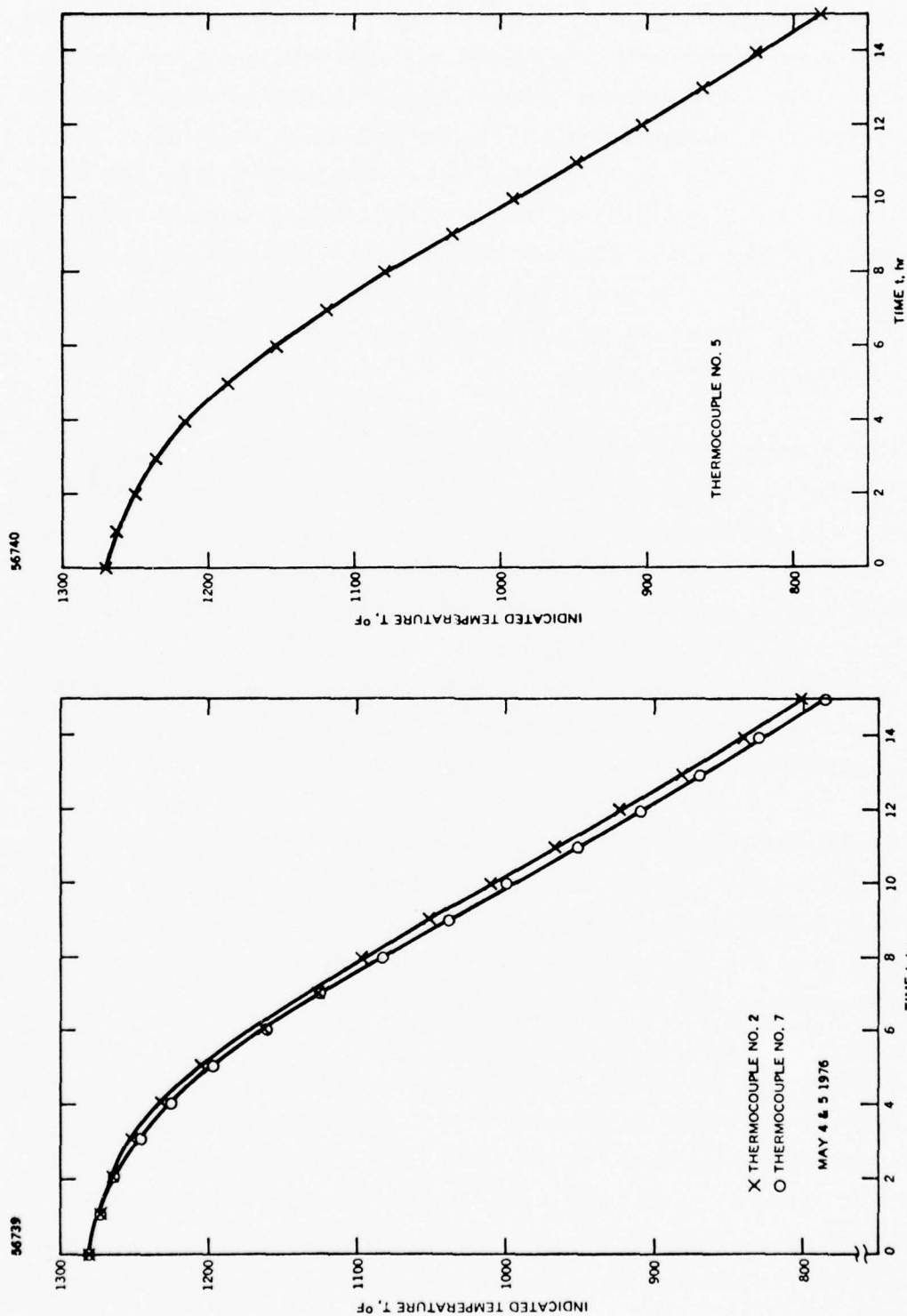


Figure 66. Temperature of Thermal Energy Storage Demonstration Unit During Cool-down

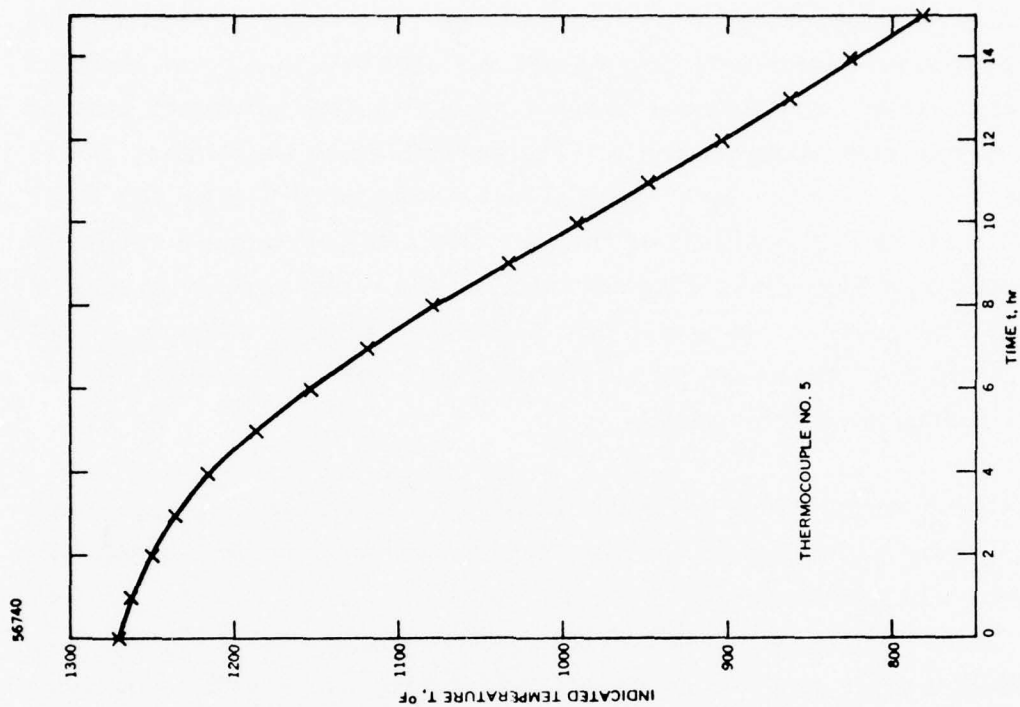


Figure 67. Temperature of Thermal Energy Storage Demonstration Unit During Cool-down

56724

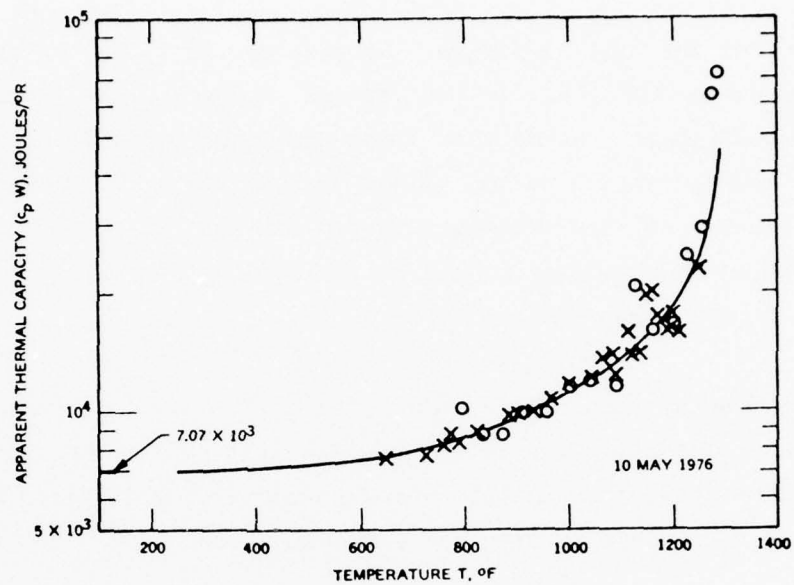


Figure 68. Apparent Thermal Capacity of Thermal Energy Storage Unit

56737

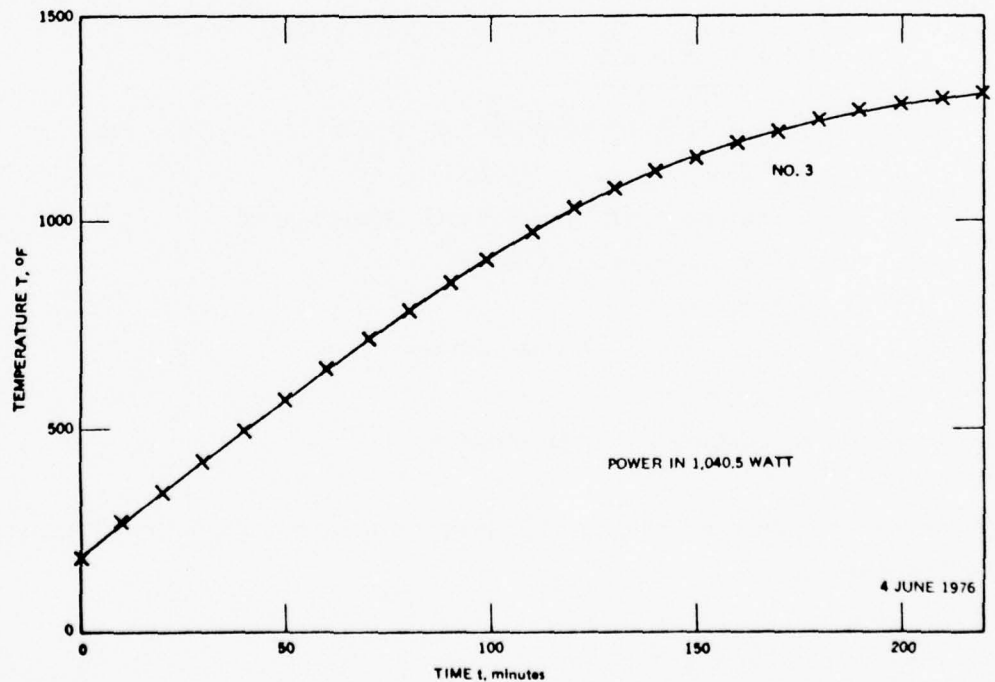


Figure 69. Measured Temperature of Thermocouple No. 3 During Charging of TES Unit

well as from the heating curves. Despite the fact that no melting should have occurred, the slope of the curves changed their trend only below 950°F, which lies considerably below the reported melting point of the thermal energy storage salt. It was thought that the variable effective heat capacity of the thermal energy storage unit could possibly be explained by the varying amount of the working fluid of the heat pipe, sodium, in the vapor state.

With increasing temperature, the amount of sodium in the vapor state increases. The effective total specific heat of the sodium vapor due to evaporation and/or condensation in the vapor volume is given by the change of latent heat capacity with temperature, i.e.,

$$(W c_p)_{\text{eff Na}} = dC_{\text{Na}}/dT \text{ joules/}^{\circ}\text{K} \quad (1)$$

where

$$C_{\text{Na}} = \frac{\Delta H \times p_v \times V \times M}{RT} \quad (2)$$

latent heat of evaporation content of sodium vapor in
the vapor volume, joules

ΔH = latent heat of evaporation, joules/gram

p_v = vapor pressure, dynes/cm²

V = volume, cm³

M = molecular weight, grams/mole

T = temperature, °K

R = gas constant, ergs/°K-mole

The vapor pressure of sodium can be expressed as a function of temperature by the relation

$$p_v = A \exp (-E/T) \quad (3)$$

where

$$\begin{aligned} A &= 3.363 \times 10^{10} \text{ dynes/cm}^2 \\ E &= 11973.4^\circ\text{K} \end{aligned}$$

The latent heat of evaporation can be found by employing Clapeyron's relation

$$\Delta H = T(v_1 - v_2) dp_v/dT \quad (4)$$

where

$$\begin{aligned} v_1 &= \text{vapor volume} \\ v_2 &= \text{fluid volume} \end{aligned}$$

Since

$$v_1 \gg v_2$$

the relation can be reduced to

$$\Delta H = T \times v_1 \times dp_v/dT \quad (5)$$

By differentiating relation 3 and employing the relation

$$p \times v = RT/M \quad (6)$$

the latent heat of evaporation can be found to be

$$\Delta H = RE/M \quad (7)$$

The effective thermal capacity of the sodium can then be expressed by

$$(c_p W)_{\text{eff Na}} = \frac{E \times (E/T - 1) \times V \times A \times \exp(-E/T)}{T^2} \text{ ergs/}^\circ\text{K}$$

The total volume V , of the vapor in the heat pipe of the unit was calculated to be 1243.9 cm^3 .

When the above relation was evaluated, as shown in the following tabulation, the change of state of the sodium was found to have only a minor effect on the apparent thermal capacity of the entire system. It could not explain the observed change in thermal capacity of the system.

<u>T, °K</u>	<u>300</u>	<u>500</u>	<u>750</u>	<u>1000</u>
$c_p W, \text{j}/^\circ\text{K}$	1×10^{-10}	1.8×10^{-4}	0.16	3.48

4.2.2.2 Latent Heat Capacity

After the completion of these initial tests, the temperature of the thermal energy storage unit was increased above the melting temperature of the thermal energy storage salt. The electric power to the heater was then turned off and the unit was permitted to cool solely by the losses through the insulation. The results of that test are shown in Figures 70 and 71. It can be seen that the solidification of the thermal energy storage salt started when the temperature of the thermocouple on the outside of the thermal energy storage unit reached 1280°F .

When the data were reduced to determine the amount of thermal energy extracted from the unit as function of time and temperature, the distribution of the total energy between sensible heat and phase change energy as shown in Figures 72 and 73 were found. The results seemed to indicate that the total phase change energy, which had been expected to consist primarily of the fusion energy of the thermal energy storage material, was not released within a $\pm 25^\circ\text{F}$ temperature range.

The thermal energy storage unit design called for a thermal energy storage of 4.32×10^6 joules in the form of fusion energy. The amount of thermal energy storage material required was based on a fusion energy of

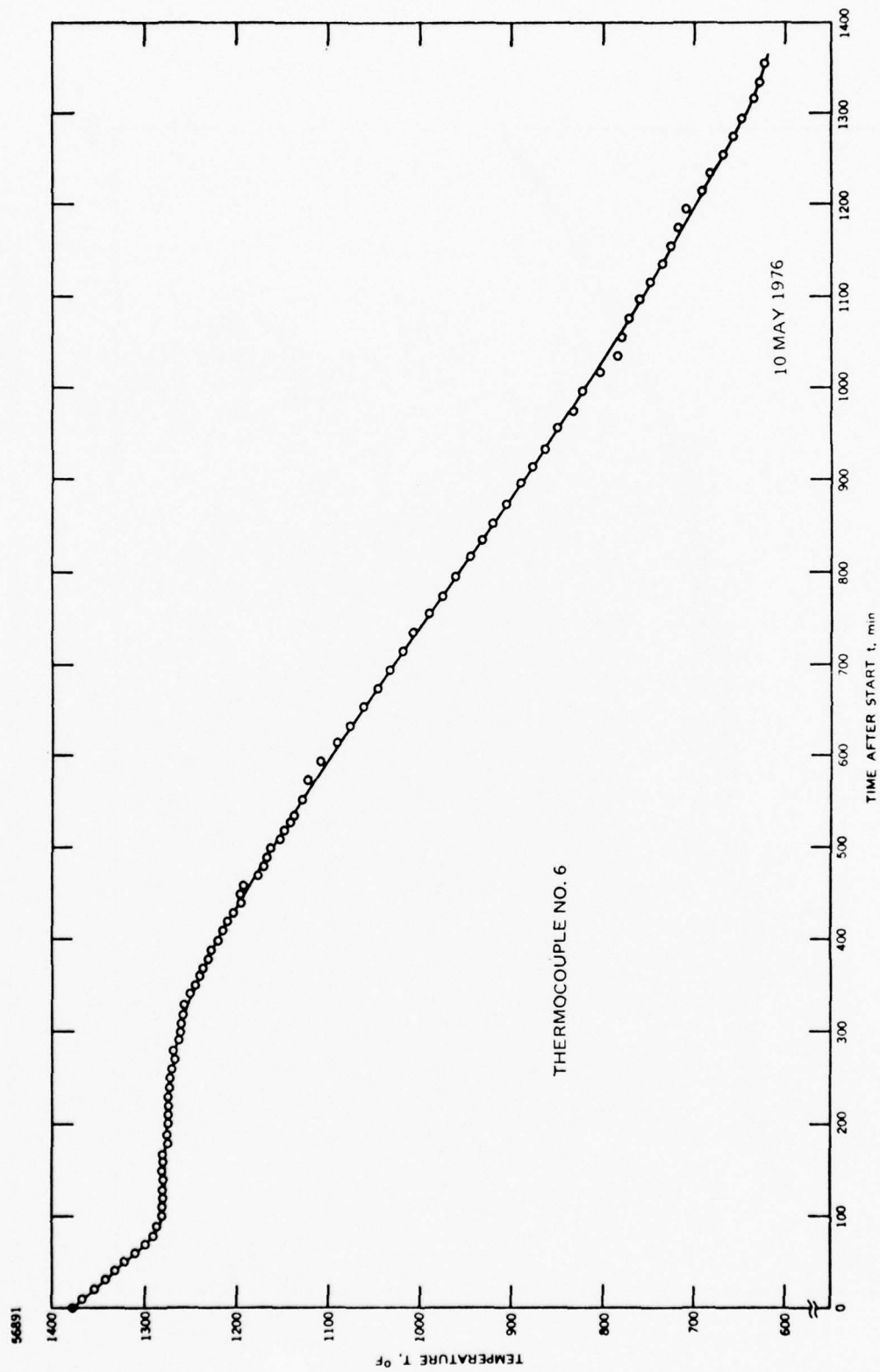


Figure 70. Cooling Data of Thermal Energy Storage Unit (Thermal Losses Only)

56738

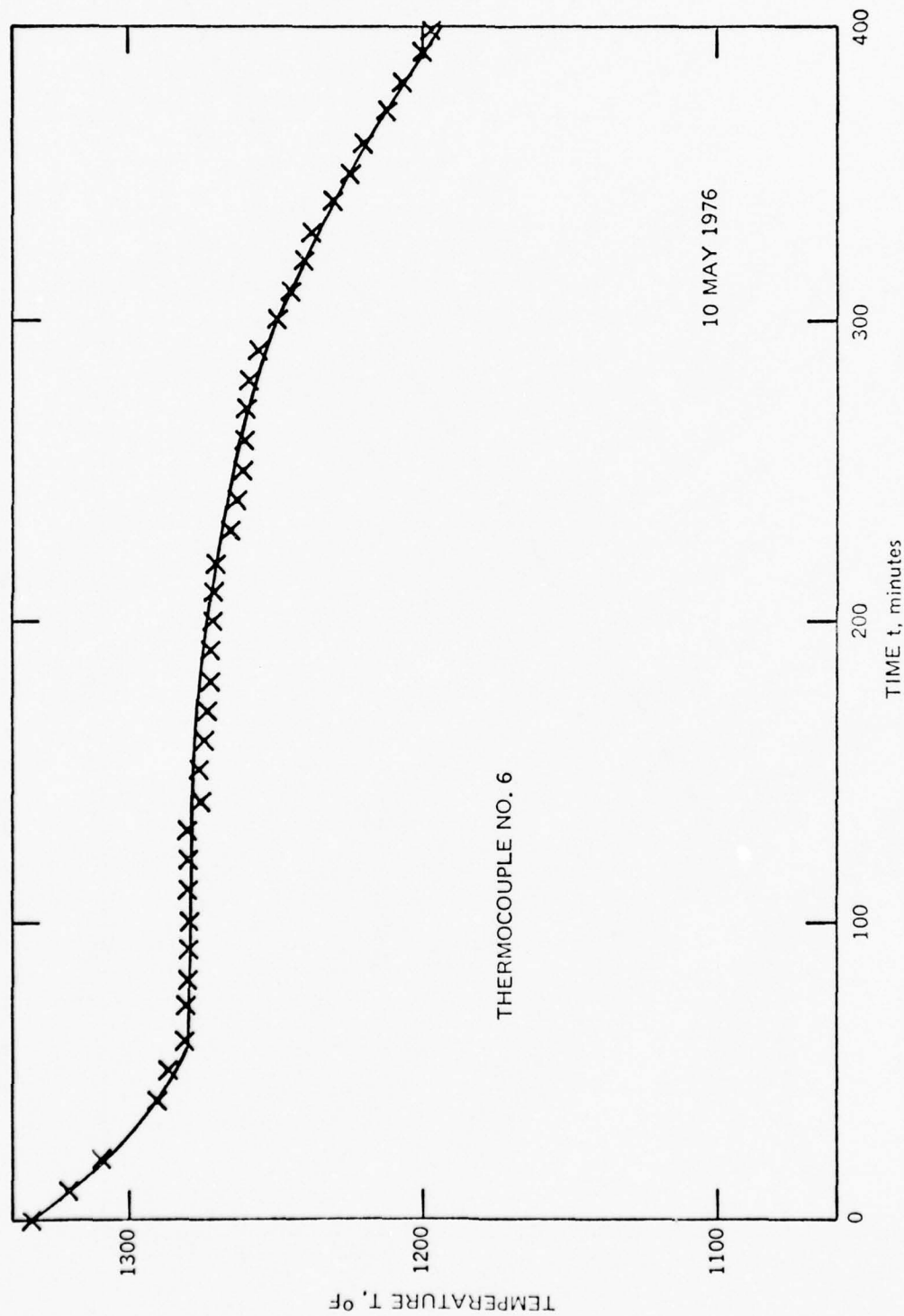


Figure 71. Temperature of Thermal Energy Storage Demonstration Unit During Cool-down

56734

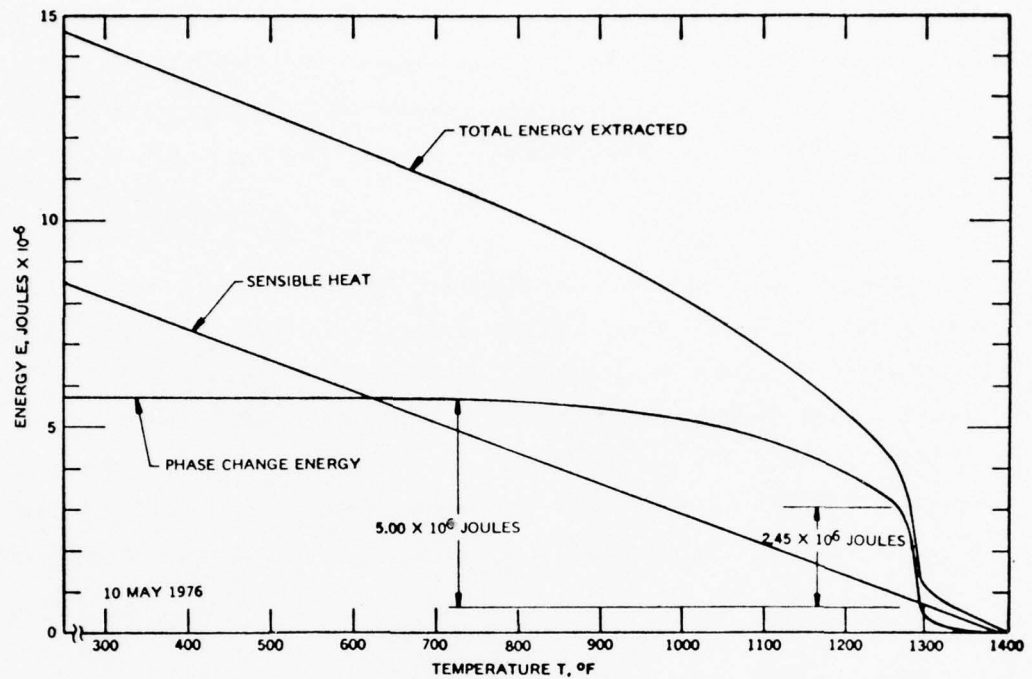


Figure 72. Extracted Energy (Cooling by Thermal Losses Only)

56729

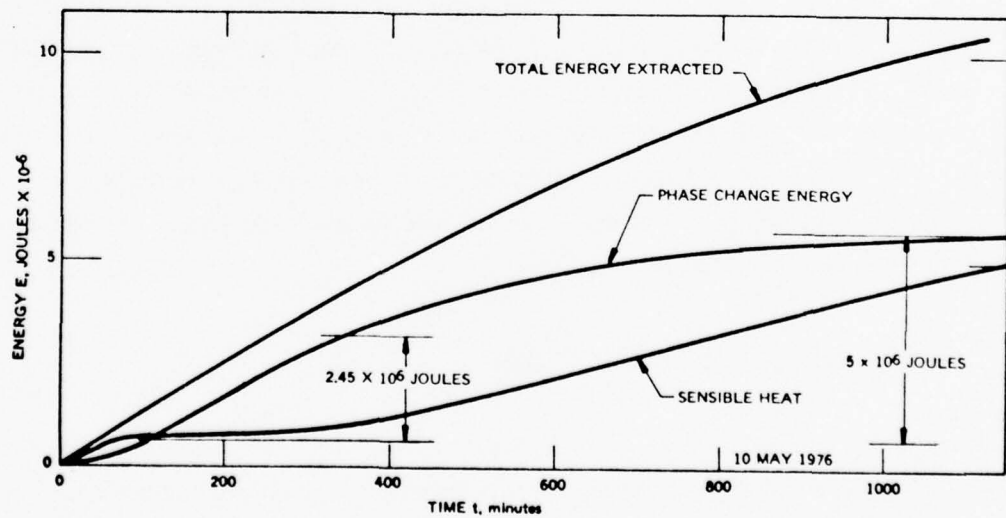


Figure 73. Extracted Energy (Cooling by Thermal Losses Only)

788.4 joules/gram (339.27 B/lb or 0.219 kW-hr/kg). This compares with the fusion energy of 944 joules/gram based on ideality of the ternary eutectic mixture of MgF_2 -LiF-KF. Based on ideality, the total fusion energy available in the thermal energy storage unit would have been 5.17×10^6 joules.

From the results plotted in Figures 72 and 73 it appears that only 2.45×10^6 joules of phase change energy was released over a temperature range of 50°F . This is about 56.7 percent of the design energy. The total amount of the design energy was extracted over a temperature range of 1285° to 1055°F , i.e., 230°F . The total amount of phase change energy appeared to be 5.07×10^6 joules. This is almost equal to the amount of energy that would have been calculated to be available as fusion energy based on ideality.

The same energy content in the TES salt as a function of temperature is exhibited in the heating curve as shown in Figure 74. This verifies that the energy content is independent of either the cooling or heating process of the salt.

The effective thermal capacity of the thermal energy storage unit as a function of time is shown in Figure 75. The curve shows two peaks in the effective thermal capacity of TES unit, one at about 1290°F and the other at 1165°F . At these two temperatures thermal energy is released with the smallest drop in temperature. It is not known what phase change coincides with the second peak at 1165°F .

4.2.2.3 Effect of Extraction Rate

The first evaluation of the thermal energy storage capacity was from test data obtained during a test in which the thermal energy storage unit was cooled only by its losses, which were a function of the temperature of the

56732

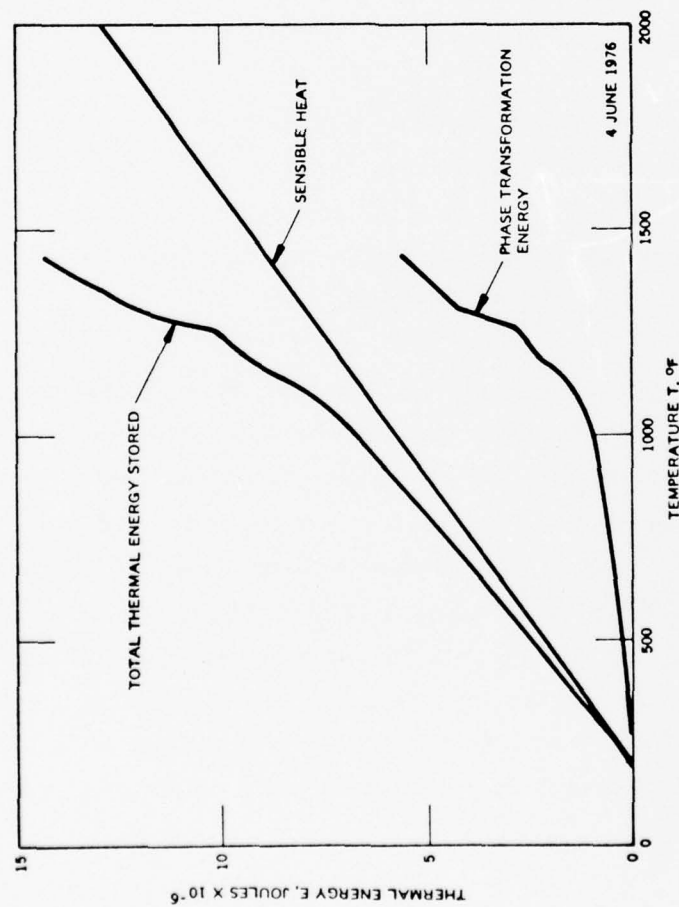


Figure 74. Amount of Stored Thermal Energy as Function of Temperature (Heating Curve)

56726

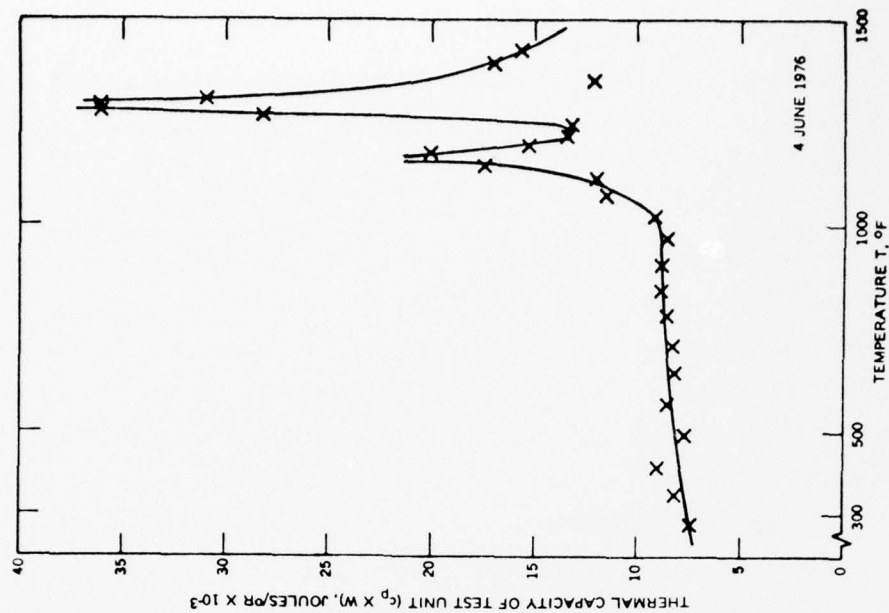


Figure 75. Apparent Thermal Capacity of Thermal Energy Storage Unit During Charging

unit. The initial loss was 213 watts decreasing with decreasing temperature, but remaining almost constant during the time at which the majority of the fusion energy was released.

Test results are shown in figures 76 and 77 of a test at which the initial total thermal power extraction from the unit was 555.6 watts. The power was extracted from the unit by losses through the insulation and by cooling the hot cylinder by an air flow of $\dot{W} = 0.76$ gram/sec. At the eutectic point the power extraction rate was 475 watts. In a third test whose test data are presented in Figures 78 and 79, the gas flow rate was $\dot{W} = 3.7$ gram/sec. At this flow rate the initial power extraction rate was 1799 watts, while at the eutectic temperature the extraction rate was 1067 watts, which was almost equal to the design extraction rate of 1200 watts, 200 watts of losses and 1000 watts of power carried away by the cooling gas in the hot cylinder.

When the amount of energy extracted from the thermal energy storage material is correlated with the extraction rate, no effect of the extraction rate on the evaluated amount of available thermal energy can be found. The variations in the reduced data are within the accuracy with which the temperatures and the times could be measured.

Thus, the test data indicated that the behavior of the thermal energy storage material selected for this application was different from that anticipated. While lithium fluoride liberated the entire fusion energy at a specific melting point, the ternary eutectic salt made up of MgF_2 , LiF , and KF , liberates phase change energy over a wide range of temperature. Since this temperature range was not known at the time of the design of the thermal energy storage unit, it was not included in the calculation of the temperature swing over which the hot cylinder would operate. Only the increasing temperature drop associated with the build-up of solidified thermal energy storage material had been considered. The overall effect of

56736

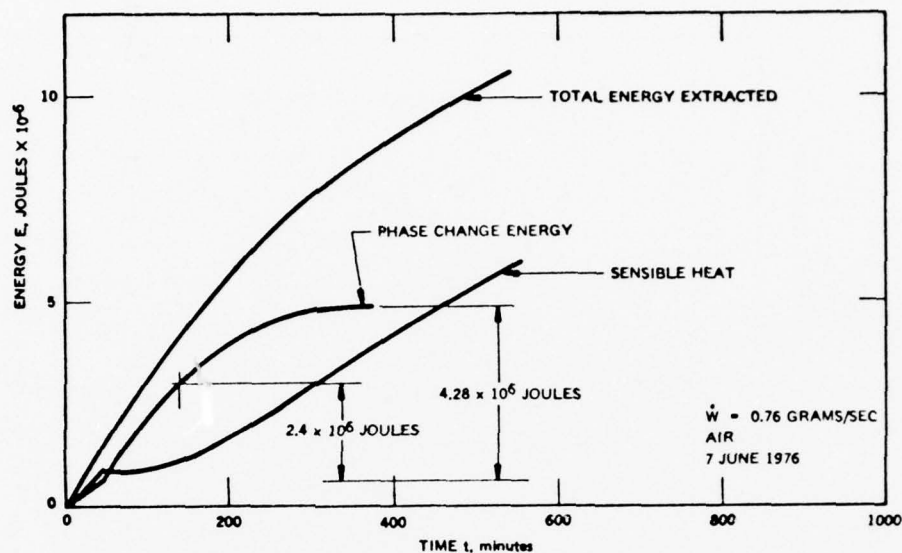


Figure 76. Extracted Energy (Cooling by Thermal Losses and by Simulated V/M Cooler Operation with Flowing Air)

56733

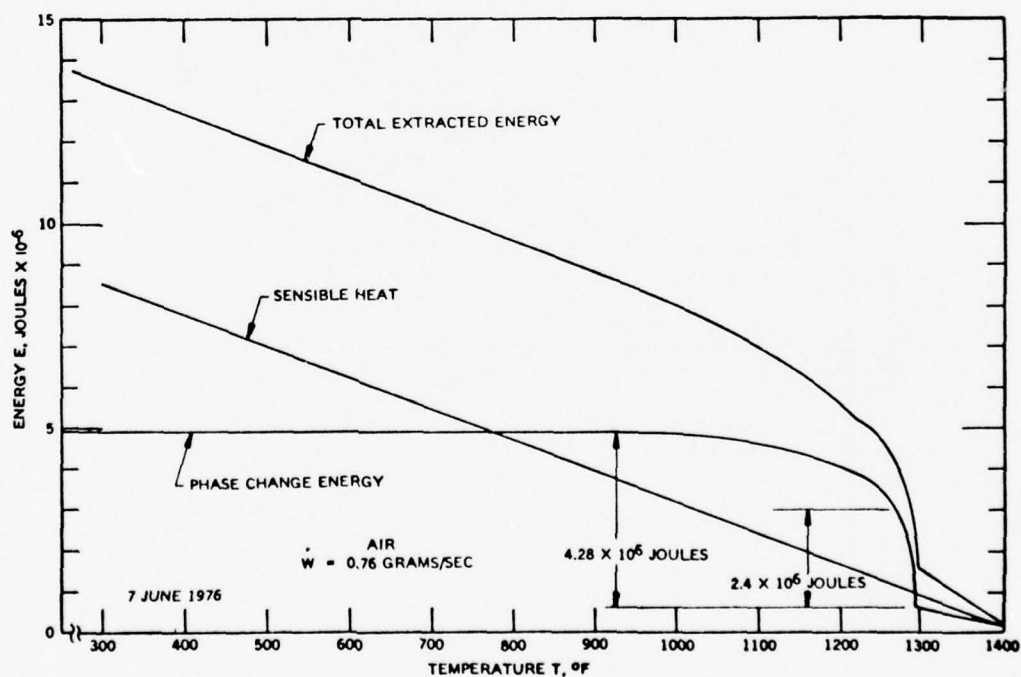


Figure 77. Extracted Energy (Cooling by Thermal Losses and by Simulated V/M Cooler Operation with Flowing Gas)

56728

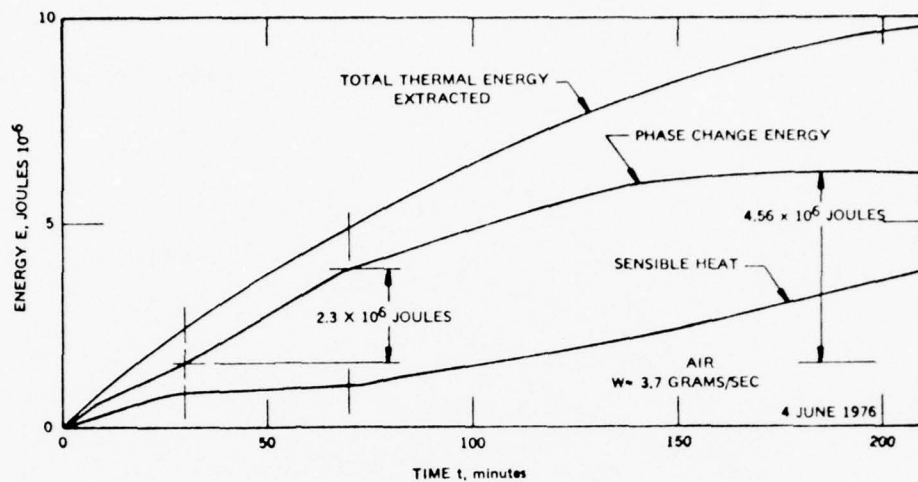


Figure 78. Extracted Energy (Cooling by Thermal Losses and by Simulated V/M Cooler Operation with Flowing Air)

56735

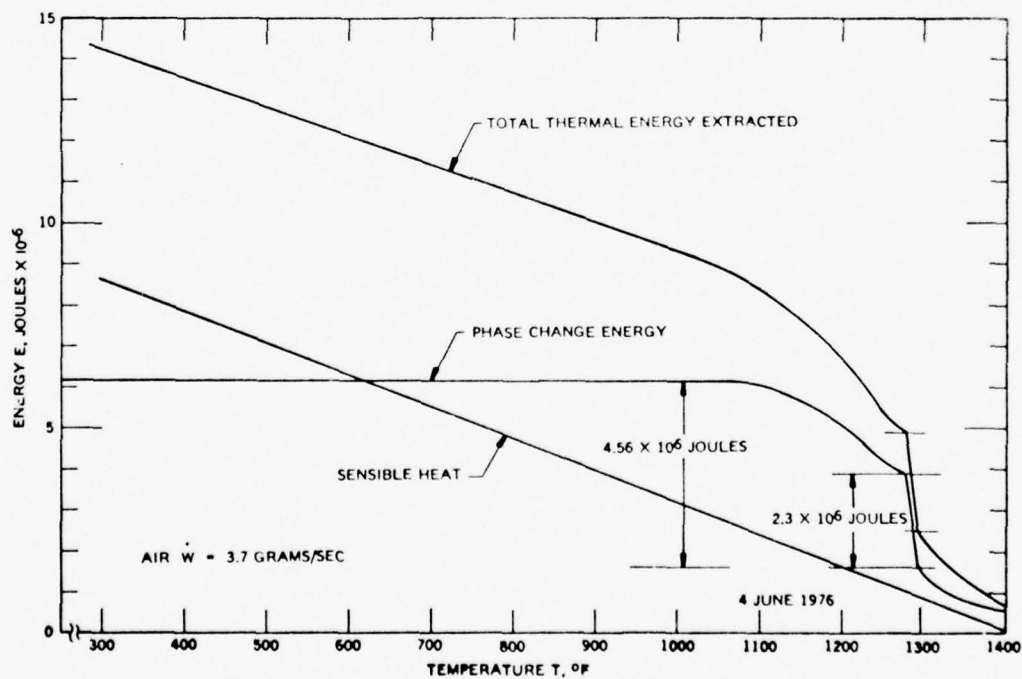


Figure 79. Extracted Energy (Cooling by Thermal Losses and by Simulated V/M Cooler Operation with Flowing Gas)

the unpredicted behavior of the chosen TES material is either the acceptance of a larger temperature swing over which the hot cylinder of the Vuilleumier cooler has to operate or a smaller energy storage density.

4.2.2.4 Temperature Distribution

The design of the thermal energy storage unit was primarily aimed at extracting energy from the thermal energy storage material and transferring it to the hot cylinder with the smallest possible temperature drop. This would permit the use of a thermal energy storage material that had a melting temperature only slightly higher than the operating temperature of the hot cylinder of the Vuilleumier cooler. The best approach for achieving the desired operating characteristic of the thermal energy storage unit was the use of the heat pipe phenomenon by which energy could be transferred over a relatively large distance with a relatively small temperature drop.

When the thermal energy storage unit was tested with energy extraction at the hot cylinder, large temperature gradients were measured in the thermal energy storage unit. In Figures 80 and 81 the temperatures which were measured and recorded on a strip chart and whose locations are presented in Figure 60 are plotted against time. The gas flow rate through the hot cylinder was set to extract a total power of 1067 watts. Since the temperature differences did not exist during charging, as can be seen from Figure 82, the observed temperature gradients could not be attributed to faulty thermocouple readings.

All evidence indicated that the heat pipe functioned only partially. Some heat pipe effect was deducted from the fact, that the power transferred at the hot cylinder could not be conducted through the structural components of the thermal energy storage unit with the indicated temperature gradients along the unit.

96746

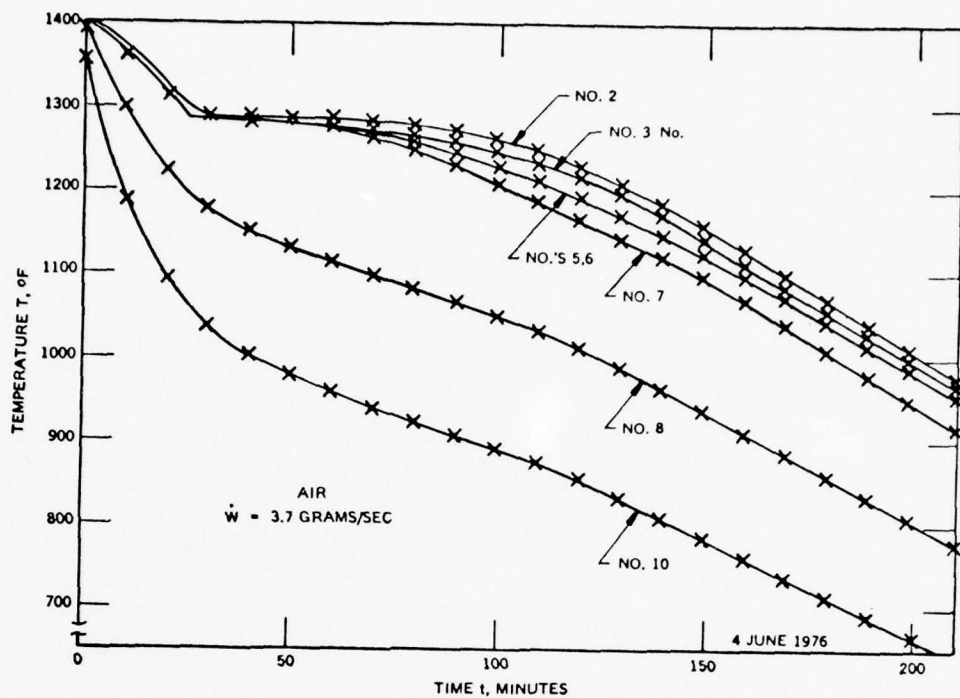


Figure 80. Measured Temperatures During Energy Extraction

96730

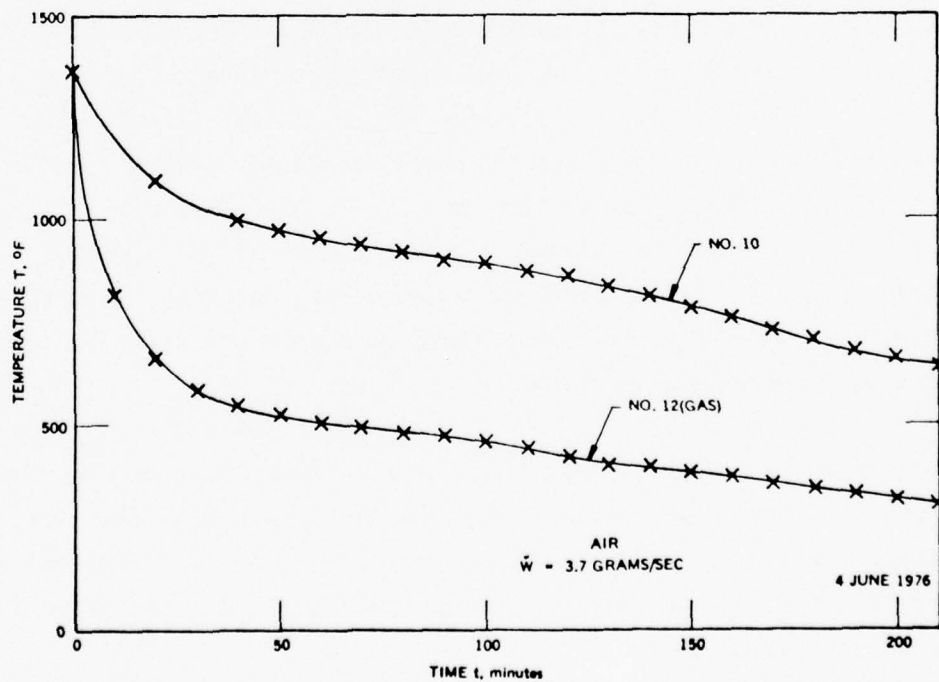


Figure 81. Measured Temperatures by Thermocouples Nos. 10 and 12

56727

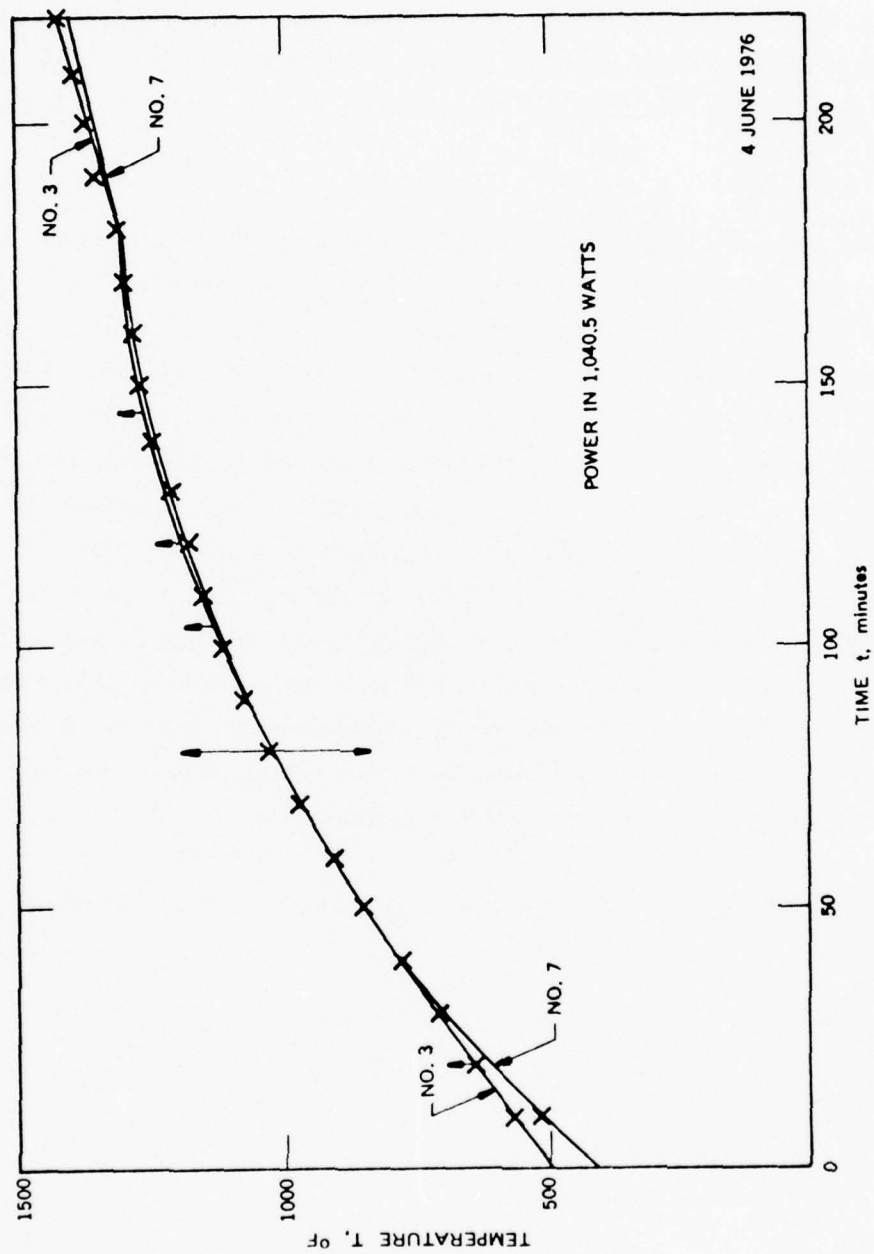


Figure 82. Temperatures During Charging of TES Unit

Three possible reasons for the malfunction of the heat pipe could be considered; (1) insufficient amount of working fluid (sodium), (2) failure of the wick, and (3) incondensable gas in the heat pipe. All three possible modes of heat pipe deficiency were investigated. (See Appendix B for wick study.) The failure was finally traced to a gas leak in the fill valve.

The heat pipe was reprocessed after the fill valve had been replaced by a new valve. When the stored energy was extracted from the unit by thermal losses and by cooling of the hot cylinder, the thermal energy storage unit exhibited the temperature distribution that had been predicted for the design (Figure 83). All temperatures along the outside of the unit remained equal, while the temperature measured inside the thermal energy storage unit (T.C. Nos. 1 and 2) was higher. The difference between the outside and inside temperatures was increasing with time as had been expected, when considering the heat transfer across the solidified TES material. The average power extraction rate was about 883 watts (figure 84) and the temperature differential between the outside temperatures and the inside temperature was 42°F . A temperature differential of 50°F at an extraction rate of 1200° watt had been predicted by the heat transfer analysis that was presented in Subsection 2.2.1.

The measured energy extracted as a function of temperature is shown in Figure 85.

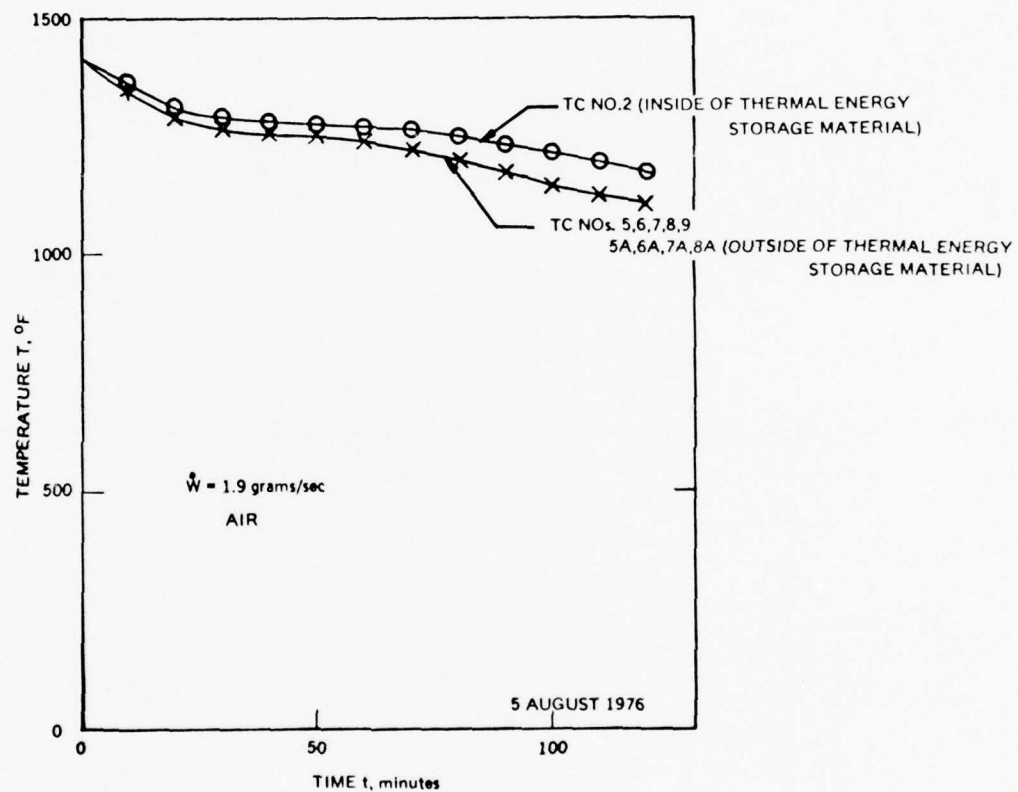


Figure 83. Measured Temperatures During Energy Extraction

56889

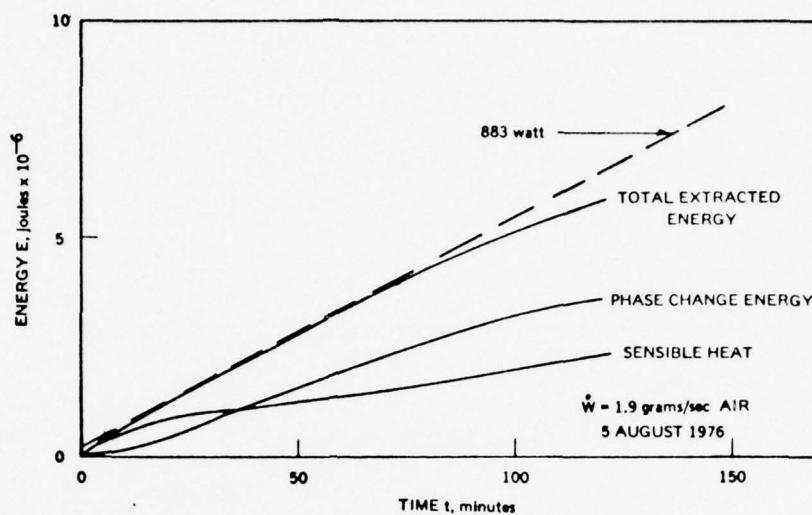


Figure 84. Extracted Energy (Cooling by Thermal Losses and by Simulated V/M Cooler Operation with Flowing Air)

56888

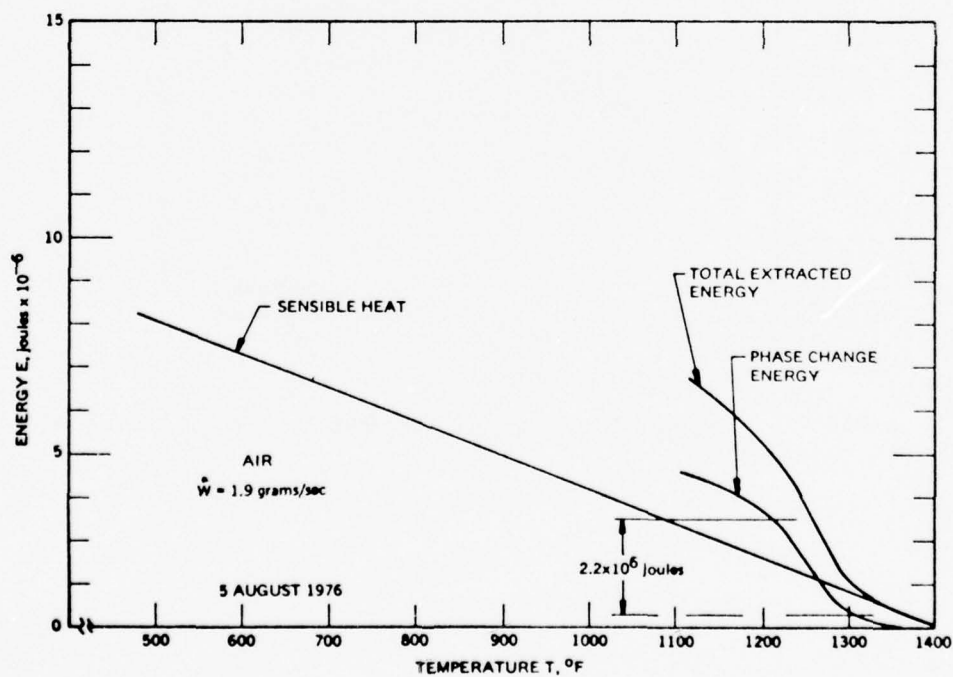


Figure 85. Extracted Energy (Cooling by Thermal Losses and by Simulated V/M Cooler Operation with Flowing Gas)

SECTION V

CONCEPTUAL FLIGHT DEVICE PARAMETER DEVELOPMENT

5.1 BASIC REQUIREMENTS

For the evaluation of the thermal energy storage concept as applied to a high capacity Vuilleumier refrigerator, requirements for the refrigerator as shown in Table 6 were assumed.

TABLE 6. REFRIGERATOR REQUIREMENTS

Orbit:	12 hr
Eclipse Time:	1 \pm 0.1 hr
Operating Temperature:	1250 $^{\circ}$ \pm 25 $^{\circ}$ F
Total Power Requirement:	1000W 1500W 2000W
No. of Hot Cylinders:	1 or 2

With the Vuilleumier cooler energy requirement given, it was further assumed that thermal losses would amount to about 10 percent of the cooler power, and that the thermal energy storage material is a ternary eutectic salt made up of 64 LiF - 30 MgF₂ - 6 KF, having an eutectic temperature of 1310 $^{\circ}$ F and a heat of fusion of 788.4 joules/gram (339.3 B/lb).

The main restrictions placed on the design of a thermal energy storage unit were:

- a. The unit must be constructed from commercially available Inconel 600 pipes.

- b. The unit must be tested in a 1-g environment.
- c. The unit will be mated to the hot cylinder of the High Capacity refrigerator.

The stipulation that the design should incorporate commercially available Inconel 600 pipes was based on the experience gained in trying to procure specially made tubing from sheet metal stock. An intensive procurement inquiry produced only two vendors who were willing to undertake the fabrication of some but not all tubes to a given design. Despite quoting a price three times higher than that quoted by the first vendor, the second vendor was not even willing to guarantee the loosest tolerances required for final welding of the thermal energy storage unit. Thus, the available sources for tube fabrication from sheet metal stock proved to be too few and the fabrication cost appeared to be relatively high.

The nonfunctional requirement imposed on the design that the unit be able to operate in a 1-g environment, has to be accepted as long as the thermal energy storage unit has to be tested and its operation verified prior to launching and operation in space. This requirement imposes a dimensional constraint on the unit which is set by the height to which the working fluid of the heat pipe can be raised in a 1-g environment by the suction pressure due to capillary forces in the wick structure of the heat pipe.

5.2 CONCEPTUAL DESIGN PARAMETERS

5.2.1 BASIC DESIGN

The basic design that evolved from the above requirements and constraints is shown in Figure 86. The length, L , of the thermal energy storage unit is determined by the power requirement of the refrigerator which is shown in Figure 87.

56684 A

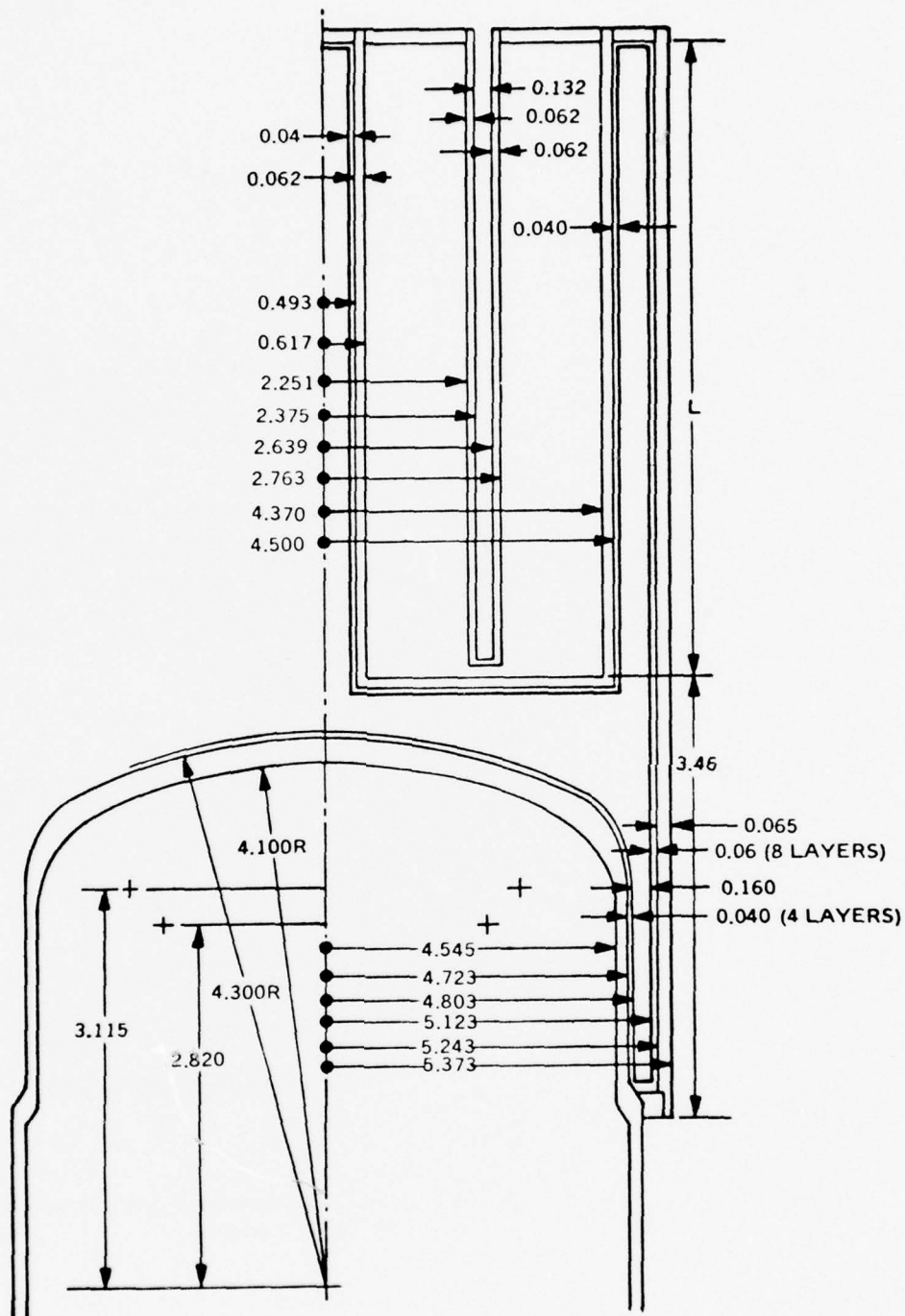


Figure 86. Thermal Energy Storage Unit Mounted on a Hi-Cap Hot Cylinder

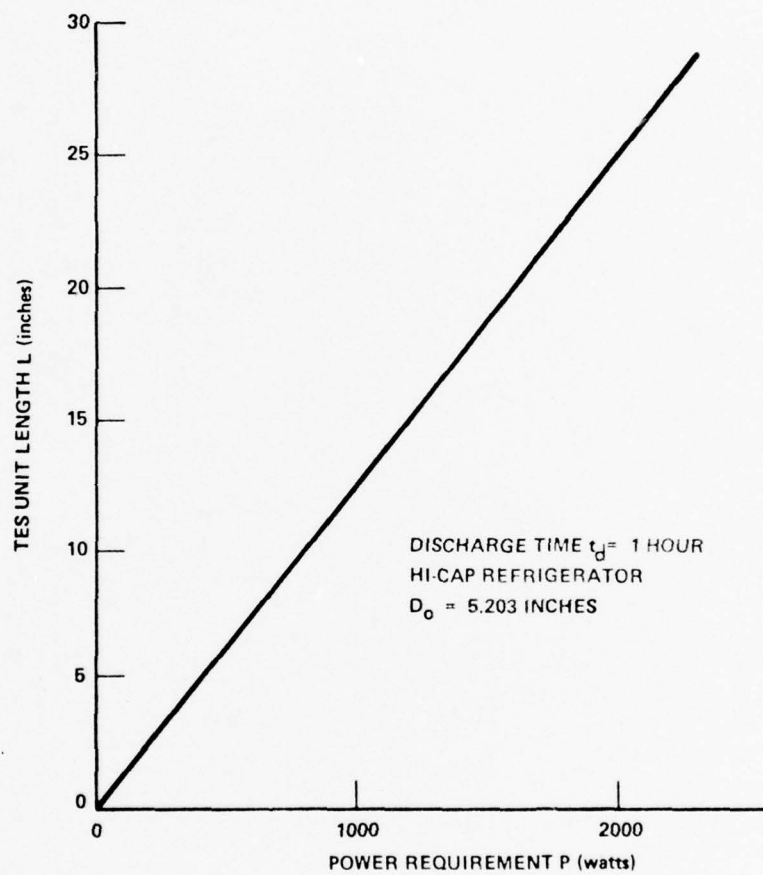


Figure 87. Correlation Between Power Requirement and TES Unit Length

54801

5.2.2 TEMPERATURE DISTRIBUTIONS

The temperature distribution in the thermal energy storage unit is shown in Figure 88. This temperature distribution is not affected by the length of the unit, because the temperature drop associated with the vapor flow pressure drop is very much less than 1°F . It remains negligible over the entire range of design lengths considered in this study.

The temperature drop across the thermal energy storage material as a function of the discharge time is shown in Figure 89. The effect of the temperature drop across the thermal energy storage material on the operating temperature of the Vuilleumier refrigerator is shown in Figure 90. At the beginning of the discharge cycle, the operating temperature is 1279°F , while at the end of the cycle the operating temperature will be either 1227°F or 1219°F for a 1-hour orbit, respectively. The operating temperature is therefore 29°F above the design operating temperature of 1250°F at the beginning of the eclipse and 23°F below the design temperature.

The operating temperature of the Vuilleumier refrigerator over the entire 12-hour cycle, which includes the charging and discharging of the thermal energy storage unit, is shown in Figure 91. It would be interesting to compare this temperature variation and the cycle frequency of a hot cylinder operated with a thermal energy storage unit with the temperature history of a hot cylinder which is heated directly with a temperature controlled electrical heater.

5.2.3 WEIGHT

The total weight of the thermal energy storage unit including all necessary components of the unit, structural, wicking, working material, and insulation, is presented in Figure 92. For comparison, the probable weight of a nickel-hydrogen battery that can satisfy the same power requirements as the thermal energy storage unit are presented. The specific weight of the

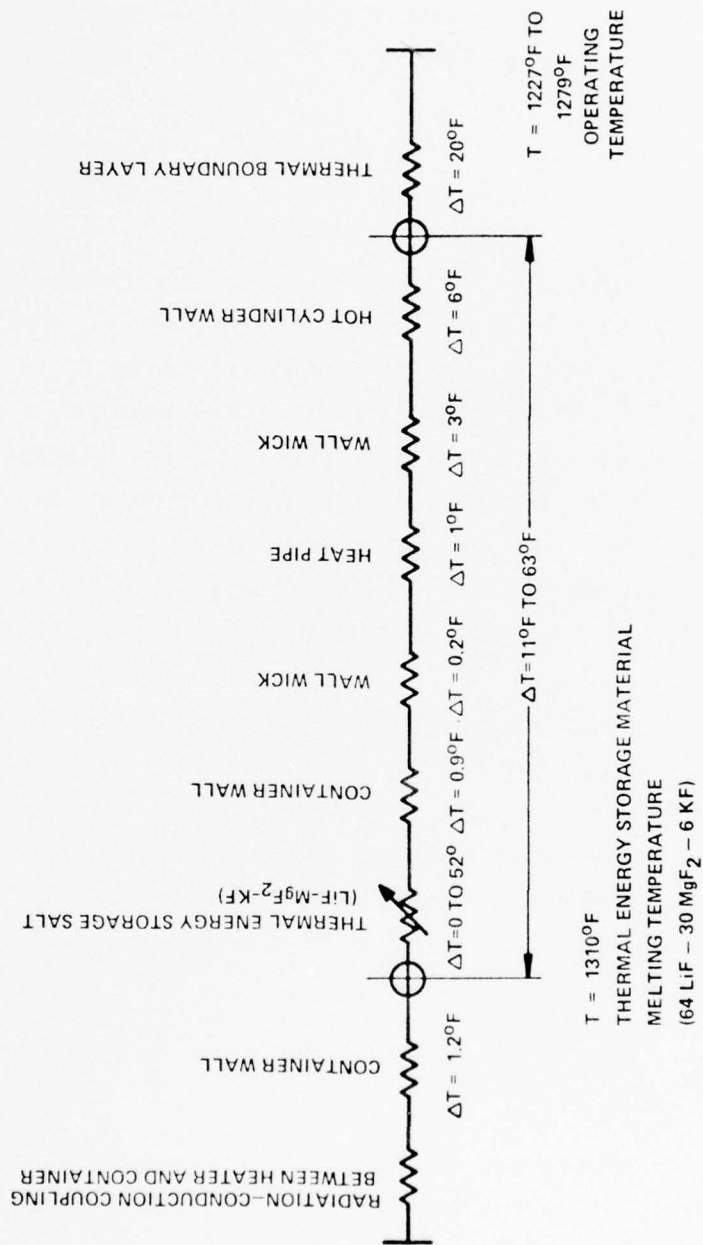


Figure 88. Temperature Distribution in the Thermal Energy Storage Unit and the Hot Cylinder of the Long Life, High Capacity Vuilleumier Refrigerator for Space Application

54796

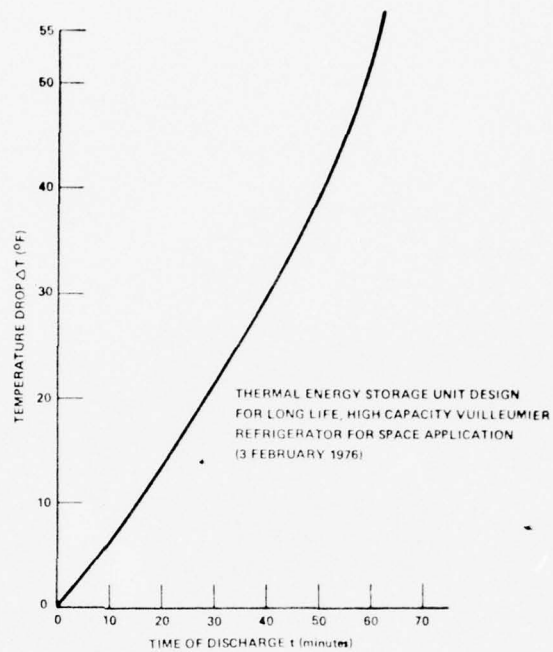


Figure 89. Temperature Drop Across Thermal Energy Storage Material

54800

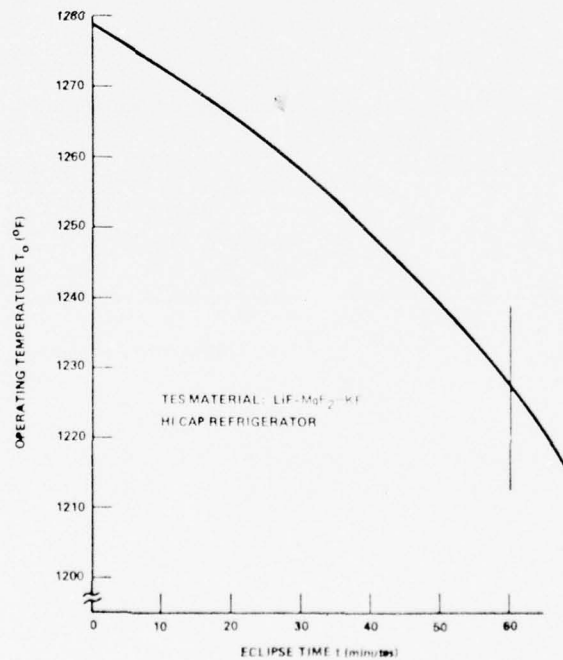


Figure 90. Vuilleumier Refrigerator Operating Temperature During Discharge of Thermal Energy Storage Unit

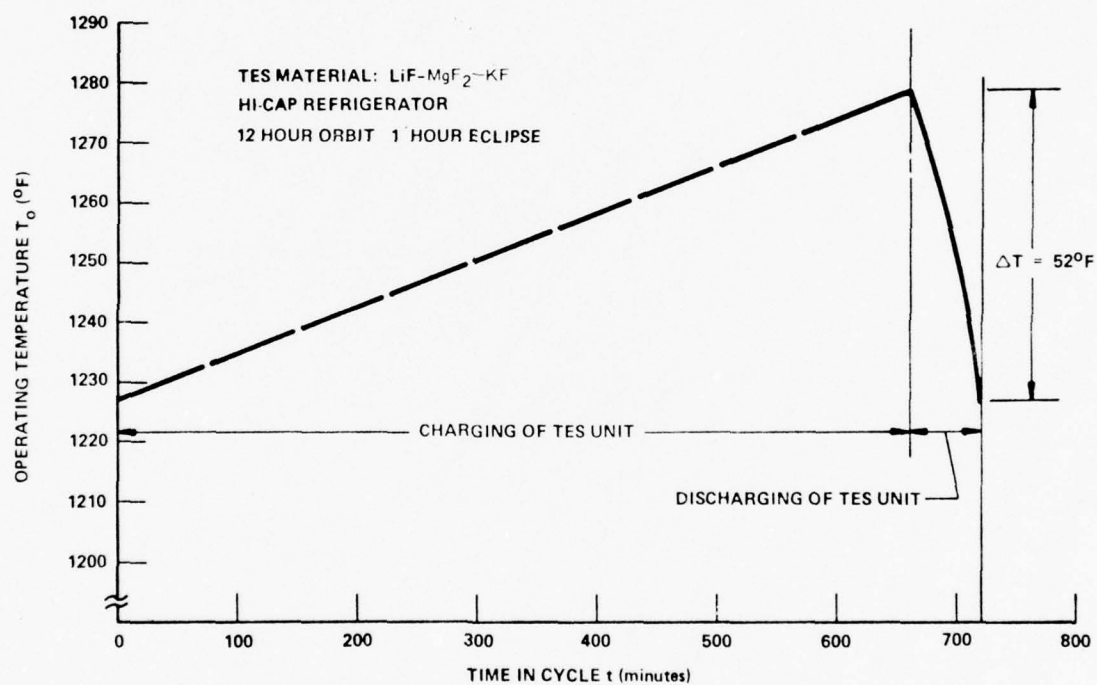


Figure 91. Operating Temperature of Vuilleumier Refrigerator During a Full Cycle of Charging and Discharging of the Thermal Energy Storage Unit

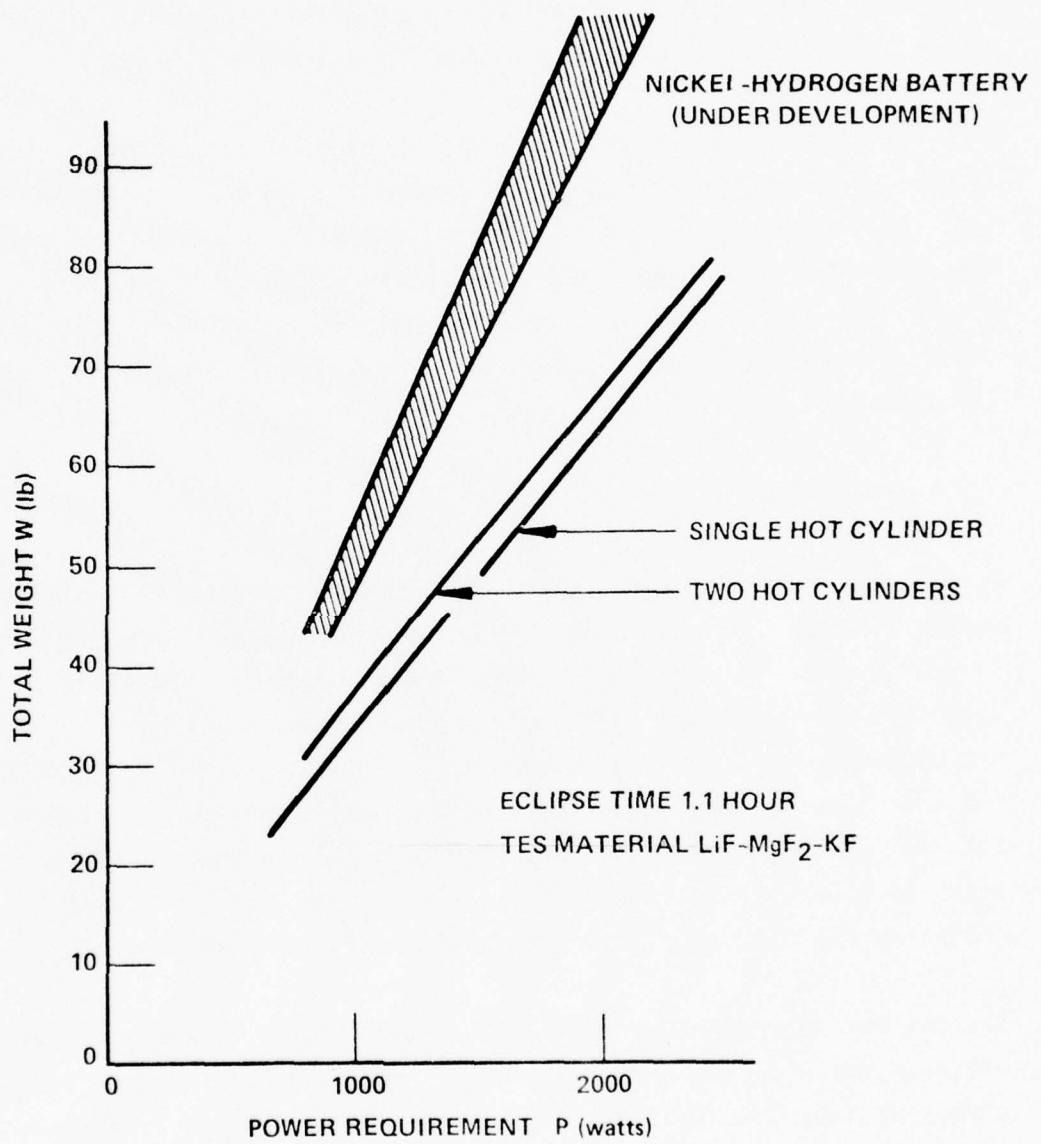


Figure 92. Total Weight of a Thermal Energy Storage Unit for a Vuilleumier Cooler

54791

thermal energy storage unit is shown in Figure 93. With increasing power requirements, the specific weight approaches asymptotically 34 watt-hr/lb for a single hot cylinder Vuilleumier refrigerator, and slightly more than 32 watt-hr/lb for a dual hot cylinder refrigerator. The specific weights for batteries are being presented only for initial evaluation.

When comparing the weights of the thermal energy storage material (Figure 94) with the weights of the container (Figure 95), it can be seen that they are equal. While the thermal energy storage material weight is determined by the energy storage requirement, the container weight could conceivably be reduced if and when, by experience and long duration testing, the minimum material thickness for the container material has been established.

5.2.4 STRUCTURE

For the outer container, the wall thickness is determined by the collapsing criteria of the cylinder. The unit has to withstand a pressure difference of one atmosphere when the thermal energy storage unit is cold and a slightly lower pressure differential when the unit is operating at its design temperature. Correspondingly, the materials properties of Inconel 600 are changing with temperature as shown in Figure 96. The correlation between wall thickness of the outer cylinder and the collapsing pressure is shown in Figure 97. If a safety factor of 4 is employed, then the wall thickness for the design indicated in Figure 86 would be about 0.060 inch.

The collapsing pressure calculations assumed a long cylinder to cover the entire range of design. The calculations can be refined to incorporate the effect of length on the wall thickness requirements. A relatively short TES unit could be constructed with a slightly thinner wall than that indicated by Figure 97.

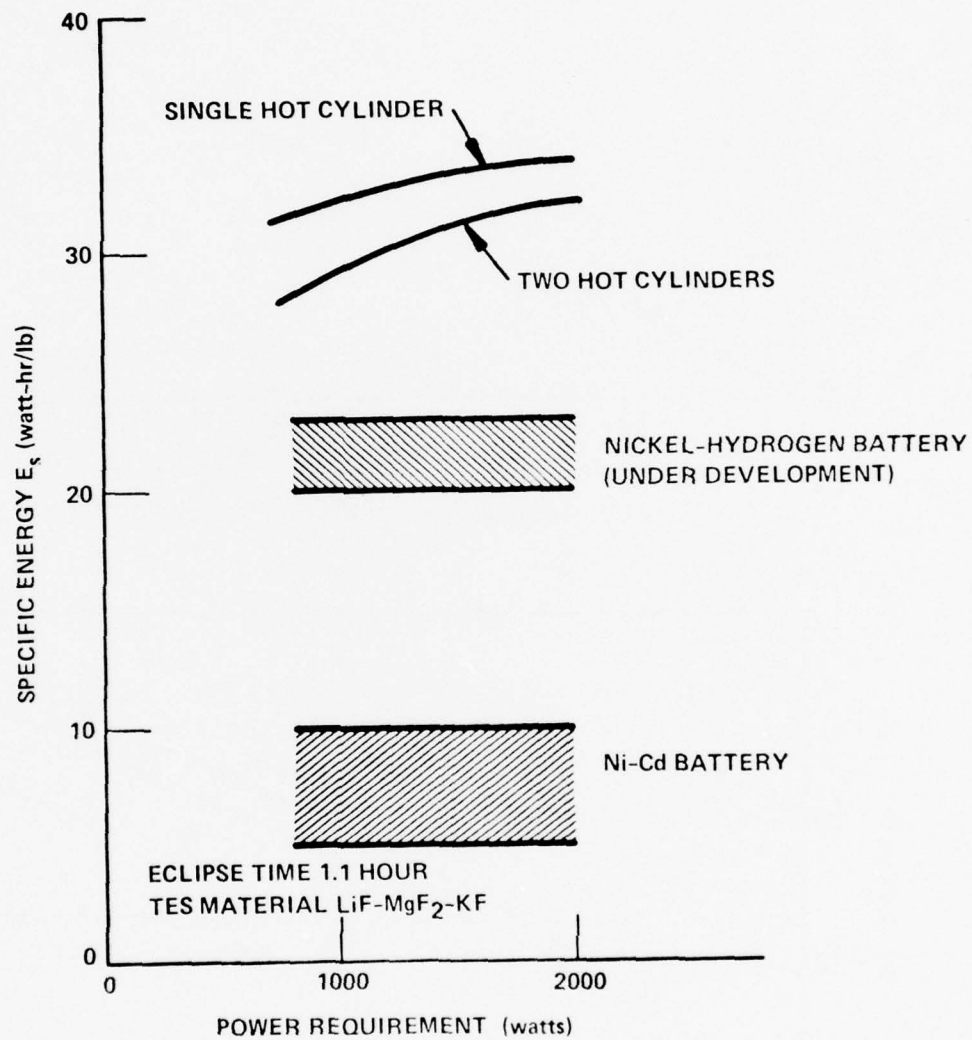


Figure 93. Specific Energy of a Thermal Energy Storage Unit for a Vuilleumier Cooler

54795

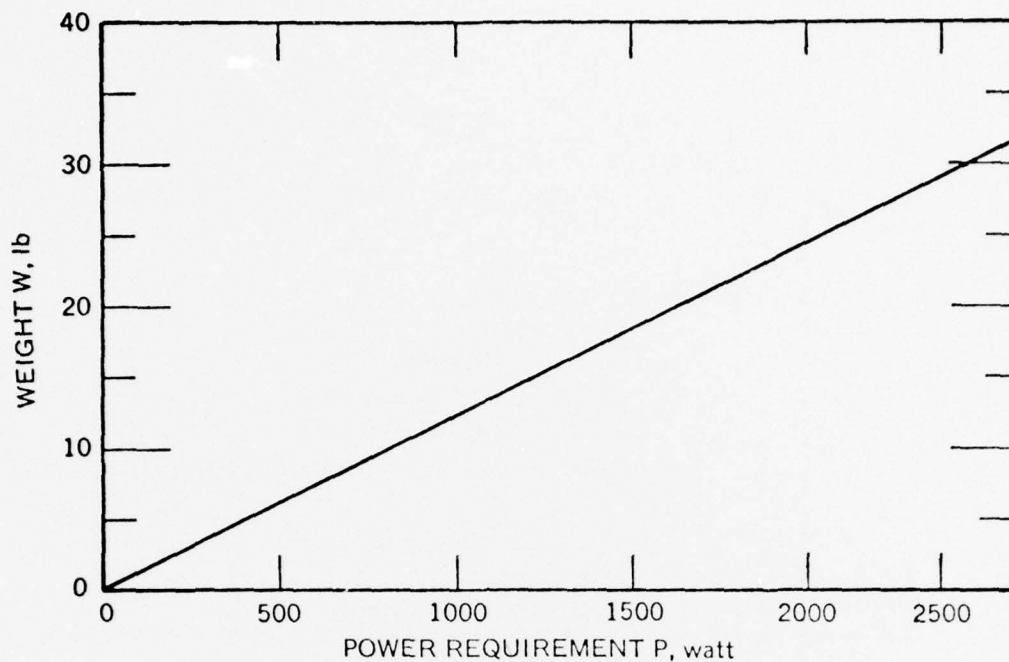


Figure 94. Thermal Energy Storage Material Weight

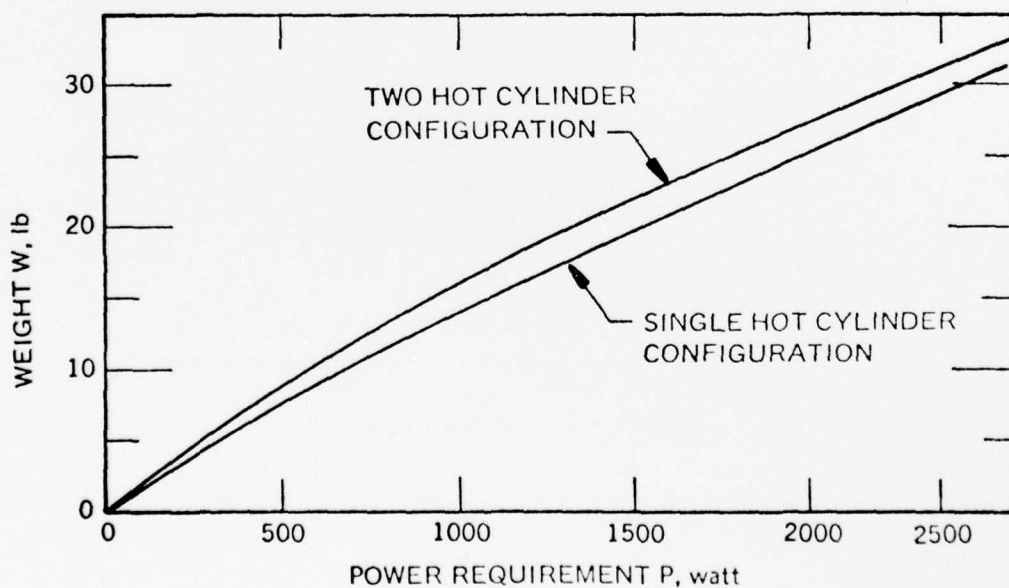


Figure 95. Total Container Weight Including Insulation and Heat Pipe Components

54793

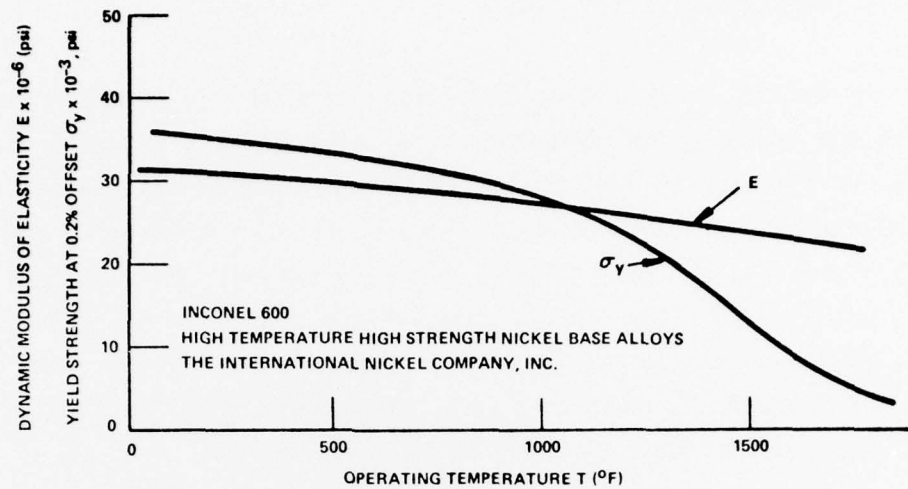


Figure 96. Dynamic Modulus of Elasticity E and Yield Strength of Inconel 600 Alloy

54794

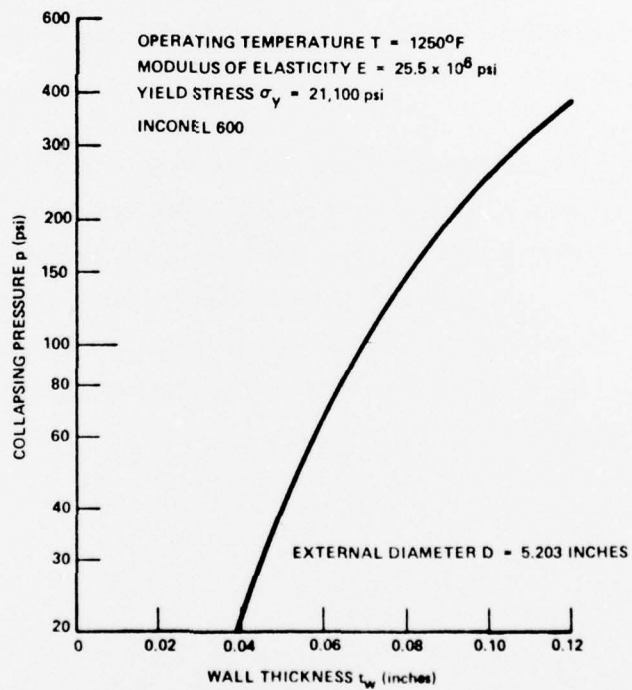


Figure 97. Collapsing Pressure of Thin-Walled Vessel

5.2.5 CONCEPTUAL FLIGHT DEVICE

For a mission using a long life, high capacity Vuilleumier refrigerator with two opposing hot cylinders, the total thermal power requirement for the refrigerator is 1150 watts. This power has to be supplied to the two opposing hot cylinders, i.e., 575 watts to each cylinder. The low earth orbit would demand only 18 minutes of thermal energy to be supplied by the TES units. Using the design underlying the TES demonstration unit which called for an energy requirement of 1000 watts for 60 minutes, the length of the TES units for the long life, high capacity Vuilleumier refrigerator (Hi-Cap V/M) hot cylinders can be estimated to be

$$L = \frac{1150}{2 \times 1000} \times \frac{18}{60} L_{\text{TESDU}} = 0.1725 L_{\text{TESDU}}$$

The hot cylinder physical layout with the TES unit is shown in Figure 98 and Figure 99 shows the Hi-Cap V/M cooler with the TES units mounted on both hot cylinders. For comparison, Figure 100 shows the cooler without the TES units.

The available pipe sizes for the construction of the TES unit are boxed in black in Figure 32. Only Schedule 40 pipes are available for larger pipe sizes. The nominal 5-inch pipe has a wall thickness of 0.258 inch, which is about three times thicker than needed. Thus, an unmachined pipe would weigh about 10 pounds, but approximately two-thirds (6.5 pounds) would have to be removed. The cost of the pipe is approximately \$16/pound indicating a waste of about \$100.

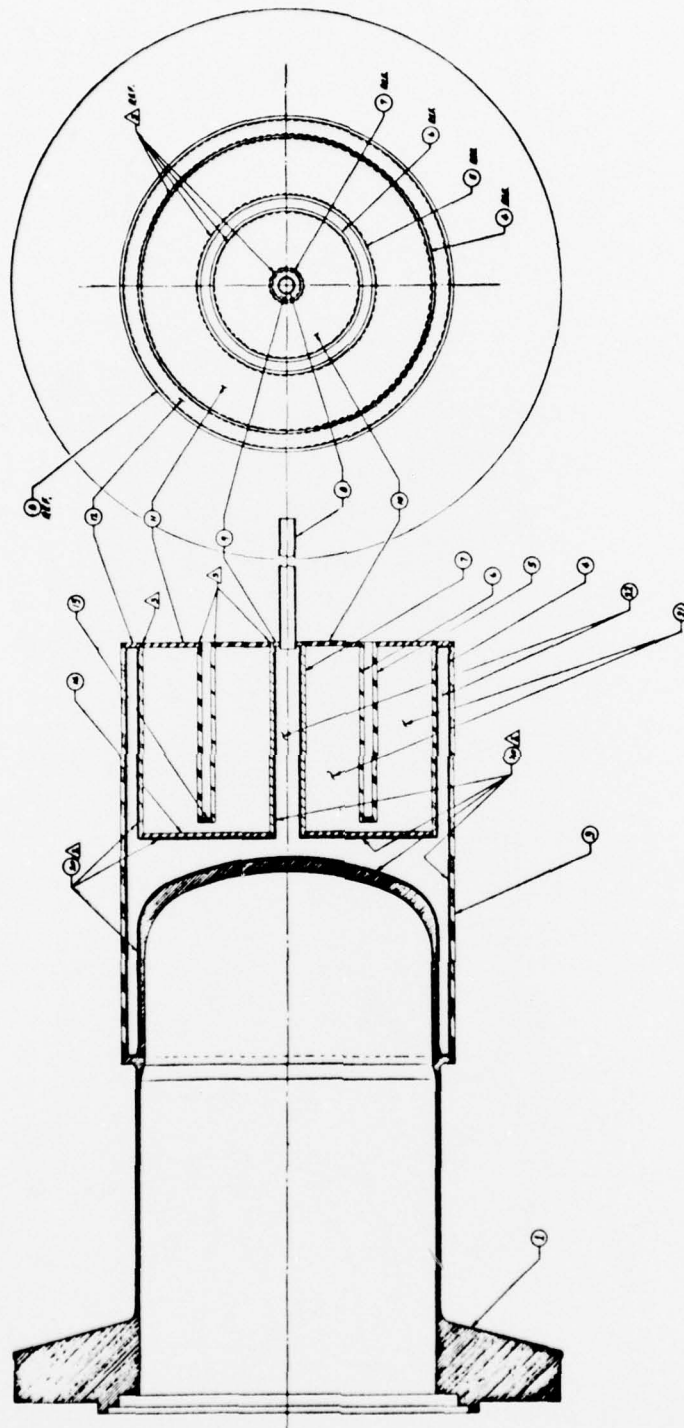


Figure 98. Conceptual Thermal Energy Storage Unit for Hi-Cap Vuilleumier Cooler

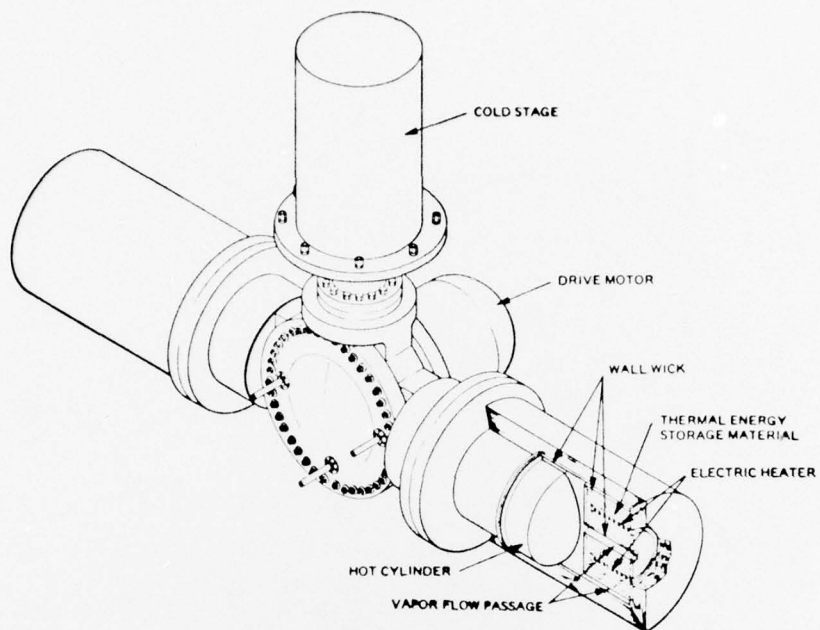


Figure 99. Long Life, High Capacity Vuilleumier Refrigerator with Thermal Energy Storage Units

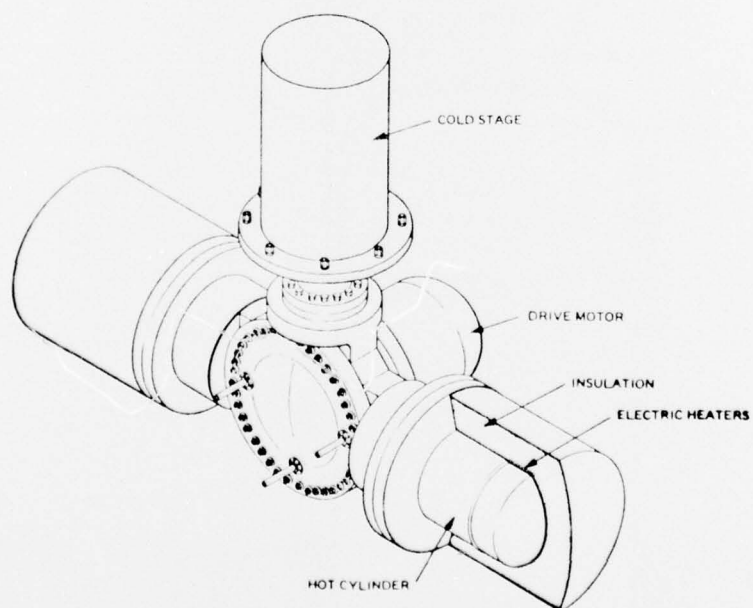


Figure 100. Long Life, High Capacity Vuilleumier Refrigerator with Battery Energized Electric Heaters (Present Hi-Cap Configuration)

SECTION VI

CONCLUSIONS

The Thermal Energy Storage Demonstration Unit program had as its objective proof of feasibility of storing energy in form of latent heat for powering a Vuilleumier cooler during the time a satellite is in the eclipse of the sun. The major technical areas that needed technical confirmation were the storing of thermal energy, the extraction of the energy over a limited temperature range, and the transfer of the thermal energy to the hot cylinder of the Vuilleumier cooler.

The design of the thermal energy storage unit confirmed the concept of storing energy from an electric heater in form of the latent heat of a thermal energy storage material. The stored thermal energy was extracted over a large area with a minimum of temperature drop and transferred to the hot cylinder by heat pipe action.

The testing of the thermal energy storage demonstration unit revealed rather unexpectedly that the phase change energy of the ternary eutectic salt, $\text{LiF-MgF}_2\text{-KF}$, was not released or absorbed entirely at the melting point of the salt, but over a relatively wide temperature range. It appeared that only about 50 percent of the "ideal" fusion energy is absorbed during heating or released during cooling at the eutectic temperature of about 1310°F . Phase transformation with energy absorption upon heating apparently takes place at temperatures below the eutectic temperature. This produces the appearance of a specific heat which is much more temperature dependent than kinetic theory would predict.

The thermal energy storage demonstration unit program demonstrated a TES unit that stored energy in the form of fusion energy, released the stored

energy at the eutectic temperature and below, and could transfer the energy by heat pipe action to the hot cylinder of a Vuilleumier cooler. The large amount of thermal energy released at the eutectic temperature and during the solidification of the thermal energy storage salt was transferred over a temperature range of about 42°F. This agreed well with the design prediction, confirming the capability of designing TES units to specific requirements when the thermodynamic properties of the TES material are known.

The evaluation of weight contributions of the various TES unit components pointed to the most fruitful areas of further investigation of all aspects of thermal energy storage, if this concept should prove to be a valid alternative to storing energy in an electrical battery. A considerable reduction of the wall thicknesses of the container could be possible, if material compatibility for long duration operation could be proven to exist between the storage salt, the heat pipe working fluid, and the container material.

APPENDIX A

EFFECT OF NONCONDENSABLE GAS ON HEAT PIPE OPERATION

When large temperature differences along the heat pipe section of the thermal energy storage unit were observed, an attempt was made to explain this apparent malfunction of the heat pipe by assuming the possibility of noncondensable gas in the heat pipe section of the thermal energy storage unit. In Figure A-1, the temperature difference between thermocouple No. 6 and thermocouple No. 10 were plotted. The temperature difference could be explained by a vapor pressure difference of the working fluid which has been calculated for the operating temperature and which has also been plotted in Figure A-1. The calculated pressure differentials which are based on the observed temperature differentials, are considerably higher than those which were calculated for the vapor flow, as can be seen from the pressure differentials shown in Figures 16, 17 and 18 of Subsection 2.2.2.3. Only the presence of noncondensable gas in the heat pipe could explain such large vapor pressure differentials. If the presence of noncondensable gas at a pressure of 1.67 mm Hg at room temperature is assumed, then temperature differentials as shown in Figure A-1 could be expected. The calculated temperature differential curve has apparently a different trend than the curve which was constructed from the measured temperature differentials. Nevertheless, some similarity in behavior seems to exist.

It was interesting to show that, if noncondensable gas should have an effect on the heat pipe operation, a heat pipe operating with potassium as the working fluid would be less affected than a heat pipe operating with sodium at the same operating temperature. This can be seen in Figure A-2. The reason for this difference between the two working fluids can be found

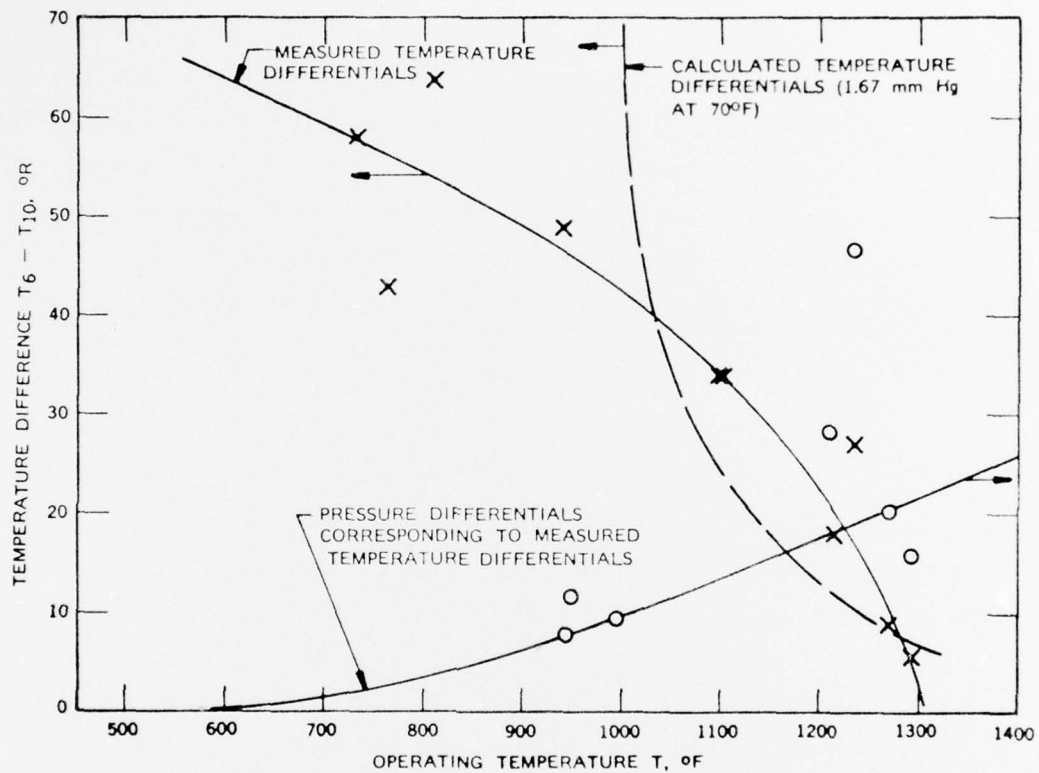


Figure A-1. Temperature Differentials and Pressure Differentials

56882

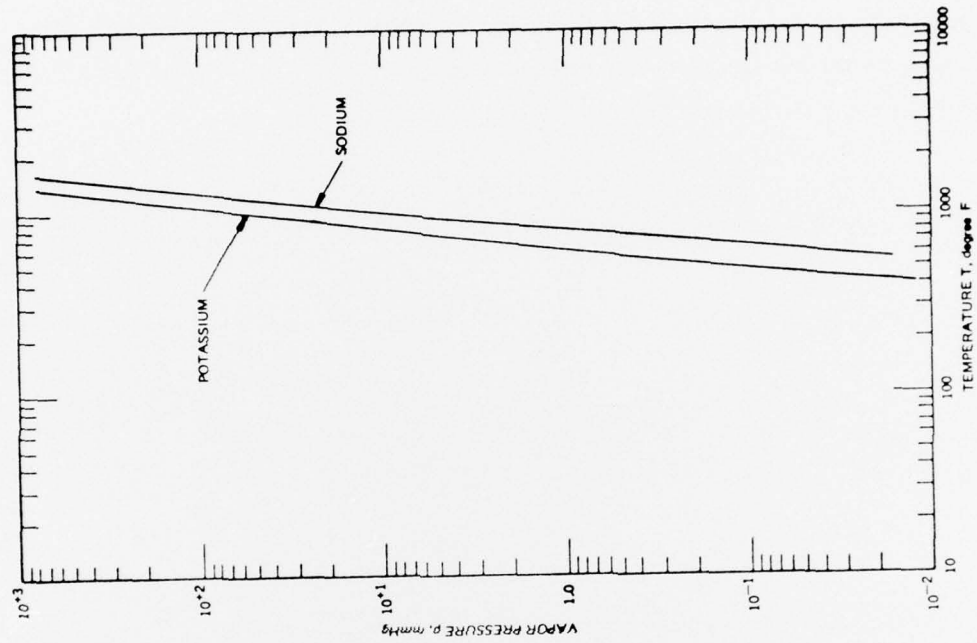


Figure A-3. Vapor Pressure of Sodium and Potassium

56142

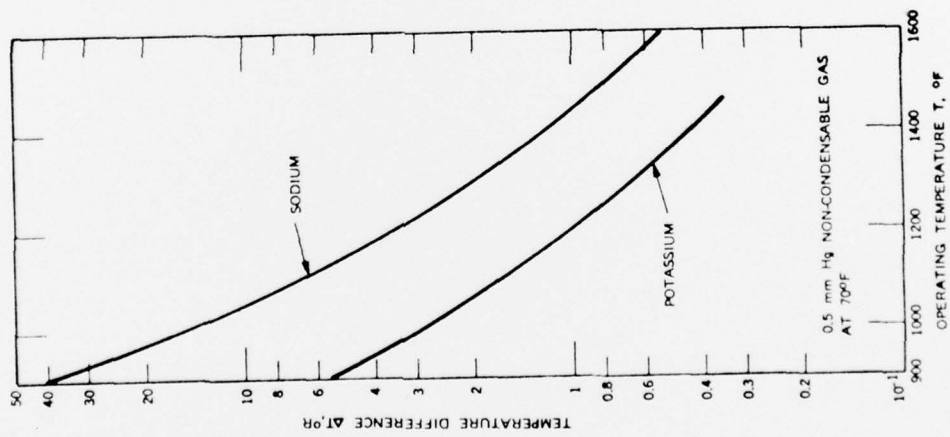


Figure A-2. Temperature Differential Due to Noncondensable Gas

from the graph showing the vapor pressure of sodium and potassium (Figure A-3). For the thermal energy storage unit operating at around 1300°F, potassium would be quite acceptable as heat pipe working fluid, as the vapor pressure at that temperature is only slightly above 1/2 atm. The unit has to be designed for a pressure differential of 1 atm to satisfy the condition in the laboratory.

APPENDIX B

TRANSIENT WICK EFFECTS

When initially it was not possible to verify the presense of noncondensable gas in the heat pipe section of the thermal energy storage unit, and it appeared that the heat pipe section had been fully evacuated, the capacity and performance of the wick structure was investigated in an informative experiment to verify the wick design.

The wick of the heat pipe was constructed with a 70 Mesh bolting cloth which has a wire diameter of 0.00375 inch. For a fluid the wicking height is

$$h = \Delta p_c / \rho g$$

where:

$$\begin{aligned} h &= \text{height, cm} \\ \rho &= \text{specific gravity of water, g/cm}^2 \\ g &= \text{gravitational constant, 981 cm/sec}^2 \\ \Delta p_c &= \text{capillary pressure, dynes/cm} \end{aligned}$$

$$\Delta p_c = 2\sigma \cos\phi / r_c$$

where:

$$\begin{aligned} \sigma &= \text{surface tension of water against air, dynes/cm} \\ \phi &= \text{contact angle, degrees} \\ r_c &= \text{effective pore radius, cm} \\ r_c &= 0.707 (1/M - d) \end{aligned}$$

where:

$$M = \text{Mesh, cm}^{-1}$$

$$d = \text{wire diameter, cm}$$

For distilled water at room temperature, the surface tension is

$$\sigma = 72.75 \text{ dynes/cm,}$$

and the wicking height is found to be:

$$h = 3.086 \text{ inch.}$$

Figure B-1 shows a fixture that was built to simulate the wick structure in the heat pipe section of the thermal energy storage unit. In step one, the dry structure was weighted. In step two, the wick structure was soaked with water and the structure was weighted again. In step three, the structure was held horizontally in water, after which it was weighted again. In the fourth step, the wick was permitted to soak up water after most of the water had been shaken out of the wick. The structure was weighted again. The fully filled 4.9 inch high screen appeared to hold 7.0 grams of water. When standing vertically, it retained 4.5 grams of water. This indicated that the height of the water in the wick was

$$h = h_0 \times W/W_0$$

$$h = 3.15 \text{ inch}$$

This compared with the predicted value of $h = 3.086$ inch. After the fourth step, the water weight was $W = 3.6$ grams, which corresponded to a wicking height of $h = 2.52$ inch, or about 80 percent of the maximum wicking

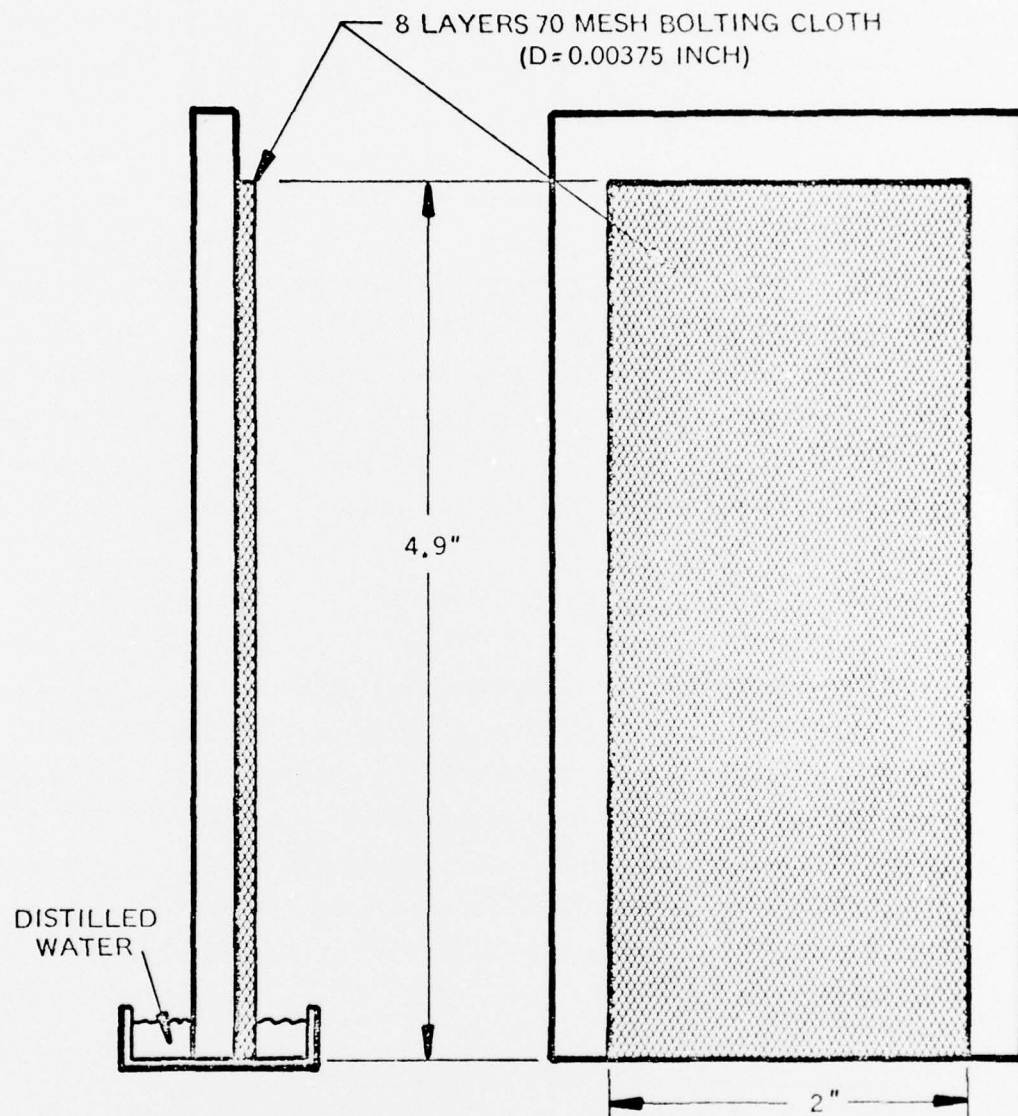


Figure B-1. Test Fixture for Wick Investigation

height. The data of Ref. 3 are difficult to correlate and do not pertain to sodium. Nevertheless it is indicated that time is a strong parameter which determines the height during continuous operation to which the wick will remain wet in a heat pipe whose diameter is close to the calculated maximum wicking height.

The small informative test indicated that some basic data should be generated in support of the design of full scale thermal energy storage units. Wick data in the literature and of other investigators are very speculative and sketchy and can therefore not be used for designs in which the limit of the capability of wick structures is being approached. The permeability investigation of wicking structures, which was performed under the previous program, proved the need for such basic studies in connection with the design of a major hardware component.

Tests might be needed to ascertain whether the heat pipe section of the thermal energy storage unit is not subject to the fast start-up phenomenon which was observed with the 15-ft long heat pipe. At an extraction rate of 1200 watts, 0.2772 g/sec of sodium has to circulate. This is equivalent to 997.92 g/hr of sodium. The entire heat pipe section contains 329 grams of sodium, indicating that the sodium has to be wicked back three times an hour during operation. This rate might make the heat pipe operation marginal for a wick height which is more than 75 percent of the maximum wicking height. Some basic investigations with water should be able to answer these questions.

-
3. H. R. Knuz, L. S. Langston, B. H. Hilton, S. S. Wyde, and G. H. Nashick, "Vapor-Chamber Fin Studies - Transport Properties and Boiling Characteristics of Wicks," NASA Contractor Report No. NASA CR-812, June 1967.